LAP SPLICING OF LARGE HIGH-STRENGTH STEEL REINFORCING BARS

By
Ryan Rulon
Rémy D. Lequesne
Andrés Lepage
David Darwin

A Report on Research Sponsored by

ELECTRIC POWER RESEARCH INSTITUTE

Structural Engineering and Engineering Materials
SM Report No. 148
March 2022

THE UNIVERSITY OF KANSAS CENTER FOR RESEARCH, INC.
2385 Irving Hill Road, Lawrence, Kansas 66045-7563

LAP SPLICING OF LARGE HIGH-STRENGTH STEEL REINFORCING BARS

By

Ryan Rulon

Rémy D. Lequesne

Andrés Lepage

David Darwin

A Report on Research Sponsored by

ELECTRIC POWER RESEARCH INSTITUTE

Structural Engineering and Engineering Materials
SM Report No. 148
THE UNIVERSITY OF KANSAS CENTER FOR RESEARCH, INC.
LAWRENCE, KANSAS
March 2022

ABSTRACT

Use of large bars is advantageous in large structures like nuclear power plants. Nevertheless, ACI 318-19 prohibits tension lap splices for bars larger than No. 11 (36 mm) because limited test data are available. Eleven large-scale reinforced concrete beams with tension lap splices were tested to failure under monotonically increasing four-point bending to support design provisions for large diameter bars (No. 14 and 18 (43 and 57 mm)). Specimens had different amounts of transverse reinforcement, nominal concrete compressive strengths of 5 or 10 ksi (34 or 69 MPa), and target bar stresses at splice failure of 60 and 100 ksi (420 to 690 MPa) for No. 14 (43 mm) bars and 60 ksi (420 MPa) for No. 18 (57 mm) bars.

The test results show that lap splices of No. 14 (43 mm) bars can develop bar stresses up to 100 ksi (690 MPa) and that lap splices of No. 18 (57 mm) bars can develop bar stresses up to at least 60 ksi (420 MPa). These limits reflect the scope of the test matrix, as there was no indication that higher bar stresses cannot be attained. Analyses showed that both the ACI 408R-03 and ACI 318-19 equations for lap splice lengths become less conservative as bar size increases. This trend was apparent when comparisons were made using prior test results between groups of specimens with No. 6 (19 mm) and smaller bars, No. 7 to No. 10 (22 to 32 mm) bars, No. 11 (36 mm) bars, and bars larger than No. 11 (36 mm). Two methods are proposed for modifying the ACI 408R-03 and ACI 318-19 development length equations to obtain similar ratios of test-to-calculated bar stresses across all bar sizes: a bar size factor (1.15 for No. 11 (36 mm) bars and 1.25 for larger bars) in the numerator of the development length equations or an increased exponent on the bar diameter term (replacing d_b with $d_b^{1.35}$ in ACI 408R-03 and $d_b^{1.25}$ in ACI 318-19, see Equations 4.6 and 4.7 in this report). A minimum clear cover of one bar diameter is recommended for large-bar lap splices. Transverse reinforcement should also be required throughout lap splices of No. 14 and 18 (43 and 57 mm) bars, as several of the weakest large-bar specimens had no transverse reinforcement and even small quantities ($K_{tr}/d_b = 0.5$) tended to reduce size effect. Other analyses showed that increasing the limit on $\left(\frac{c_b+K_{tr}}{d_b}\right)$ in the ACI 318-19 development length provisions from 2.5 to 3.5 results in similar ratios of test-

to-calculated bar stresses for all amounts of confinement. It is also recommended that development length ℓ_d be limited to $50d_b$ when designing unconfined lap splices (and thus unconfined lap splices classified as Class B in ACI 319-19 should not be longer than $65d_b$).

ACKNOWLEDGMENTS

Support for this research was provided by the Electric Power Research Institute. Material support for the study was provided by Commercial Metals Company and Dayton Superior.

TABLE OF CONTENTS

CHAPTER 1 – INTRODUCTION

1.1 Motivation

Reinforced concrete members contain steel reinforcement for strength, toughness, and crack control. The bond between the steel reinforcement and concrete must allow forces to transfer between the materials for the reinforcement to be effective. In design, adequate bond strength is ensured by satisfying member-specific reinforcement detailing requirements and providing adequate lap splice and development lengths. Lap splices, which are the focus of this study, refer to the overlap between parallel discontinuous bars designed to allow for force transfer between the bars through bond with the concrete. The development length of a bar, which is also discussed in this report, is the bonded length needed to transfer a given force between a reinforcing bar and concrete.

Research on bond has examined the effects of a wide range of variables, including bar size, bar stress, bar deformation geometry, bar coating, concrete compressive strength, concrete density, clear cover, bar spacing, depth of concrete below the bar, and confinement. Design provisions and recommendations (ACI 318-19 and ACI 408-03), therefore, account for these variables. However, because of very limited data from tests of large-bar lap splices, current design provisions do not permit lap splices of bars larger than No. 11 (36 mm). Large diameter No. 14 and 18 (43 and 57 mm) reinforcing bars are advantageous in very large members like foundation mats or thick walls in nuclear power plants. There is need to study the strength of lap splices of No. 14 and 18 (43 and 57 mm) bars to establish safe design criteria. In addition, there is a general lack of data on development of these large bars, and because development and splice strengths have been shown to be the same, additional data on splice strength adds to the understanding bond strength more generally.

1.2 Scope & Objectives

The purpose of this study is to understand the behavior of large-diameter bar lap splices so that design provisions can be adapted for use with No. 14 and 18 (43 and 57 mm) bars. The authors are aware of only six studies of lap splices that included specimens with bars larger than No. 11 (36 mm). The two most relevant are included in ACI Committee 408 (2021). Taken together, these studies include only 17 specimens with bottom-cast lap splices with lengths representative of common practice tested within a constant moment region. Furthermore, several of the 17 specimens had low-strength concrete or threaded bars that are not representative of conventional concrete or reinforcing bars. There is a need for more tests using materials representative of modern practice.

For this study, 11 tests of full-scale beams were conducted. There were seven specimens with No. 14 (43 mm) longitudinal bars and four specimens with No. 18 (57 mm) longitudinal bars. Each specimen was loaded monotonically in four-point bending until lap splice failure. Tension lap splices were located at midspan in a region with constant moment. The specimens were designed so that lap splice failures limited the beam strength and bar yielding did not occur. Test variables included the lap splice length (14 to 72 times the bar diameter), bar diameter (No. 14 and 18 (43 and 57 mm)), amount of transverse reinforcement (with and without), and nominal concrete compressive strength (5 and 10 ksi (34 and 69 MPa)). Specimens were designed to obtain bar stresses between 60 and 100 ksi (420 and 690 MPa).

CHAPTER 2 – LITERATURE REVIEW

2.1 Bond Mechanism

Force transfer between concrete and steel reinforcement (referred to as bond) is essential in reinforced concrete members. The mechanisms of transfer are illustrated in Figure 2.1 and include bearing of the bar deformations (ribs) against concrete and frictional forces from the surface roughness of bars. These are balanced by both normal (perpendicular to bar) and shear (parallel to bar) forces. The force components perpendicular to the bar are prone to cause splitting cracks to form parallel to the bar. If cover, bar spacing, or transverse reinforcement are not adequate, a splitting failure will limit the bond strength. If clear cover, bar spacing, and transverse reinforcement are sufficient to prevent a splitting failure, a pullout failure will limit bond strength.

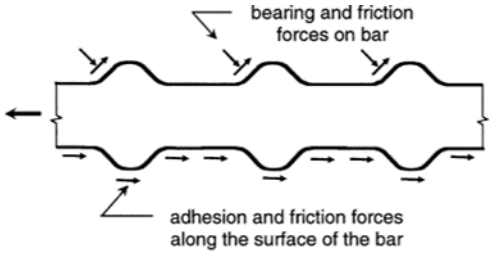

Figure 2.1: Bond force transfer (ACI 408R-03)

Bond strength is a structural property that depends on details such as transverse reinforcement, cover, bar size, concrete strength, and geometry. When a reinforced concrete member is loaded, there is initially strong adhesion between the steel and concrete that persists while there is relatively little slip. As loads are increased, cracks develop at the bar deformations and extend outward. As the bar slips, adhesion diminishes and force transfer occurs entirely through the bearing of bar deformations on concrete and friction. A further increase in loading causes longitudinal cracks to open, which increases slip. With low confinement or concrete cover, cracks may extend to the surface and result in a splitting failure (Figure 2.2). High amounts

of confinement will resist concrete splitting, which can instead result in a bar pullout failure involving crushing of concrete between bar deformations (Figure 2.3). In commonly proportioned reinforced concrete members, splitting failures tend to be more common than pullout failures (Orangun, Jirsa, and Breen, 1977).

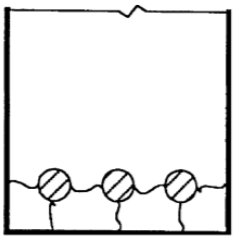

Figure 2.2: Cross-sectional view of a splitting failure (ACI 408R-03)

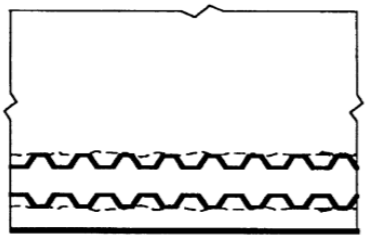

Figure 2.3: Side view of a pullout failure (ACI 408R-03)

A critical bond condition in design occurs where bars are terminated or lap spliced. In either case, designers must ensure that bond force demands are low enough to prevent splitting or pullout failures under expected loads. ACI 318 approaches this using the concept of development length: the minimum embedment length needed for a terminated bar to develop a force equal to the bar area times the specified yield stress. Lap splices, which are used to transfer the force in one bar to another by overlapping them, are designed using the concept of development. The following sections describe key parameters affecting bond strength, and thus required development and lap splice lengths, followed by descriptions of relevant prior work and development length provisions in selected consensus documents including building codes/standards and committee reports.

2.2 Relevant Parameters

2.2.1 Transverse Reinforcement and Concrete Cover

Transverse reinforcement increases bond strength by resisting the opening of cracks parallel to the bar axis that may cause splitting failures (Orangun, Jirsa, and Breen, 1977) and carrying tension across cracks (Ferguson and Krishnaswamy, 1971). There is, however, a limit to the benefits of transverse reinforcement. If sufficient reinforcement is present to change the failure mode from splitting to pullout, further increases in transverse reinforcement are not correlated with increases in bond strength (Orangun, Jirsa, and Breen, 1977).

These effects are demonstrated in results reported by Frosch, Fleet, and Glucksman (2020). Figure 2.4 shows results from tests of two specimens that were nominally identical, except for the amount of transverse reinforcement. Specimen C3/60/2-40-5-50 (red) had transverse reinforcement equivalent to 50 psi (0.34 MPa), calculated as $(A_v f_y)/(b_w s)$, where A_v is the area of shear reinforcement within stirrup spacing s, f_y is the reinforcement yield stress, and b_w is the beam width. C3/60-40-5-100 (blue) had transverse reinforcement equivalent to 100 psi (0.69 MPa). In these specimens clear cover was 1.9 times the bar diameter and clear spacing was 2 times the bar diameter. Figure 2.4 shows that doubling the amount of transverse reinforcement produced a 12% increase in lap splice strength. The longitudinal bar stresses at failure were 83 and 92 ksi (570 and 630 MPa) in this case.

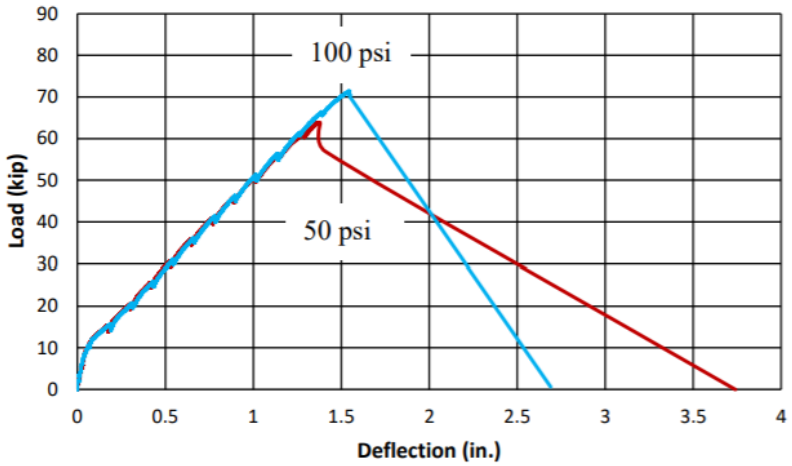

Figure 2.4: Effect of confinement on bond strength (Frosch, Fleet, and Glucksman, 2020) (1 kip = 4.448 kN, 1 in. = 25.4 mm, 100 psi = 0.6895 MPa)

Increased concrete cover and bar spacing also increase bond strength. This is because larger concrete cover and greater bar spacing require greater energy for splitting cracks to propagate from the bar (or bars) being developed to the concrete surface or between bars. When c_{bc} (bottom cover) is less than c_{so} (side cover) and c_{si} (one-half the clear spacing between bars), splitting cracks tend to initiate at the reinforcing bars and progress towards the bottom surface. Cracks tend to form through the side cover or between bars when c_{bc} is greater than c_{so} *or* c_{si}. However, it is not just the minimum of c_{bc}, c_{so}, and c_{si} that will control behavior; Orangun, Jirsa, and Breen (1977) showed that relative values also have an effect. This led to the development of the cover definitions in ACI 408-03 described in Section 2.4.2.

2.2.2 Bar Geometry

Increasing lap splice and development length will increase the force in the bar associated with bond failure, but the relationship is not proportional. Lap splice specimens have flexural cracks and often longitudinal splitting cracks that initiate at the ends of the lap splice and then propagate towards the center until failure. This is often accompanied by small amounts of concrete crushing near the bar deformations. Many studies show that "failure occur(s) by slow wedging action followed by rapid final slip of the bar at failure" (ACI 408R-03). Common design practice, consistent with ACI 318 equations, assumes a proportional relationship between length and force. This is conservative for short lap splices and development lengths but becomes less conservative as the length or stress values increase because additional length does not produce a proportional increase in bond strength. Limited data show that very long unconfined lap splices ($\ell_s/d_b > 80$) reach an asymptote where additional lap splice lengths do not provide any increase in bond strength (Glucksman, 2018). This is discussed in greater depth in Chapter 4.

As bar diameter increases, a longer lap splice length is required to reach a given bar stress. This is because the perimeter of a bar over which bond is active is a function of diameter whereas bar force is a function of diameter squared. For the same reason, larger bars will develop larger bar forces (but lower

stresses) than smaller bars using the same lap splice length when cover and confinement are constant (Orangun, Jirsa, and Breen, 1977).

Most of what is known about bond is based on tests with bar sizes between No. 5 and No. 11 (16 and 36 mm) (inclusive). Only five previous studies have included specimens with larger bars: Ferguson and Thompson (1965), Ferguson and Krishnaswamy (1971), Thompson et al. (1979), Hassan, Lucier, and Rizkalla (2012), and Hegger et al. (2015). Between these five studies, 17 tests had large bar bottom-cast lap splices within a zero-shear region of a beam span and only 9 are included in the ACI 408 Database (2021). The remaining specimens were side casted and tested, so the correlation to modern practice is not as direct. Thompson et al. (1979) reported tests on two specimens with No. 14 (43 mm) bars and a lap splice length of 35 times the bar diameter. Both specimens failed before exhibiting a bar stress of 60 ksi (420 MPa). Hassan et al. (2012) tested eight beam-splice specimens that used No. 20 (64 mm) threaded bars and had a lap splice over bar diameter ratio (ℓ_s/d_b) range from 52 to 94. The relative rib area of the threaded bars was reported as 0.16, which is much larger than the average value of 0.0727 provided in ACI 408R-03 for conventional reinforcing bars. Hegger et al. (2015) reported tests on specimens with bar diameters of 1.56 and 1.97 in. (40 and 50 mm). Results from Thompson et al. (1979), Hassan et al. (2012), and Hegger et al. (2015) will be used in comparisons with results from the current study.

A size effect has also been observed in tests performed with large diameter bars. Ichinose et al. (2004) investigated size effect on bond strength using both pullout and lap splice tests with short lap splice lengths. There were 18 beam-splice tests in this study, with and without transverse reinforcement. Ichinose et al. (2004) observed that less confinement (concrete cover and/or transverse reinforcement) results in a larger bar size effect. The study also explained that splitting cracks, due to their inherent brittle nature, were the main factor in the size effect. Ichinose et al. (2004) concluded that "bond strength is proportional to about -0.2 to -0.3 power of bar diameter." A possible limitation to the test matrix of the study was lap splice length, as the only investigated value was $\ell_s = 12.6d_b$. The fib Model Code (2010) appears to have

accepted these findings, as the basic bond strength equation is multiplied by bar diameter to the 0.3 power for bars with diameters larger than 1 in. (25 mm).

Hassan, Lucier, and Rizkalla (2012) also reported similar observations. This study used both No. 9 (29 mm) deformed bars and No. 20 (64 mm) threaded bars. Hassan et al. (2012) concluded that ACI 318 design equations provided less conservative estimates of bar stress for large diameter bars. They also described a strong correlation between transverse reinforcement quantity and the apparent effect of size on lap splice strength.

Another feature of bar geometry that impacts bond strength is the size and spacing of bar deformations. A measure of this is called relative rib area (R_r). The relative rib area is a ratio of bearing area of deformations to the shearing area in between as shown in Figure 2.5, which can be simplified to approximately the deformation height, h_r, divided by rib spacing, s_r. Higher relative rib areas tend to increase the effectiveness of confining reinforcement on bond strength (ACI 408R-03).

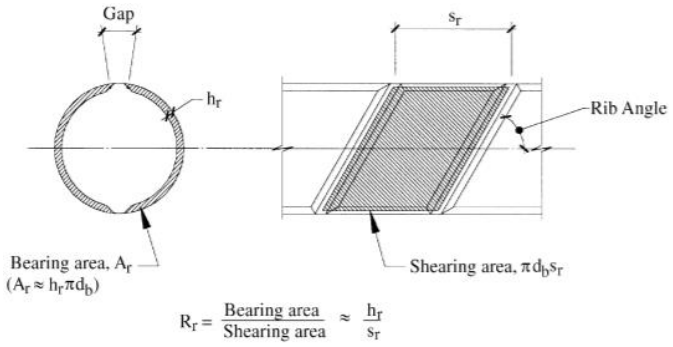

Figure 2.5: Relative Rib Area (ACI 408R-03)

2.2.3 Concrete Compressive Strength

Bond strength increases with concrete compressive strength because higher strength concrete is more resistant to splitting and crushing near the bar deformations. Development and lap-splice lengths have traditionally been calculated as a function of $\sqrt{f'_c}$. These functions apply to reinforcing bars in tension and are accepted for design for $f'_c \leq 10{,}000$ psi (69 MPa). The amount of contribution above this value has

been the subject of many studies. Zuo and Darwin (1998) showed that the average bond strength normalized to $\sqrt{f'_c}$ decreases with an increased concrete strength, and that the rate of decrease is more pronounced as the lap splice length increases. Zuo and Darwin (2000) used statistical analyses of a large database of lap splice test results to show that bond strength is more closely correlated to $f'^{1/4}_c$ than $\sqrt{f'_c}$. ACI Committee 408 recommends using $f'^{1/4}_c$ to represent the concrete contribution to bond strength (see Section 2.4).

2.2.4 Bar Stress

There is a lack of development length and lap splice test data that includes large bar diameters with bond failures above 80 ksi (550 MPa). Most prior tests with bars larger than No. 11 (36 mm) have failed below this threshold value, so there is a need to include tests that reach bar stresses of 100 ksi (690 MPa). Longer lap splice lengths are needed to obtain higher bar stresses. However, evidence shows (refer to Section 2.2.2) that very long lap splices, $\ell_s/d_b > 80$, may not be effective in reaching high stresses, particularly when there is no transverse reinforcement. Some specimens in this study are designed for high stresses.

2.2.5 Other Factors

ACI Committees 318 and 408 address a few other factors that have an impact on bond strength. One is bar casting position. Top-cast bars, defined as having at least 12 in. (300 mm) of concrete below the bars at the time of casting, exhibit lower bond strengths than bottom-cast bars located near the bottom of a beam (Thompson et al., 1979). The negative effect is a result of bleed water migrating upwards and materials like aggregate and cement paste settling downwards while the concrete is placed and consolidated. These effects result in weaker concrete further from the bottom of a concrete placement. For design, a 30% increase of development or lap splice length is recommended in ACI 318 if the longitudinal reinforcement is top cast. Specimens can also be side-cast and thus show bond strengths that vary with depth (Ferguson and Krishnaswamy, 1971).

A reinforcement coating factor is applied in design to epoxy-coated bars. Epoxy coatings are usually applied to prevent corrosion, but they also reduce the surface roughness and available friction and can affect the effective R_r. The use of coatings can decrease bond strength up to 35%, so ACI 318 requires a factor of 1.2 or 1.5, depending on bar spacing, be applied to development and lap splice lengths.

The type of aggregate used also affects bond strength. Lightweight aggregate such as blast furnace slag, pumice rock, or recycled materials are sometimes used to reduce concrete density. These aggregates tend to lower the tensile and compressive strengths of concrete, requiring longer development and lap splice lengths.

2.3 Test and Specimen Setup

Many bond studies have been performed, but only a few test setups provide realistic results. The pullout-test schematic shown in Figure 2.6 has been widely used due to its simplicity, but the results are not representative of conditions in practice because the concrete surrounding the bar is compressed at the support where the bar is being pulled out. This setup provides apparent bond strengths that are much larger than can be achieved using other more realistic test setups. For this reason, ACI 408R-03 recommends that pullout specimens not be used.

Figure 2.6: Pullout test schematic (ACI 408R-03)

In practice, the bar and surrounding concrete are commonly both in tension parallel to the bar axis when the bar is being developed or lap spliced in tension. In this case, the only compression on the deformed bars is mechanical bearing of the concrete on the bar deformations. These boundary conditions are commonly

achieved experimentally using a beam lap-splice specimen, shown schematically in Figure 2.7. Beginning with ACI 318-95, data used as a basis for ACI 318 bond requirements have been obtained from tests of beam lap-splice specimens (ACI 408R-03).

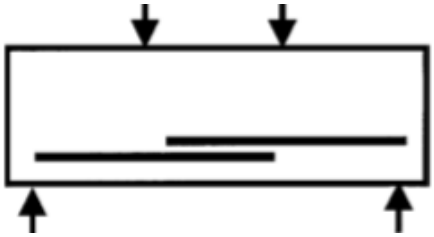

Figure 2.7: Lap splice test schematic (ACI 408R-03)

Dozens of previous studies have used variations of the lap splice test setup, each of which is fundamentally similar to the schematic shown in Figure 2.7. Briggs et al. (2007) reported tests of beam lap-splice specimens to determine relationships between bond characteristics and high steel stresses. Each of the 22 specimens were cast with longitudinal bars on the bottom to avoid top-bar effects. The specimens were then inverted for testing, which allows easy (and safe) access to the concrete faces nearest the lap splice for crack marking and measurement. A photograph of the test setup is shown in Figure 2.8. Steel spreader beams were used to apply force to the ends of the specimen. The spreader beams were loaded through the laboratory strong floor with threaded rods and hydraulic jacks.

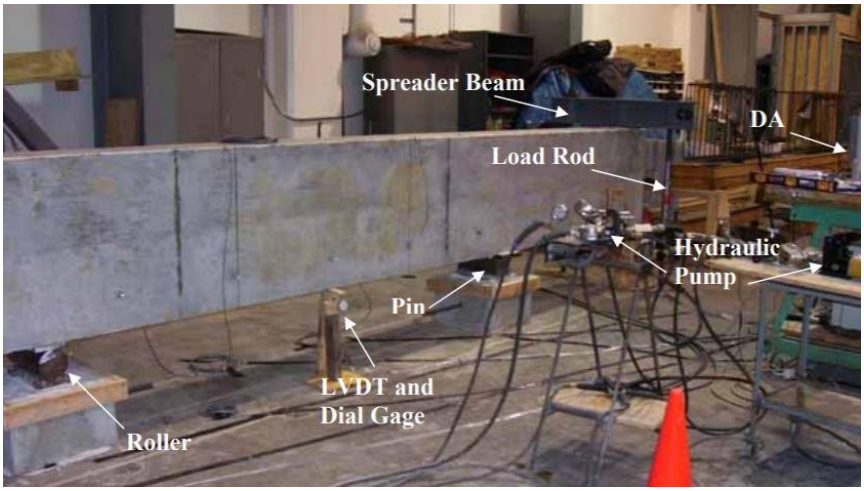

Figure 2.8: Briggs et al. (2007) test setup

Glucksman (2018) also used a four-point bending setup to test beam lap-splice specimens. It was important in this study for the setup to allow free rotation at all points of contact with the beam and free translation at supports. It was also important in design of the setup to locate the pin and roller supports far from the ends of the lap splice. Glucksman states that "supports were placed at least 1.5 times the beam height away from the lap splice ends" because bending stresses will distribute over a distance equal to the beam height.

2.4 Design Recommendations

2.4.1 Equation Development

Expressions for development and lap splice length are empirical and not based on theoretical derivations. Orangun, Jirsa, and Breen (1977) performed statistical analyses to obtain equations for bond strength using results from tests of specimens with and without confinement. These equations were refined by Darwin et al. (1992), Darwin et al. (1996a,b), and Zuo and Darwin (2000) using a larger database of test results and including a wider range of variables. The database developed and used by Zuo and Darwin (2000) was published, with some modifications, by ACI Committee 408 in 2001. This database includes results from several hundred tests of lap-splice specimens. An updated version of this database (ACI Committee 408 2021) will be used herein for some analyses.

Most equations proposed by researchers can be referred to as "descriptive" or "analysis" equations, which are meant to be best fits of a dataset with mean test/calculated results near 1.0. These equations can be very accurate for conditions similar to those represented by the specimens in the database and are useful for research purposes. Design equations used in practice must be straightforward and safe for industry to systematically apply in a wide range of conditions, so simplification of the descriptive equations and application of safety factors is required. Development and lap splice requirements in several consensus documents are described below.

2.4.2 ACI 408R-03

The ACI 408R-03 descriptive equation for total bond force is shown in Equation 2.1. The last term is included only if confinement is present.

$$\frac{T_b}{f'^{1/4}_c} = \frac{T_c + T_s}{f'^{1/4}_c} = \frac{A_b f_s}{f'^{1/4}_c} =$$

$$[59.9\ell_d(c_{min} + 0.5d_b) + 2400A_b]\left[0.1\frac{c_{max}}{c_{min}} + 0.90\right] + \left[30.88t_r t_d \frac{NA_{tr}}{n} + 3\right] f'^{1/2}_c \quad \text{Equation 2.1}$$

Where:

$A_b =$ area of bar being developed or spliced

$A_{tr} =$ total cross sectional area of each stirrup crossing splitting plane

$c_{bc} =$ bottom concrete clear cover to bar being developed

$c_{max} =$ maximum of c_{bc} and c_s

$c_{min} =$ minimum of $c_{so}, c_{bc},$ and $c_{si} + \frac{d_b}{2}$

$c_s =$ minimum of c_{so} and $c_{si} + 0.25$ in. (6 mm)

$c_{si} =$ half of clear bar spacing

$c_{so} =$ side concrete clear cover to bar being developed

$d_b =$ bar diameter

$f'_c =$ concrete compressive strength

$f_s =$ bar stress

$\ell_d =$ development or lap splice length

$n =$ number of bars being developed or lap spliced

$N =$ number of stirrups within the development or lap splice length

$t_d = 0.78d_b + 0.22 =$ effect of bar size on T_s

$t_r = 9.6R_r + 0.28 =$ effect of relative rib area on T_s

$T_b =$ total bond force of a developed or lap − spliced bar

$T_c =$ concrete contribution to total bond force

$T_s =$ transverse steel contribution to total bond force

$R_r =$ relative rib area (see Section 2.2.2)

The following restriction applies to Equation 2.1 because bond strength is not sensitive to transverse reinforcement quantity in addition to that required to prevent splitting failures:

$$\frac{1}{d_b}\left[(c_{min} + 0.5d_b)\left(0.1\frac{c_{max}}{c_{min}} + 0.90\right) + \left(\frac{0.52t_r t_d A_{tr}}{sn}\right) f'^{1/2}_c\right] \leq 4.0 \qquad \text{Equation 2.2}$$

ACI 408R recommends Equation 2.3 for both development and lap splice length calculations in design. The design equation was produced by solving Equation 2.1 for ℓ_d/d_b, substituting f_y for f_s, incorporating a ϕ-factor for safety, and simplifying the equation. Equation 2.4 is a form of Equation 2.3 that is used to calculate bar stress based on a lap splice length, with ℓ_s substituted for ℓ_d, f_{cm} for f'_c, f_s for f_y, and φ set equal to 1.

$$\ell_d = \frac{\left(\frac{f_y}{\varphi f'^{1/4}_c} - 2400\omega\right)\alpha\beta\lambda_{408}}{76.3\left(\frac{c\omega + K_{tr,408}}{d_b}\right)} d_b \geq 12 \text{ in. (300 mm) and } 16d_b \qquad \text{Equation 2.3}$$

$$f_s = \left(\frac{76.3\frac{\ell_s}{d_b}\left(\frac{c\omega + K_{tr,408}}{d_b}\right)}{\alpha\beta\lambda_{408}} + 2400\omega\right) f^{1/4}_{cm} \qquad \text{Equation 2.4}$$

where:

$c = c_{min} + d_b/2$

$d_b =$ bar diameter

$f'_c =$ concrete compressive strength

$f_y =$ yield stress of bar being developed or lap spliced

$K_{tr,408} = \frac{0.52t_r t_d A_{tr}}{sn} f'^{1/2}_c$

$\ell_d =$ development or lap splice length

$s =$ spacing of transverse reinforcement

$\alpha =$ reinforcement location factor (1.3 for more than 12 in. (300 mm) of concrete below bars)

β = reinforcement coating factor (1.2 for epoxy coated bars)

λ_{408} = lightweight aggregate concrete factor (1.3 for lightweight concrete)

φ = capacity reduction factor, to be taken as 0.82 for design.
A value of 1.0 is used herein to obtain a descriptive equation for comparisons with test data.

$$\omega = 0.1\frac{c_{max}}{c_{min}} + 0.9 \leq 1.25$$

ACI 408R-03 recommends using an upper limit of 4 for the confinement term $\left(\frac{c\omega+K_{tr,408}}{d_b}\right)$ instead of the 2.5 value in ACI 318-19, although it is important to note that ACI 408R-03 and ACI 318-19 define cover and confinement terms differently. The ACI 408R-03 recommendation is based on analyses that showed that bond strength is a function of $\left(\frac{c\omega+K_{tr,408}}{d_b}\right)$ for values as large as 5 (Zuo and Darwin, 2000).

2.4.3 ACI 318-19

The ACI 318-19 design equation for calculating development length is shown in Equation 2.5. The expression is a modification of the equation proposed in Orangun, Jirsa, and Breen (1977) with f_y substituted for f_s. An analysis published in ACI 408R-03 showed that this equation is generally conservative except for small bars. ACI 408R-03 recommends use of ψ_s = 1.0 for all bar sizes. Equation 2.6 is a form of Equation 2.5 that is used to calculate bar stress based on a lap splice length, with ℓ_s substituted for ℓ_d, f_{cm} for f'_c, and f_s for f_y.

$$\ell_d = \left(\frac{3}{40}\frac{f_y}{\lambda\sqrt{f'_c}}\frac{\psi_t\psi_e\psi_s\psi_g}{\left(\frac{c_b+K_{tr}}{d_b}\right)}\right)d_b \geq 12 \text{ in. } (300 \text{ mm}) \qquad \text{Equation 2.5}$$

$$f_s = \frac{40\lambda\frac{\ell_s}{d_b}\sqrt{f_{cm}}\left(\frac{c_b+K_{tr}}{d_b}\right)}{3\psi_t\psi_e\psi_s\psi_g} \qquad \text{Equation 2.6}$$

where: c_b= lesser of: (a) the distance from center of a bar or wire to nearest concrete surface, and (b) one-half the center-to-center spacing of bars or wires being developed

d_b = bar diameter

f'_c = concrete compressive strength

f_y = yield stress of bar being developed

$K_{tr} = \frac{40A_{tr}}{sn}$

ℓ_d = development length

s = spacing of transverse reinforcement

λ = lightweight aggregate concrete factor (0.75 for lightweight concrete)

ψ_t = reinforcement location factor (1.3 for more than 12 in. (300 mm) of concrete below bars)

ψ_e = reinforcement coating factor (1.5 or 1.2 for epoxy-coated conditions)

ψ_s = reinforcement size factor (0.8 for No. 6 (19 mm) and smaller bars)

ψ_g = reinforcement grade factor (1.0 for Grade 60 (420), 1.15 for Grade 80 (550), 1.3 for Grade 100(690))

$\left(\frac{c_b+K_{tr}}{d_b}\right) \leq 2.5$

There is a restriction on both the concrete compressive strength and the bar yield stress values for Equations 2.5 and 2.6. Values of $\sqrt{f'_c}$ and f_y are capped at 100 psi [0.69 MPa] and 100,000 psi (690 MPa), respectively. These limits exist due to either limited test data or evidence that Equation 2.5 is unconservative outside these limits. ACI 318-19 also requires that $\ell_s = 1.3\ell_d$ for most cases even though the development length equation is, itself, based on tests of lap splices. The 1.3 factor is intended to provide some measure of ductility and serves as a motivation for designers to stagger lap splice locations. The 1.3 factor might also allow steel reinforcing bars to yield in the case of an overload instead of exhibiting a lap splice failure.

2.4.4 fib Model Code 2010

The fib Model Code equation for development (anchorage) length is provided as Equation 2.7.

$$\ell_b = \frac{\emptyset \sigma_{sd}}{4 f_{bd}} \geq \ell_{b,min} \qquad \text{Equation 2.7}$$

The fib Model Code equation for tension lap splice length is shown in Equation 2.8. Minimum lap splice length requirements are in Equation 2.9. Minimum cover is equal to one bar diameter.

$$\ell_b = \alpha_4 \frac{\emptyset f_{yd}}{4 f_{bd}} \geq \ell_{b,min} \qquad \text{Equation 2.8}$$

$$\ell_{b,min} > \max\left\{0.7 \frac{\emptyset}{4} \frac{f_{yd}}{f_{bd}}; 15\emptyset; 200 \text{ mm}\right\} \qquad \text{Equation 2.9}$$

$$f_{bd} = (\alpha_2 + \alpha_3) f_{bd,0} - \frac{2 p_{tr}}{\gamma_c} < 2.5 f_{bd,0} - \frac{0.4 p_{tr}}{\gamma_c} < \frac{1.5\sqrt{f_{ck}}}{\gamma_c} \qquad \text{Equation 2.10}$$

$$f_{bd,0} > \eta_1 \eta_2 \eta_3 \eta_4 \left(\frac{f_{ck}}{25 \text{ MPa}}\right)^{0.5} \frac{1}{\gamma_c} \qquad \text{Equation 2.11}$$

where: $f_{ck} =$ characteristic concrete compressive strength

$f_{yd} =$ design yield stress of reinforcing bars in tension

$\ell_b =$ design anchorage or lap splice length

$\ell_{b,min} =$ minimum anchorage or lap splice length

$p_{tr} =$ mean compression stress perpendicular to the potential splitting plane

$\alpha_2 =$ factor for confinement from cover (1.0 for cases satisfying minimums)

$\alpha_3 =$ factor for confinement from transverse reinforcement (conservatively 0)

α_4 = reduction factor, may be taken as 0.7 where the calculated stress in reinforcement does not exceed 50% of the characteristic reinforcement strength, or no more than 34% of bars lapped at the section, otherwise = 1.0

γ_c = safety factor

η_1 = bar coating coefficient (1.75 for uncoated and galvanized, 1.4 for epoxy coated)

η_2 = casting position coefficient (1 for good bond conditions defined in Section 6.1.3.2 of fib Model Code)

η_3 = bar size factor (1 for $\emptyset < 1$ in. (25 mm) and (1 in. or 25 mm/$\emptyset$)$^{0.3}$ otherwise)

η_4 = bar grade factor (1.2 for 400 MPa, 1.0 for 500 MPa, 0.85 for 600 MPa, 0.75 for 700 MPa, and 0.68 for 800 MPa, where 1 ksi = 6.895 MPa)

σ_{sd} = steel stress to be anchored by bond over distance ℓ_b

$\emptyset$ = nominal bar diameter

The η_3 factor is particularly relevant to the current study. This factor is proportional to $\emptyset^{-0.3}$ for bars with diameters larger than 1 in. (25 mm). This means that for cases where p_{tr} is zero, f_{bd} and $f_{bd,0}$ are both proportional to $\emptyset^{-0.3}$ (see Equations 2.10 and 2.11). Equation 2.8 shows that ℓ_b is inversely proportional to f_{bd}. So, for cases where p_{tr} is zero and $\emptyset$ is greater than 1 in. (25 mm), use of η_3 is effectively multiplying the equation for ℓ_b (Equation 2.8) by $\emptyset^{0.3}$, resulting ℓ_b being proportional to $\emptyset^{1.3}$.

2.4.5 Other Building Codes

Although not described in detail here, many other building codes have limitations on large-bar tension lap splices similar to the limitations in ACI 318-19. For example, the Korea Concrete Institute building code prohibits tension lap splices of bars larger than No. 11 (36 mm) (S.-C. Chun, personal communication, August 22, 2021). Likewise, the Taiwan Concrete Institute and Japan Concrete Institute building codes also prohibit tension lap splices of bars larger than No. 11 (36 mm) and 1.38 in. (35 mm), respectively (M.-Y. Cheng, personal communication, December 20, 2021).

2.5 Prior Studies of Lap Splices

2.5.1 Large (No. 14 and 18 (43 and 57 mm)) Bars

ACI 318-19 and other standards do not allow tension lap splices of bars larger than No. 11 (36 mm) because of the limited test data available to provide a basis for safe design provisions. Despite the large number of studies on bond and lap splice strength, as evidenced by the ACI 408 Database (2021), the authors are aware of only five prior studies that reported tests of specimens with lap-spliced No. 14 or 18 (43 or 57 mm) bars.

Ferguson and Krishnaswamy (1971) reported results from tests of nineteen specimens containing large bars. However, because the bars were side-cast, it is difficult to draw comparisons with bottom-cast bars to isolate effects of bar size. Specimens with Grade 60 (420) No. 14 (43 mm) lap-spliced bars had concrete compressive strengths of 2.7 to 3.6 ksi (19 to 25 MPa) and were either unconfined or had u-stirrup or spiral confinement. The Grade 60 (420) No. 18 (57 mm) lap-spliced bar specimens had concrete compressive strengths of 2.6 to 4.7 ksi (18 to 32 MPa) and either u-stirrups, spirals, or hairpin confinement. During testing, many specimens failed in flexure, while the remainder failed at the lap splice by “face and side split.” The report recommended that the use of transverse reinforcement be required for large lap-spliced bars. Ferguson and Krishnaswamy concluded with design recommendations and stated that lap splices with No. 14 and 18 (43 and 57 mm) bars should “no longer be prohibited.”

Thompson et al. (1979) reported tests of two specimens with lap-spliced No. 14 (43 mm) bars. They stated that lap splice behavior is important to understand because of a lack of redundancy in structural members that contain lap splices. Wide sections, or wall type specimens, were the research focus in this study. The concrete compressive strength was approximately 3 ksi (20 MPa). The study found that the lap splice provisions in ACI 318 at the time were conservative. Transverse reinforcement was shown to have many different benefits, including minimized crack widths and less brittle failures. The failure pattern described in Thompson et al. (1979) is very similar to the description reported in Orangun, Jirsa, and Breen

(1977): flexural cracks initiated at the lap splice ends and then progressed towards the center of the lap splice as splitting cracks developed parallel to the lap-spliced bars.

Ichinose et al. (2004) reported pullout and lap-splice tests of bars with diameters up to 2 in. (52 mm). Their results demonstrated a clear size effect on bond strength, and that this size effect was most pronounced when conditions favored a splitting failure, such as in specimens with high-relative-rib-area bars and small amounts of transverse reinforcement. The lap splice tests in this study were, however, limited to lengths of 12.6 times the bar diameter, which is lower than the $16d_b$ recommended in ACI 408R-03.

Hassan, Lucier, and Rizkalla (2012) reported results from tests of lap-spliced No. 9 and No. 20 (28 and 63.5 mm) bars. Although the large-diameter bars in this study were threaded, and thus not representative of bars commonly used in practice, they showed that tension lap splices can be effective for large bars. They showed that transverse reinforcement has a more pronounced effect for large-diameter bars than for more conventional bar sizes, and that ACI 318 development length equations are less conservative for large-bars.

Hegger et al. (2015) reported tests of specimens with two different bar sizes larger than No. 11 (36 mm), seven of which are included in the ACI 408 Database (2021). The bars had diameters of 1.58 and 1.97 in. (40 and 50 mm). The specimens reached bar stresses up to 87 ksi (600 MPa) and included lap splice lengths of 23 to 44 times the bar diameter.

Although prior tests of lap-spliced No. 14 and 18 (43 and 57 mm) bars appear to show that such lap splices can be effective, there is a need for more tests of specimens with bottom-cast bars that include a wider range of concrete compressive strengths, steel stresses, lap splice lengths, and amounts of confinement. This study is aimed at better understanding the behavior of large-diameter bar lap splices over a range of variables representative of modern practice.

2.5.2 Recent Studies of Lap Splices

Since ACI 408 published its database of lap splice test results in 2001, there have been several other important studies of lap splices that inform the present work.

The ACI 408 database includes a large number of tests with high strength concrete and normal strength steel, but Seliem et al. (2009) showed that lap splices can be effective for high strength steel bars in normal strength concrete. ASTM A1035 Grade 100 (690) steel reinforcing bars, produced by MMFX, were used in 69 beam lap-splice specimens to evaluate bond behavior of high-strength steel. Lap splices developed bar stresses between 68 and 155 ksi (470 and 1070 MPa) at failure. The report showed that the development length equation in ACI 408R-03 is accurate for both confined and unconfined specimens at high bar stresses. Seliem et al. (2009) also observed that unconfined specimens failed in a highly brittle (explosive) manner. The use of transverse reinforcement resulted in more gradual failures at bar stresses that approached bar yielding of the lap-spliced bars. Based on these results, and the recent addition of high strength steel to ACI 318-19, it is important to examine lap splices of large bars with high strength steel in combination with varying levels of confinement.

Large and high-strength bars may require long lap splices for the lap splice to be effective. It is therefore relevant that Richter (2012) reported results from tests of specimens with long lap splices. Their focus on long lap splices was motivated by the fact that (1) most design provisions are based on tests with specimens containing lap splice lengths shorter than $40d_b$ and (2) failure of long and unconfined lap splices has been observed in practice. Richter tested lap splices under direct tension in concrete prisms and in T-shaped and rectangular beams. Test results showed that strength does not increase proportionally with lap splice length, as discussed in Section 2.2.2 and ACI 408R. Furthermore, the results imply that unconfined lap splices may reach a point where increasing the splice length does not produce any increase in bar stress (Figure 2.9).

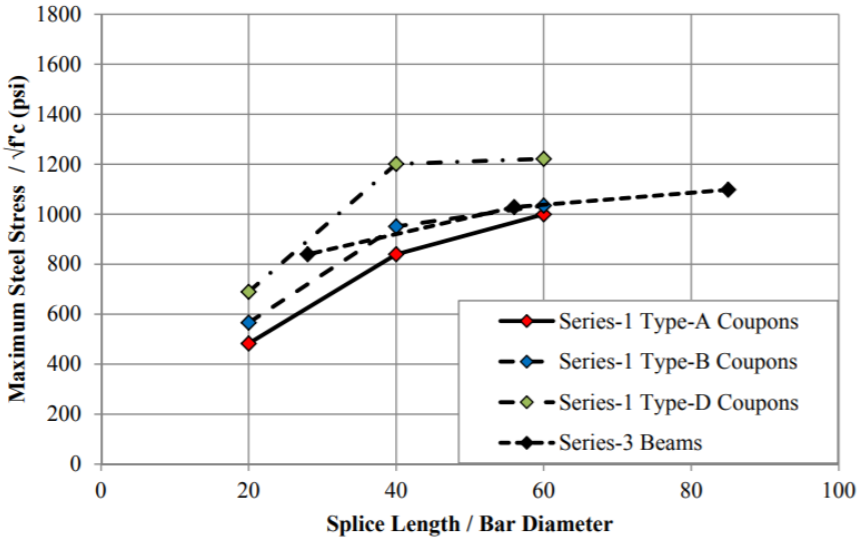

Figure 2.9: Lap splice strength vs. lap splice length (Richter, 2012) (1 psi = 6.895 Pa)

Glucksman (2018) reported results from tests of lap splice specimens with high strength reinforcement and lap splices longer than $40d_b$. Twenty-two beam specimens with No. 8 (25 mm) Grade 100 (690) longitudinal bars and a nominal concrete compressive strength of 5 ksi (34 MPa) were tested. Similar to prior studies, Glucksman (2018) found that lap splice strength is not proportional or linearly related to lap splice length and suggested that lap splice strength is a function of $\ell_s^{0.5}$. Frosch, Fleet, and Glucksman (2020) analyzed results from Glucksman (2018) that focused on very long lap splices of No. 8 (25 mm) bars. They concluded that bar stress at failure increases with lap splice length for unconfined lap splices shorter than $80d_b$, but not for longer lap splices. Glucksman (2018) U-60-5 (ℓ_s/d_b=60) reached a bar stress of 68.4 ksi (472 MPa), U-80-5 (ℓ_s/d_b=80) failed at 102.2 ksi (704.6 MPa), and U-100-5 (ℓ_s/d_b=100) failed at 103.7 ksi (714.9 MPa). Splice strengths increased until near the $80d_b$ lap splice length threshold.

CHAPTER 3 – TEST PROGRAM

3.1 Specimen Design

Eleven large-scale beams with bars lap-spliced at midspan were tested to failure in four-point bending under monotonically increasing force. Generic elevation and section views of the specimens are shown in Figures 3.1 and 3.2 (see Appendix A for specimen-specific figures). Specimen details are listed in Table 3.1.

The specimens were designed to obtain a lap splice failure of the longitudinal bars at midspan. Beam cross-sectional dimensions (18 by 32 in. (460 by 810 mm) for specimens with No. 14 (43 mm) bars and 24 by 36 in. (610 by 910 mm) for specimens with No. 18 (57 mm) bars) were selected to avoid flexural compression damage prior to lap splice failure.

The overall length of each beam was either 25 or 31 ft (7.6 or 9.5 m) and consisted of a support span, two shear regions, and two overhangs (Figure 3.1). The support span length was not less than the lap splice length plus two times the overall beam depth, *h*. This limited localized effects from supports with the lap splice region. Shear region lengths and reinforcement spacing (S2) were designed to preclude shear failures. The overhang length was 24 in. (610 mm) for all specimens and was adequate to prevent longitudinal reinforcement anchorage failures near the beam ends.

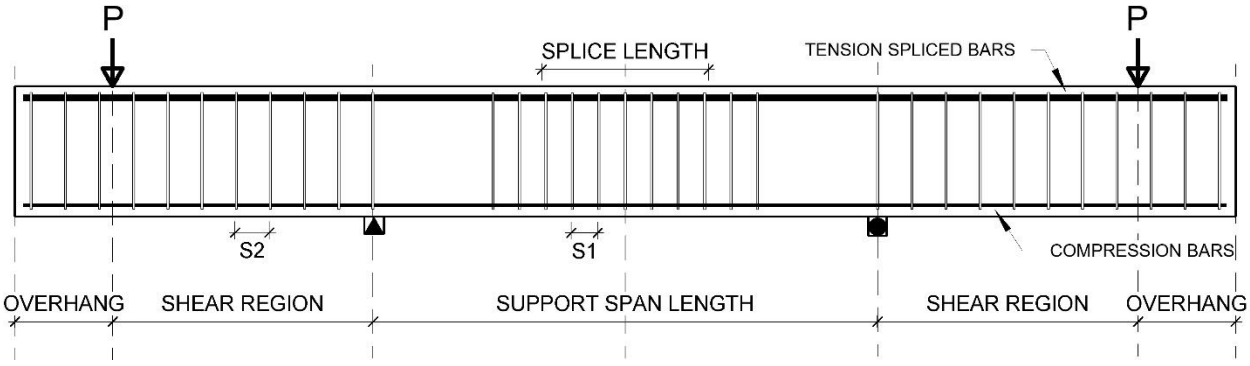

Figure 3.1: General elevation view of a test specimen

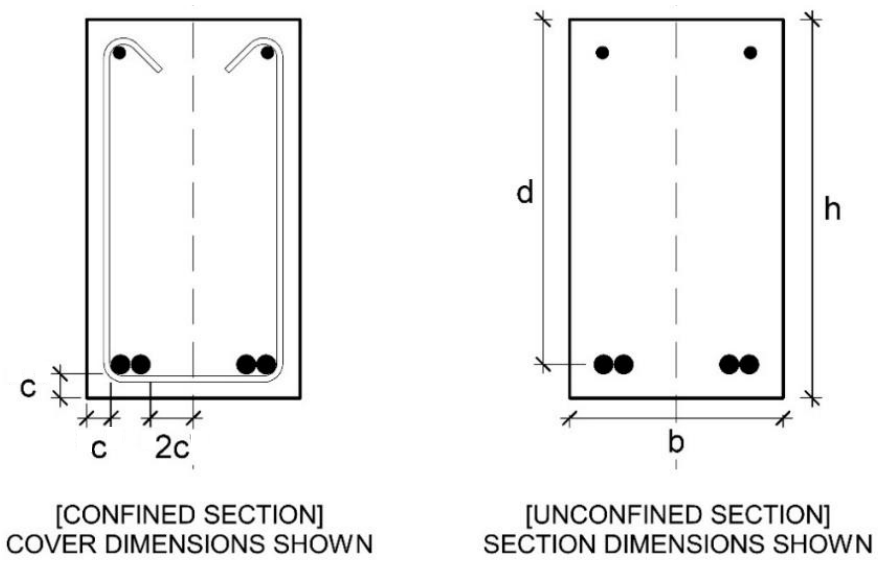

Figure 3.2: General cross sections of the lap splice region

Lap splice lengths (ℓ_s) were selected to obtain a nominal bar stress of either 60 or 100 ksi (420 or 690 MPa) to represent the range of bar stresses used in practice. Grade 80 (550) longitudinal reinforcement was used for the five specimens with No. 14 (43 mm) bars and a target stress of 60 ksi (420 MPa), while Grade 120 (830) longitudinal reinforcement was used for the two No. 14 (43 mm) bar specimens with a target stress of 100 ksi (690 MPa) and all of the specimens with No. 18 (57 mm) bars. None of the specimens exhibited bar yielding before lap splice failure.

Other variables included concrete compressive strength, cover, spacing, and amount of confinement. Nominal concrete compressive strengths of 5 and 10 ksi (34 and 69 MPa) were used. Concrete cover values were set to realistic values to simulate construction methods in the field, but in no case was a clear cover less than one bar diameter used. The No. 14 (43 mm) bar specimens had clear bottom and side cover to the longitudinal bars of 2 in. (51 mm), resulting in nominal cover to the bar center of 2.85 in. (72.4 mm). The No. 18 (57 mm) bar specimens had clear bottom and side cover to the longitudinal bar of 2.5 in. (64 mm), resulting in nominal cover to the bar center of 3.63 in. (92.2 mm). These cover values coincided with standard "chair" dimensions, easing construction, but also resulted in (cover to bar center)/$d_b \approx 1.65$ and

(clear cover to bar)/d_b ≈ 1.15 for all specimens. Conventional U-shaped hooked No. 4 (13 mm) Grade 60 (420) stirrups were used for transverse reinforcement within the lap splice. The spacing of the confinement (S1) was set to obtain K_{tr}/d_b ratios near target values of 0, 0.5, 1.0, or 2.0. A summary of variables is shown in Table 3.2.

Table 3.1: Nominal specimen properties [a]

Specimen ID	h (in.)	d (in.)	b (in.)	ℓ_s (in.)	ℓ_s/d_b	f_s [b] (ksi)	f'_c [b] (ksi)	c [c] (in.)	K_{tr}/d_b (target)	Transv. Bar Size	S1 [d] (in.)	S2 [d] (in.)
14-a	32	29.2	18	61	36	60	5	2	0	No. 4	N/A	8.4
14-b	32	29.2	18	41	24	60	5	2	1	No. 4	6.5	8.4
14-c	32	29.2	18	30	18	60	5	2	2	No. 4	3.3	8.4
14-d	32	29.2	18	47	28	60	10	2	0	No. 4	N/A	13.3
14-e	32	29.2	18	24	14	60	10	2	2	No. 4	4.6	13.3
14-f	32	29.2	18	122	72	100	5	2	0	No. 4	N/A	4.6
14-g	32	29.2	18	61	36	100	5	2	2	No. 4	3.3	4.6
18-a	36	32.4	24	81	36	60	5	2.5	0.5	No. 4	8.0	6.5
18-b	36	32.4	24	63	28	60	5	2.5	2	No. 4	4.0	6.5
18-c	36	32.4	24	54	24	60	10	2.5	0.5	No. 4	8.0	9.4
18-d	36	32.4	24	41	18	60	10	2.5	2	No. 4	4.0	9.4

[a] 1 in. = 25.4 mm, 1 in^2 = 645 mm^2, 1 ksi = 6.9 MPa, 1 psi = 0.0069 MPa, No. 4 = 13 mm bars
[b] f_s = target bar stress at which lap splice failure is nominally expected. Bar yield stresses were always greater than f_s. f'_c = target concrete compressive strength.
[c] Clear cover to longitudinal bar, equals 1.18d_b and 1.11d_b for specimens with No. 14 and 18 (43 and 57 mm) bars. The clear side cover and clear bottom cover equaled c and clear spacing between lapped bars within the lap splice was 4c.
[d] Stirrup spacing within lap-splice (S1) and shear span (S2) (see Figure 3.1)

Table 3.2: Summary of variables of interest

Group #	Specimens	Target Concrete Strength ksi (MPa)	Target Bar Stress ksi (MPa)	Variable K_{tr}/d_b Confinement Range	ℓ_s/d_b (Within Group)
1	14-a, 14-b, 14-c	5 (34)	60 (420)	0, 1.0, 2.0	1.0, 0.7, 0.5
2	14-d, 14-e	10 (69)	60 (420)	0, 2.0	1.0, 0.5
3	14-f, 14-g	5 (34)	100 (690)	0, 2.0	1.0, 0.5
4	18-a, 18-b	5 (34)	60 (420)	0.5, 2.0	1.0, 0.8
5	18-c, 18-d	10 (69)	60 (420)	0.5, 2.0	1.0, 0.8

3.2 Materials

The properties of the steel reinforcement based on the average of two tests of each bar type are reported in Table 3.3. Grade 60 (420) bars were used for all transverse reinforcement in the lap splice regions, with bars from a single heat used throughout the No. 14 (43 mm) bar specimen set and bars from a second heat used throughout the No. 18 (57 mm) bar specimen set. Compression reinforcement consisted of Grade 60 No. 7 or No. 8 (22 or 25 mm) bars. The lap-spliced No. 14 (43 mm) and No. 18 (57 mm) bars were either Grade 80 (550) or 120 (830). The grade of these bars was selected to ensure that lap splice failure occurred at bar stresses below the yield stress based on the 0.2% offset method. Plots of stress versus strain results from tensile tests are in Appendix B.

Table 3.3: Steel reinforcement properties [a]

Bar Size	Grade	Steel Bar Use [b]	Yield Stress [c], ksi (MPa)	Peak Stress, ksi (MPa)	Uniform Elongation [d]	Fracture Stress, ksi (MPa)	Fracture Elongation [e]	Relative Rib Area
No. 4 (13 mm)	60 (420)	T, 14-a to 14-g	62.2 (429)	98.2 (678)	0.120	86.8 (599)	0.164	0.0693
No. 4 (13 mm)	60 (420)	T, 18-a to 18-d	74.0 (511)	91.3 (630)	0.102	73.8 (509)	0.136	0.0695
No. 14 (43 mm)	80 (550)	L, 14-a to 14-e	92.6 (638)	130.3 (898)	0.092	124.1 (856)	0.131	0.0642
No. 14 (43 mm)	120 (830)	L, 14-f to 14-g	134.6 (928)	169.6 (1169)	0.055	128.9 (889)	0.137	0.0843
No. 18 (57 mm)	120 (830)	L, 18-a to 18-d	129.4 (892)	- [f]	- [f]	- [f]	- [f]	0.0626

[a] Tests were conducted in accordance with ASTM A370
[b] T = transverse reinforcement, L = longitudinal (lap-spliced) reinforcement
[c] Determined with 0.2% offset method
[d] Strain at peak stress
[e] Calculated as the strain at fracture minus fracture stress / 29,000 ksi (200 GPa) to approximate the fracture elongation defined in ASTM E8
[f] Test terminated after bar yielding due to limitations of testing apparatus

Concrete was obtained from a local ready-mix plant using the specified mixture proportions in Table 3.4. The specified nominal compressive strength was 5,000 or 10,000 psi (34 or 69 MPa). The concrete contained Type I/II Portland cement, 0.75 in. (19 mm) maximum size crushed limestone aggregate, Kansas

river sand, and a high-range water reducing admixture for the 10,000 psi (69 MPa) mixture. Each beam specimen was placed individually based on the specified mixture proportions.

Table 3.5 shows test-day and 28-day strengths. Test-day concrete compressive strengths ranged from 5,010 to 6,020 psi (34.6 to 41.5 MPa) for specimens with a nominal strength of 5,000 psi (34 MPa) and from 9,610 to 10,920 psi (66.3 to 75.3 MPa) for specimens with a nominal strength of 10,000 psi (69 MPa). Plastic concrete properties are given in Appendix C for each batch.

Table 3.4: Concrete mixture proportions (SSD)

Material	f'_c = 5000 (34)	f'_c = 10000 (69)
Type I/II Cement [a], lb/yd^3 (kg/m^3)	590 (350)	750 (445)
Water [b], lb/yd^3 (kg/m^3)	295 (175)	218 (129)
Crushed EUCA-5 Limestone [c], lb/yd^3 (kg/m^3)	1670 (991)	1957 (1161)
Kansas River Sand [d], lb/yd^3 (kg/m^3)	1395 (828)	1255 (744)
Estimated Air Content, %	1	1
High-Range Water Reducer [e], oz/yd^3 (L/m^3)	-	75 (2.9)
Water-to-Cement Ratio	0.50	0.29

[a] Compliant with ASTM C150 requirements
[b] Compliant with ASTM C1602 requirements
[c] Compliant with ASTM C33 requirements, 0.75 in. (19 mm) maximum size
[d] Compliant with ASTM C33 requirements
[e] ADVA 600, compliant with ASTM C494 Type A and F and ASTM C1017 Type I requirements

Table 3.5: Concrete compressive strengths [a]

Specimen ID	Nominal, f'_c (psi)	Measured, f_{cm} [b] (psi)	Measured, $f_{cm,28}$ [b] (psi)
14-a	5000	6020	6420
14-b	5000	5990	6640
14-c	5000	5920	6480
14-d	10000	9610	9710
14-e	10000	10920	11750
14-f	5000	5540	5900
14-g	5000	5010	5580
18-a	5000	5670	6290
18-b	5000	5410	6230
18-c	10000	9730	10700
18-d	10000	10190	11210

[a] 1 ksi = 6.9 MPa, 1 psi = 0.0069 MPa
[b] Measured from tests following ASTM C39 of 6 by 12 in. (150 by 300 mm) cylinders

3.3 Construction Details

3.3.1 Formwork

All specimens with No. 14 (43 mm) lap-spliced bars used the same set of wooden formwork, while the No. 18 (57 mm) specimens used a separate larger set. The set used for Specimens 14-a through 14-g is shown in Figure 3.3.

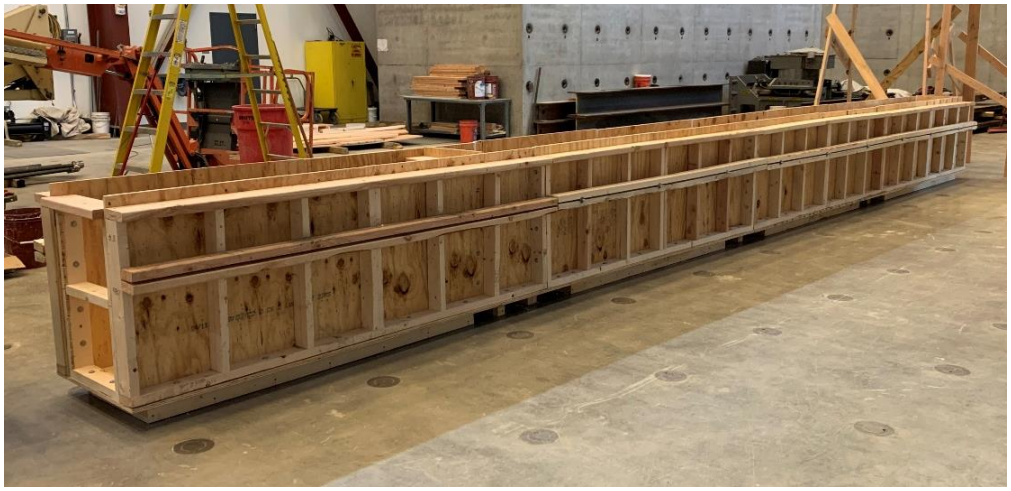

Figure 3.3: No. 14 (43 mm) bar specimen formwork

Beams were cast individually to conserve space and allow each specimen to be tested near its respective target concrete compressive strength. The formwork was constructed using dimension lumber and 3/4 in. (19 mm) thick plywood with sufficient strength and stiffness to maintain its shape during concrete placement. To ensure that the cross section remained at the desired width, 3/8-in. (9.5-mm) diameter steel all-thread rods were used as through-width-ties. The rods passed through the specimen at an elevation that was approximately 1/3 of the beam height from the top surface during casting. These rods were placed at regularly spaced intervals along the beam length and cut flush with the side face after formwork removal. Interior faces of the formwork were coated with clear polyurethane to protect surfaces in contact with concrete and allow reuse of formwork. The exterior faces of the formwork were wrapped in plastic. Caulking was added to seams between adjoining plywood sections and painters' putty was added around

openings where threaded rods and lifting bars protruded through the formwork to prevent moisture loss and seepage. A form oil release agent was added before concrete placement as a final measure to aid formwork removal. Care was taken to ensure no oil landed on the lap-spliced bars.

3.3.2 Reinforcement Assembly

Specimens were fabricated and tested at the West Campus Structural Testing Facility at the University of Kansas. The No. 14 or 18 (43 or 57 mm) lap-spliced longitudinal bars extended up to 2 in. (50 mm) from the beam ends (Figure 3.1) to allow for construction tolerances and ease of placement into formwork. Each specimen also had a pair of No. 7 (22 mm) longitudinal compression bars to support the transverse reinforcement. Shear reinforcement, which was used to prevent failure outside the lap splice region, initiated at the pin and roller support locations and was continued to the ends of the beam. The shear stirrups varied in quantity and spacing by specimen based on the expected shear demand. Figures 3-4 and 3-5 show reinforcement cages after assembly.

Figure 3.4: Reinforcement after assembly (18-a)

Standard wire ties were used to assemble the reinforcement. Bars were cut with a band saw or table saw, dictated by grade of steel and bar diameter. The clean-cut ends of large bars were used within the lap

splice region to maintain consistent bar geometry at points of interest. During construction, the reinforcement was laterally supported using additional inclined bars (Figure 3.4) tied to the transverse reinforcement. These bars were removed before concrete placement if located in or near the center lap splice region. Although adequate length was provided to prevent bond failures at the beam ends, additional anchor bars were also welded perpendicular to and at the ends of the longitudinal bars to ensure adequate bar development. Standard metal bar chairs were used to provide the desired concrete cover and to prevent movement during concrete placement.

Figure 3.5: Heavily confined lap splice (14-g)

The side and bottom cover were measured at several locations along the lap splices after the reinforcement was set in place and secured to the formwork. These measurements were used to identify deviations from target values before concrete placement and are not reported here. The values of concrete cover reported in Chapter 4 were obtained from measurements made after testing.

3.3.3 Concrete Placement and Curing

Beams were cast individually using concrete from a local ready-mix concrete company. All beams had bottom-cast lap splices, as specimens were inverted prior to testing. Photos of specimens before and after concrete placement are shown in Figures 3.6 and 3.7. The concrete was placed in layers using a process

that started at the beam ends, progressed through the middle where the lap splice was located, then ended back at the beam ends. Concrete in the lap splice region was from the middle portion of the overall batch.

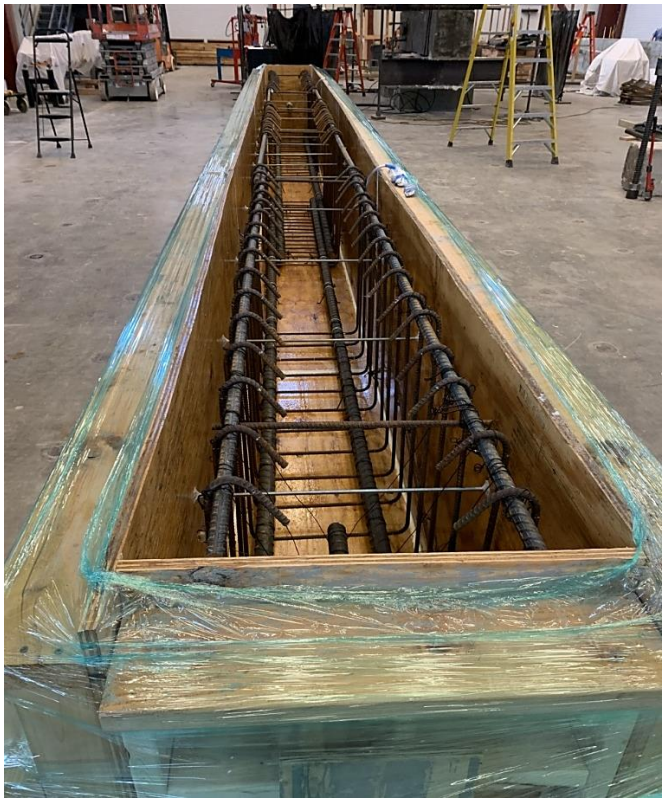

Figure 3.6: Formwork before concrete placement (18-b)

Samples were taken from the middle portion of the batch at regularly spaced intervals in accordance with ASTM C172. This concrete was used for standard tests, including slump, temperature, and unit weight. Both 4 by 8 in. (75 by 150 mm) and 6 by 12 in. (150 by 300 mm) cylinders were cast using steel molds in accordance with ASTM C192. Specimens were cured in the formwork with wet burlap and plastic tarps covering the open faces until the compressive strength was approximately 3,000 psi (21 MPa). Formwork was then removed from the specimen and cylinders were removed from the molds. Cylinders were stored next to the beam specimens while the concrete was dry cured until testing. Two 4 by 8 in. (75 by 150 mm) cylinders were tested every seven days until the concrete reached its target compressive strength, at which point the beam specimen was tested (approximately 14 to 21 days after concrete placement). Three standard

6 by 12 in. (150 by 300 mm) cylinders were then tested in accordance with ASTM C39 and the results are reported as the test-day compressive strength in Table 3.4. Table 3.4 also reports the 28-day compressive strength of each batch.

Figure 3.7: Formwork after concrete placement (14-b)

3.4 Test Setup

Figure 3.8 shows 14-b set up for testing. A reverse four-point bending test setup was used wherein downward force was applied to the beam ends. This produced a condition of zero shear force within the middle portion of the beam span where the lap splices were located. Testing with the tension face upwards also provides easier and safer access for marking cracks during testing. As previously discussed, the specimens were cast with the longitudinal lap-sliced bars at the bottom to avoid top-bar effects. The beam was then rotated about its longitudinal axis and placed upon “pin” and “roller” supports. The “roller” consisted of a 2-in. (51-mm) diameter steel rod placed between steel plates. This rod was free to rotate, thereby allowing free horizontal translation of the beam at this support. Gypsum plaster cement was used between all steel and concrete surfaces.

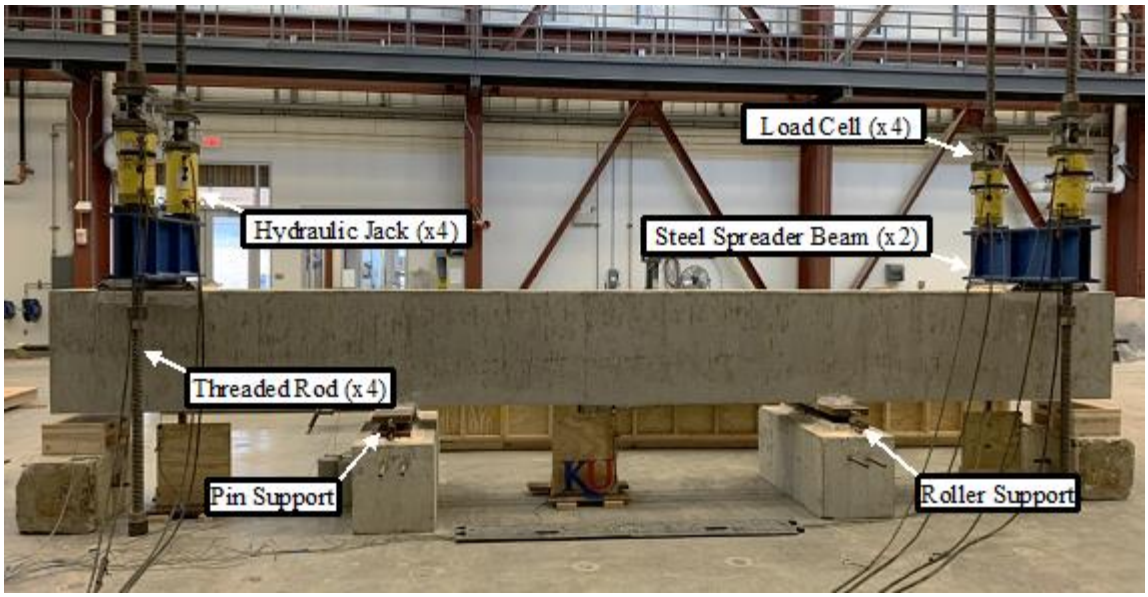

Figure 3.8: Setup prior to testing (14-b)

Force was applied using four hollow-core hydraulic jacks acting on two steel built-up spreader beams in contact with the top face of the beam. Forces from the hydraulic jacks were transmitted to the strong floor by threaded rods with nuts above the setup and below the floor (Figure 3.9). Hollow-core load cells were placed above the hydraulic jacks to measure the imposed force. The steel spreader beams were constructed with C15x33.9 channels welded to 0.5-in. (13-mm) thick top and bottom plates. A 3-in. (76-mm) gap between the channels provided room for threaded rods to pass through the centroid of the member cross-section. To compensate for beam-end rotation during testing, a 4-in. (102-mm) diameter steel half-cylinder was welded to the bottom face of each spreader beam to act as a pin support. When the concrete beam ends deflected downwards, the threaded rods and components stayed vertical.

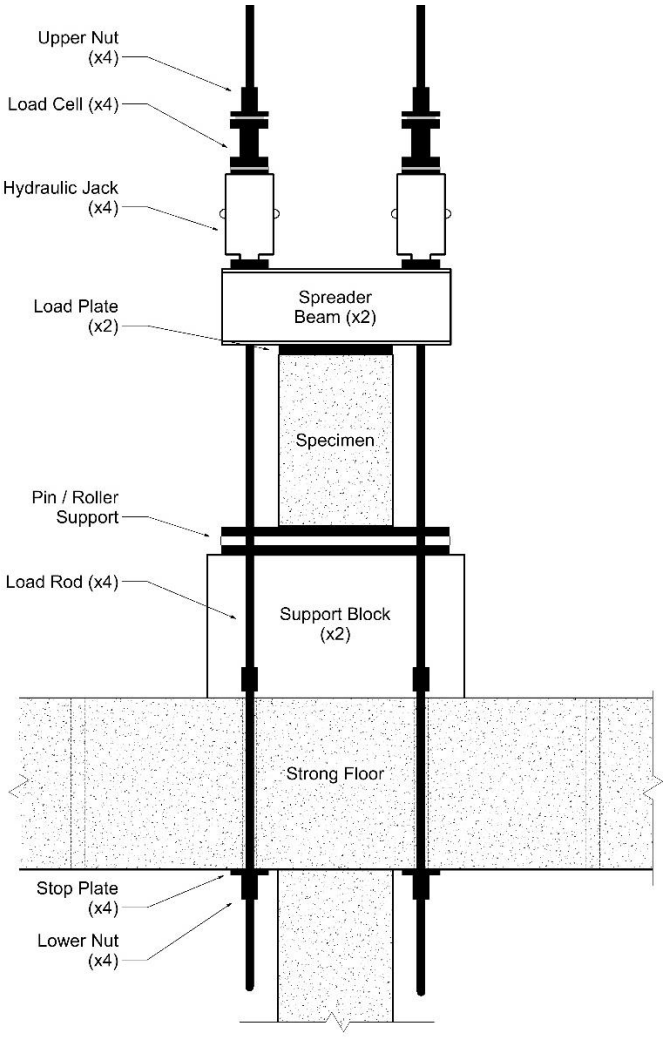

Figure 3.9: End view of test setup

The specimens were loaded using the four hydraulic jacks, high-pressure hoses, and a manual pump. Force was applied at a slow rate until specimen failure, with pauses to allow for marking, measuring, and photographing cracks. Load was paused at half the estimated cracking load and at the estimated cracking load, followed by pauses at forces associated with increments in estimated lap-spliced bar stresses of 10 or 20 ksi (70 or 140 MPa), depending on the final target strength. For example, loading might be paused at loads associated with estimated bar stresses of 20, 30, and 40 ksi (140, 210, and 280 MPa) if the target stress at failure was 60 ksi (420 MPa). The final pause was at 60 to 80% of the expected failure force, at

which point the specimen was covered with a tarp for safety (this tarp contained the debris that can become airborne when a lap splice fails but did not affect test results). In some cases, such as 14-f (see Figure E-6), loose debris remained in-place after tarp removal.

At each load step, the beam sides and the top (tension) face were inspected, and cracks were marked and measured. A crack comparator card was used and the largest crack at each load step within or near the lap splice region was recorded. Photographs of the marked cracks were taken during each pause and after failure. Load increments took approximately 5 minutes, while each pause took approximately 10 minutes.

3.5 Instrumentation

Hydraulic pressure was recorded using an electronic pressure gauge. Force applied by each jack was measured using load cells (Figures 3.8 and 3.9).

Bar strains were measured using four 120-ohm strain gauges with a gauge length of 5 mm applied to the lap-spliced bars in each specimen. Each of the four strain gauges (for all 11 specimens) were located just outside the splice region, or a nominal distance of 1¾ to 2¾ in. (44 - 70 mm) from the splice ends (Figure 3.10). Strain gauges were located underneath the longitudinal bars and protected by multiple coating layers during concrete placement. Although bar force at failure was inferred from the beam moment (see Table 4.2), results from these gauges provide a secondary basis for estimating bar force at failure.

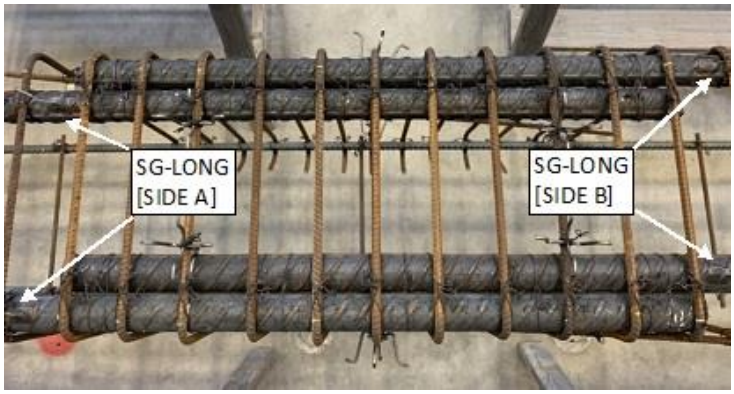

Figure 3.10: Strain gauge placement

In addition, 18-c and 18-d had strain gauges on the transverse reinforcement within the lap splice. Specimen 18-c was instrumented with four additional gauges and 18-d had six additional gauges (Figure 3.11).

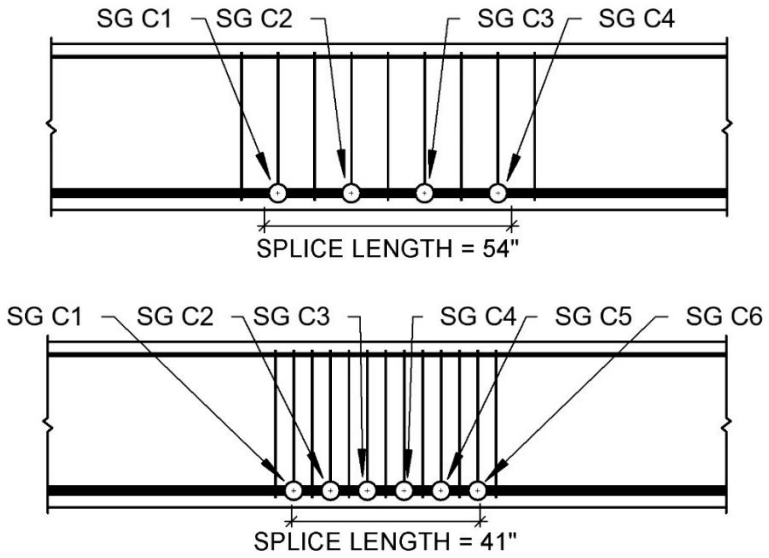

Figure 3.11: Additional strain gauge locations on transverse reinforcement for 18-c (top) and 18-d (bottom) (1 in. = 25.4 mm)

Vertical beam displacements were recorded using three potentiometers. Potentiometer #2 was located below the beam at midspan, while potentiometers Potentiometers #1 and #3 were under the loading points near the beam ends (Figure 3.12). Beam deflection was taken as the difference between the mid-span (upward) displacement and the average of the (downward) displacements measured under the loading points.

An optical tracking system was used during the tests of 18-c and 18-d that allowed for measurement in three-dimensional space of the positions of multiple markers fixed to the surface of the specimens. Figures 3.12 and 3.13 show the locations of the markers used for 18-c and 18-d, respectively. Seven columns of two markers each were attached to one face of each specimen at selected points of interest that included outside the lap splice ends, inside the lap splice ends, beam centerline, support location, and loading point.

Among other things, these data can be analyzed to determine the relative rotation between vertical sections along the beam length, as described in Section 4.5.

One data acquisition system was used for the pressure gauge, load cells, strain gauges, and potentiometers. A separate data acquisition system was used for the optical tracking system. These data were combined after testing using a common event, such as failure, to synchronize the recorded data.

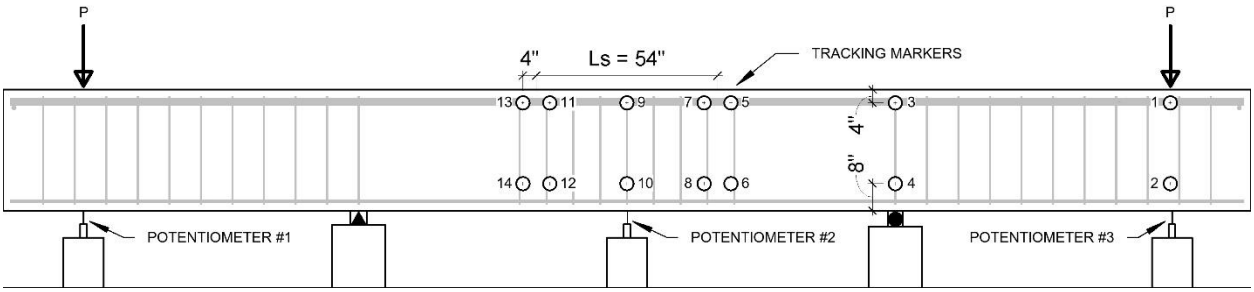

Figure 3.12: Displacement instrumentation: 18-c (1 in. = 25.4 mm)

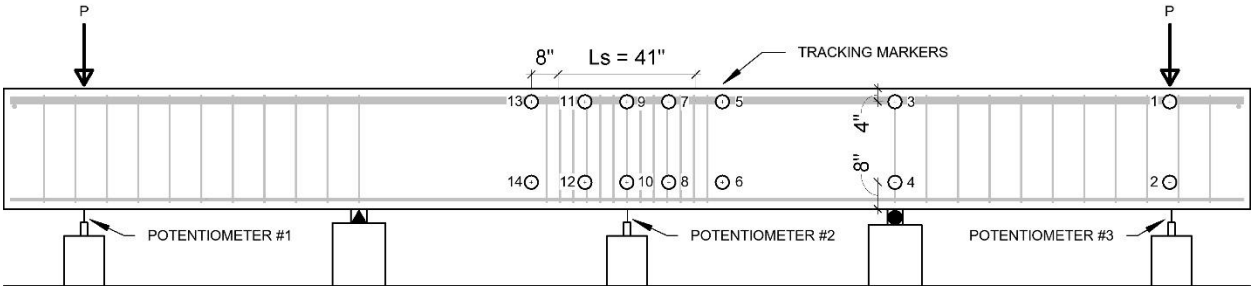

Figure 3.13: Displacement instrumentation: 18-d (1 in. = 25.4 mm)

CHAPTER 4 – ANALYSIS

4.1 Load-Deflection Results

The applied load versus midspan deflection results had similar characteristics in all tests. Sample plots are shown in Figure 4.1. Plots for all specimens are included in Appendix D. The applied load is the sum of the recorded forces in the four individual load cells, and the deflection is the vertical displacement of midspan minus the average vertical displacement at the supports (Section 3.5). The specimen self-weight and test frame weight are not included in the applied load versus deflection plots.

The general response shows an initial linear-elastic region that continues until beam cracking, followed by a change in slope of the plotted data. After cracking, changes in applied load and deflection were approximately linearly related. In specimens with no confinement (Figure 4.1(a)), lap splice failure occurred suddenly and with no apparent reduction in stiffness prior to failure. Specimens with confinement exhibited some minor softening prior to lap splice failure (Figure 4.1(b)) that was not a result of reinforcement yielding (Section 4.3). This softening may be a result of bar slip within the lap splice prior to lap splice failure. Load step pauses are also visible as drops in both load and deflection.

The maximum applied load and deflection values at failure are shown in Table 4.1. Specimens 14-f and 14-g, which nominally targeted bar stresses of 100 ksi (690 MPa), showed the largest deflections.

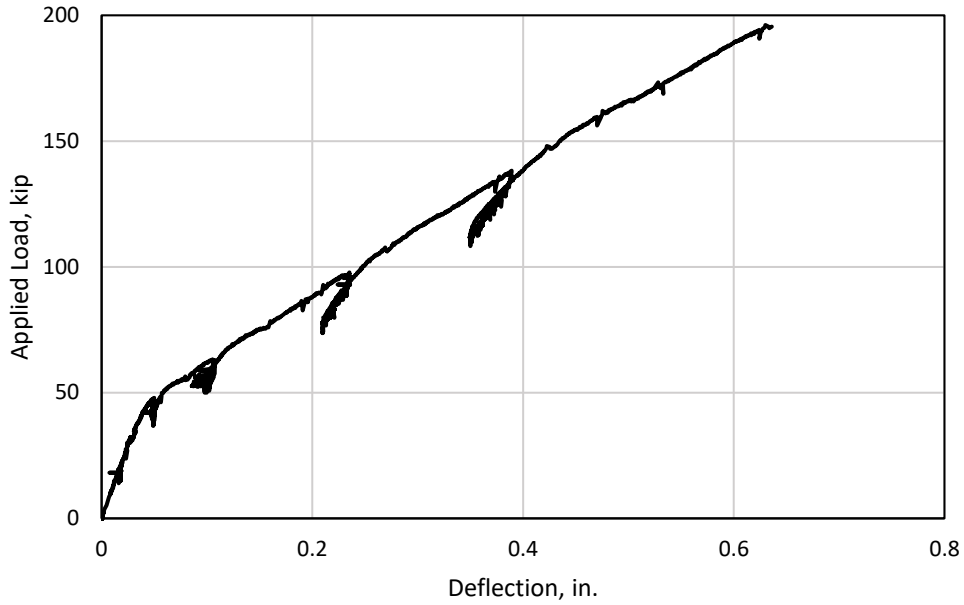

(a)

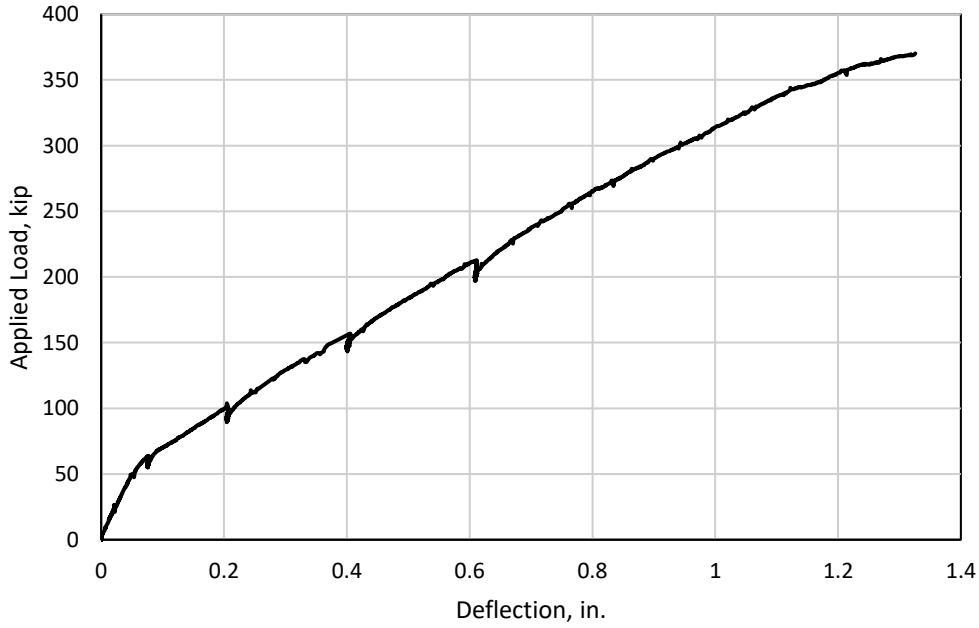

(b)

Figure 4.1: Sample load-deflection behavior: (a) 14-a and (b) 18-a (1 kip = 4.448 kN, 1 in. = 25.4 mm)

Table 4.1: Maximum applied load and deflection at failure

Specimen ID	Maximum Applied Load kips (kN)	Maximum Deflection in. (mm)
14-a	196 (872)	0.64 (16.3)
14-b	200 (890)	0.81 (20.6)
14-c	218 (970)	0.89 (22.6)
14-d	190 (845)	0.57 (14.5)
14-e	196 (872)	0.72 (18.3)
14-f	247 (1099)	1.38 (35.1)
14-g	395 (1757)	1.69 (42.9)
18-a	370 (1646)	1.33 (33.8)
18-b	361 (1606)	1.28 (32.5)
18-c	347 (1544)	1.19 (30.2)
18-d	355 (1579)	1.18 (30.0)

4.2 Cracking Behavior

4.2.1 Description of Cracking and Lap Splice Failure

Photos of all specimens after failure are in Appendix E. All specimens failed by splitting/spalling along the lap splice before yielding of the bars (Section 4.3). Most specimens with unconfined lap splices failed explosively whereas specimens with confined lap splices failed more gradually.

Each test had load pauses for marking crack locations and measuring crack widths. Figures 4.2 and 4.3 show specimens with confined lap splices, and Figure 4.4 shows a specimen with unconfined lap splices. Cracking was largely similar across all specimens, but there were specific differences between specimens with confined and unconfined lap splices. The first observed cracks initiated at or near the ends of the lap splices. Cracks then propagated vertically down the beam sides and across the tension (top) face as the load increased. For confined lap splices, cracks were commonly observed at locations where transverse reinforcement was present, as shown in Figure 4.2. For unconfined specimens, there was relatively less cracking along the lap splice length until failure (Figure 4.4b). Flexural-tension cracks (transverse to the beam axis) were the predominant crack type throughout most of the tests. Splitting cracks were also observed on the tension face parallel to the longitudinal reinforcement (Figure 4.5). At failure, specimens with confined lap splices usually exhibited spalling of the cover (Figure 4.3c). Specimens with unconfined

lap splices exhibited extensive spalling along with wide cracks at the lap splice ends perpendicular to the beam axis at failure (Figures 4.4c and 4.6). Specimen 14-f appears in the photo (see Figure E-6) to be an exception to this, but the concrete surrounding the lap splices was loose after testing and happened to be held in place by the tarp.

Figure 4.2: Cracking along transverse reinforcement on tension face (14-b)

(a) Initial cracking

(b) Cracking during increased loading

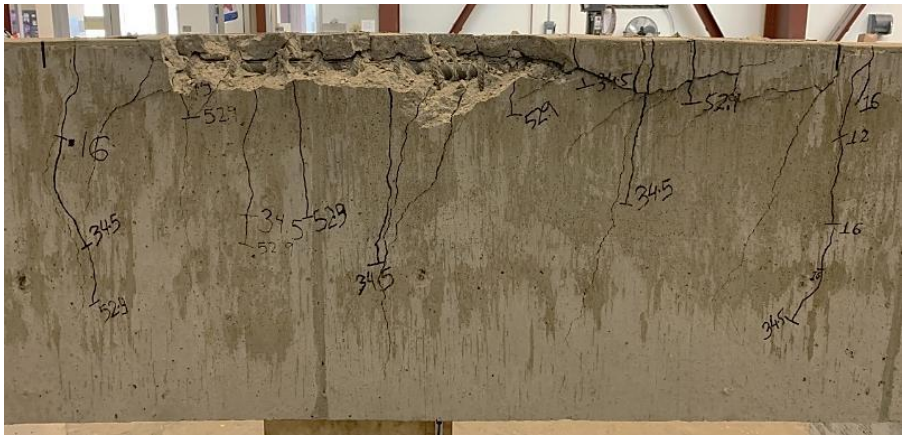

(c) After failure

Figure 4.3: Photos of 14-g (heavily confined) during testing

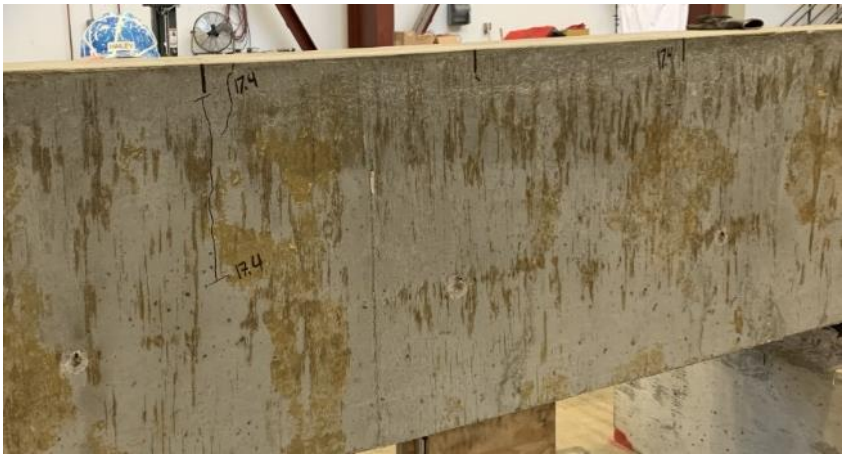

(a) Initial cracking

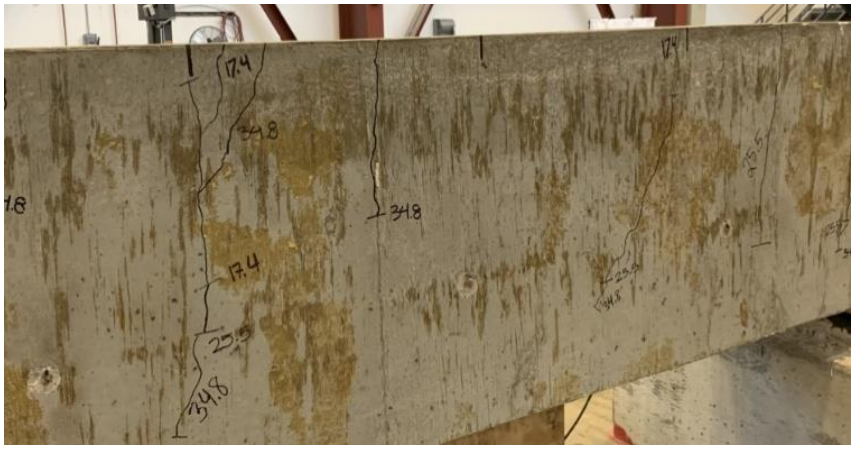

(b) Cracking during increased loading

(c) After failure

Figure 4.4: Photos of 14-d (unconfined) during testing

Figure 4.5: Longitudinal splitting cracks (14-f)

Figure 4.6: Unconfined lap splice failure (14-a)

4.2.2 Crack Widths

Crack widths were manually measured during each test when the loading was paused (Section 3.4). Figures 4.7 and 4.8 show the largest crack width measured at each pause in loading for specimens with No. 14 and 18 (43 and 57 mm) lap-spliced bars, respectively, plotted versus estimated longitudinal bar stress. Values for bar stress in Figures 4.7 and 4.8 were estimated based on nominal section properties and concrete compressive strength measured on the day of testing. Bar stresses include the effects of the applied loads,

weight of the test frame, and specimen self-weight. More detail about the calculation is provided in Section 4.4. Generally, the widest cracks were the vertical cracks occurring at the ends of the lap splice.

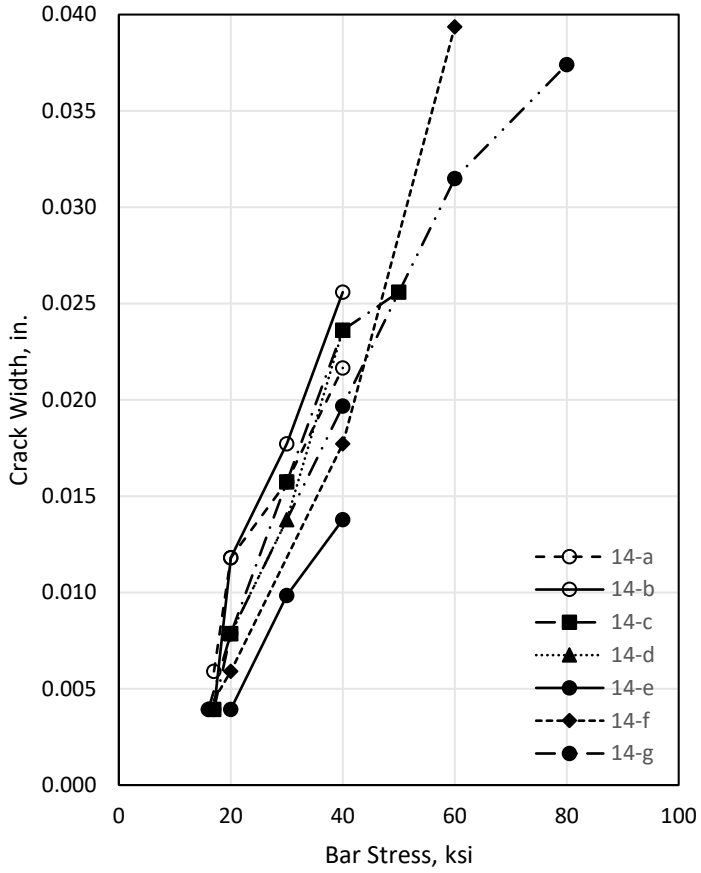

Figure 4.7: Crack width versus bar stress for specimens with No. 14 (43 mm) bars (1 in. = 25.4 mm, 1 ksi = 6.895 MPa)

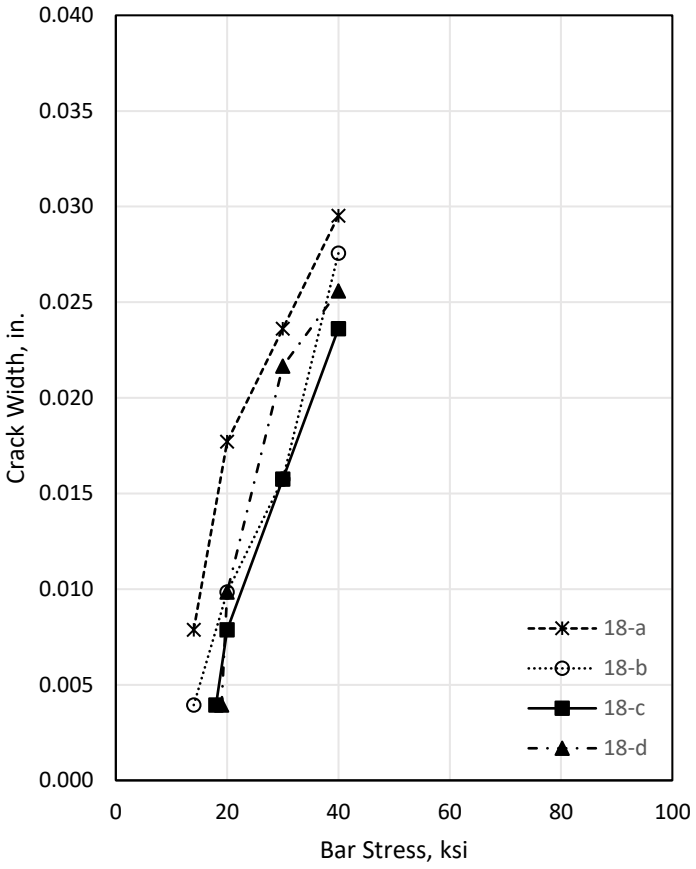

Figure 4.8: Crack width versus bar stress for specimens with No. 18 (57 mm) bars (1 in. = 25.4 mm, 1 ksi = 6.895 MPa)

As the load increased, so did the bar stress and crack widths. Specimens 14-f and 14-g, shown in Figure 4.7, follow the trends of the specimens designed to reach 60 ksi (420 MPa), but eventually reached higher bar stresses and, thus, larger crack widths. Specimens with the same nominal dimensions and reinforcement areas, therefore, exhibited similar crack widths at a bar stress of 40 ksi (280 MPa) regardless of the target stress, as expected. Specimens targeting a bar stress near 100 ksi (690 MPa) had much larger crack widths at bar stresses near 2/3 of the target stress than specimens targeting bar stresses near 60 ksi (420 MPa). Plots of crack width versus bar stress in terms of a percentage of measured stress are shown in Appendix E.

Specimens with No. 14 and 18 (43 and 57 mm) bars showed similar trends. However, at a given bar stress, specimens with No. 18 (57 mm) bars had larger crack widths. At a load step correlating to

approximately 40 ksi (280 MPa) of bar stress, the specimens with No. 14 (43 mm) bars had an average maximum crack width of 0.021 in. (0.533 mm) and the specimens with No. 18 (57 mm) bars had an average maximum crack width of 0.027 in. (0.686 mm). These differences are statistically significant based on a two-tailed Student's t-test assuming equal variances, with $p = 0.03$, where p values less than 0.05 are interpreted as evidence of statistical significance. No other trends between crack width and other variables of interest (concrete compressive strength, amount of confinement, etc.) were observed. All maximum crack width data collected are also provided in Appendix E.

4.3 Measured Strains

The specimens had strain gauges on the longitudinal bars near the ends of the lap splices and two specimens had strain gauges on transverse reinforcement within the lap splice (Section 3.5). Plots of measured strain versus time for each specimen are in Appendix F, along with a tabulated summary of bar stress at failure inferred from the strain gauge measurements.

Figure 4.9 shows longitudinal reinforcement strain versus time for 14-b. In general, the strains from all the gauges followed the same trend: strain increased with load, which increased with time except for the pauses in loading. However, a closer look shows differences. It appears that bar strains increased until failure at two of the gauges, whereas data from two of the gauges exhibited slight declines in strain shortly before failure. Interestingly, the gauges that showed declines were A-2 and B-2, located at each end of the splice on beam face 2. A possible explanation is that the lap splice on beam face 2 started to slip and shed force while the lap splice on beam face 1 continued to attract force as beam load increased. This implies that the lap splices did not fail simultaneously; rather, one lap splice started to slip and shed force to other lap splices until the group of lap splices could not take additional load. The plots in Appendix F show that this behavior is evident in several specimens with transverse reinforcement but not for specimens without transverse reinforcement. Transverse reinforcement, therefore, appears to facilitate sharing of force among lap splices.

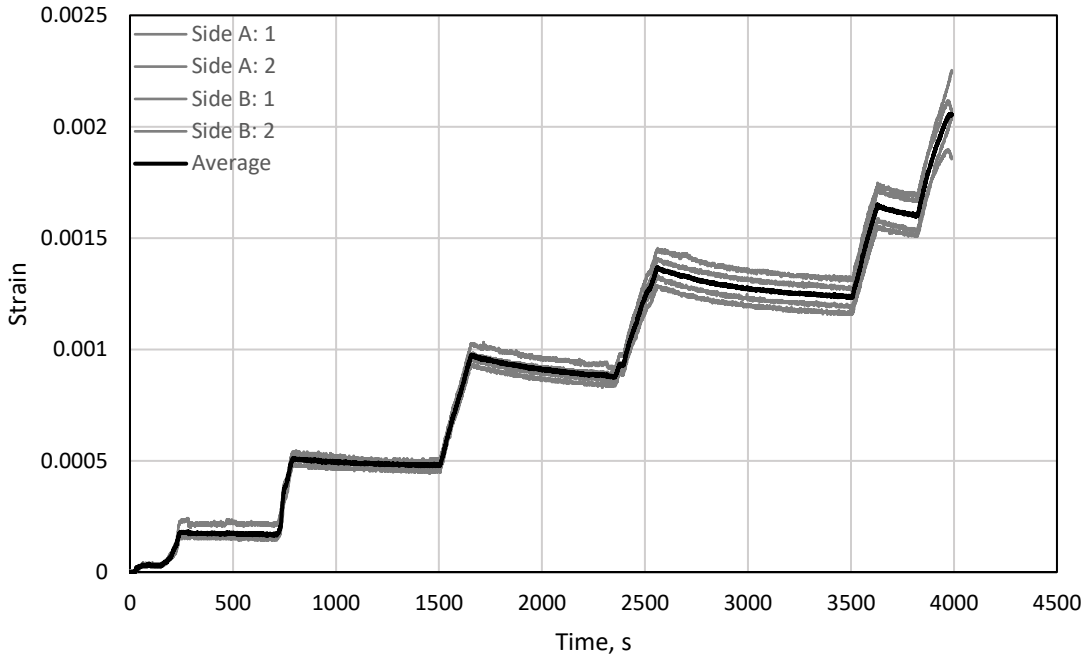

Figure 4.9: Longitudinal bar strain for 14-b

Figure 4.9 also shows that the largest recorded strain (0.00216 for 14-b) was smaller than the strain associated with yielding, which is 0.0032 based on the measured yield stress in Table 3.3, an assumed modulus of 29000 ksi (200 GPa), and assuming zero bar strain at the start of the test. This was the case for all specimens; there is no evidence of longitudinal bar yielding in these tests.

Figure 4.10 shows a plot of the transverse reinforcement strain versus time for 18-d. The figure shows that the transverse reinforcement strains were much smaller than the longitudinal (lap-spliced) bar strains, and certainly much smaller than strains associated with transverse bar yielding (the strain at yield is approximately 0.00255 based on Table 3.3, an assumed modulus of 29,000 ksi (200 GPa), and assuming zero bar strain at the start of the test). It has been previously observed that transverse reinforcement confining a tension lap splice in a constant moment region does not yield (ACI 408R-03). The data in Figure 4.10 imply that this finding applies even to specimens with high strength concrete and large (No. 18, 57 mm) bars, which have large bar deformations that might be expected to induce wider splitting cracks.

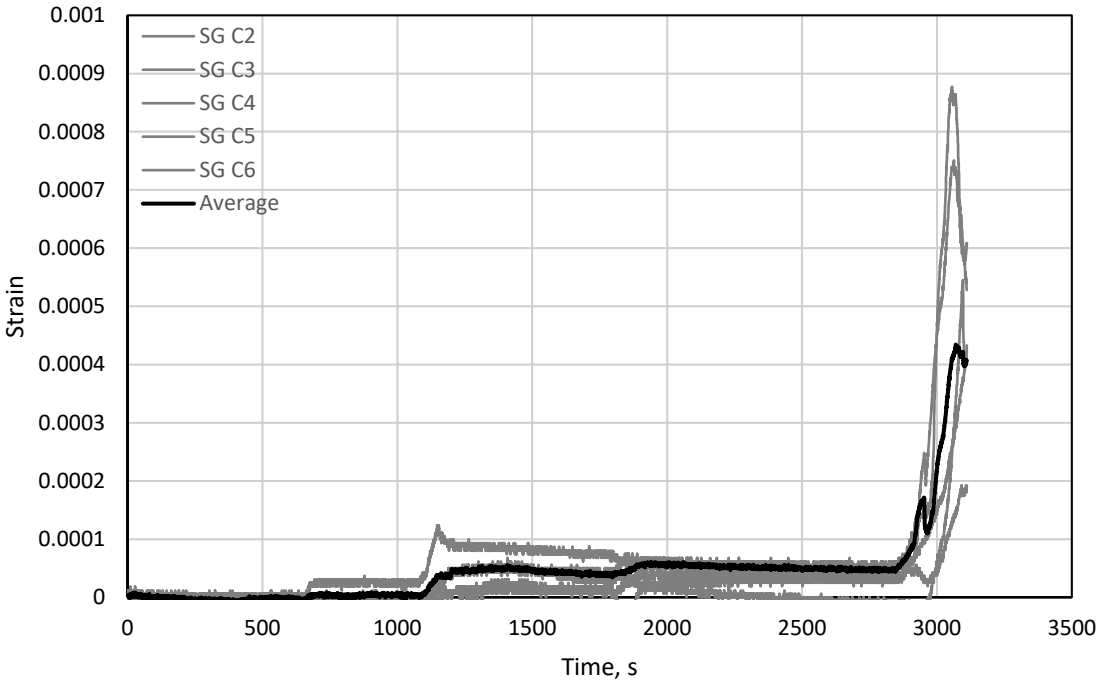

Figure 4.10: Transverse reinforcement strain for 18-d (SG C1 not recorded)

The two gauges that recorded the largest transverse reinforcement strains in 18-d were C2 and C5, which were located on transverse reinforcement 8.5 in. (220 mm) from the ends of the lap splice. It was expected that transverse reinforcement near the splice ends would be more highly stressed than transverse reinforcement near mid-splice because the longitudinal bar stresses and slip are largest near the lap splice ends. It is not clear why C6, located on the stirrup at the end of the lap splice, recorded much smaller strains than C2 or C5.

4.4 Bar Stress Calculations

The stress at failure in the lap-spliced bars was estimated for each specimen. The results are shown in Table 4.2. These bar stresses are based on the beam moment at the center of the lap splice (midspan), which was calculated based on the applied loads, test frame weight, and specimen self-weight. The stress in the longitudinal bars was estimated from the midspan moment using a moment-curvature analysis, assuming a concrete stress-strain relationship consisting of a parabola up to peak stress and a linear descending branch

from Hognestad (1951) (Equation 4.1). The peak stress was taken equal to the measured concrete compressive strength on the day of testing and the strain at peak stress, ε_o, was from the plots of experimental data shown in Darwin and Dolan (2021). The concrete stress is shown as f_c and the strain is ε_c.

$$f_c = f_{cm}\left[\frac{2\varepsilon_c}{\varepsilon_o} - \left(\frac{\varepsilon_c}{\varepsilon_o}\right)^2\right] \text{ for } \varepsilon_c \le \varepsilon_o \qquad \text{Equation 4.1a}$$

$$f_c = f_{cm}\left[1 + \frac{0.15}{0.0038 - \varepsilon_o}(\varepsilon_o - \varepsilon_c)\right] \text{ for } \varepsilon_c > \varepsilon_o \qquad \text{Equation 4.1b}$$

The steel stress-strain curves were determined through tensile tests and sample plots are included in Appendix B. The constitutive relationships used for the steel were proportional for Grade 80 (550) bars up to the yield strain. An exponential best-fit was used to represent the relationships for the Grade 120 (830) bars based on Seliem et al. (2009). Following a similar equation form, the following two exponential best-fit equations were used for the Grade 120 (830) bars used in this study: $f_s = 162(1 - e^{-212\varepsilon_s})$ for No. 14 (43 mm) bars and $f_s = 200(1 - e^{-175\varepsilon_s})$ for No. 18 (57 mm) bars. This process was the same as described in ACI Committee 408R-03. The stresses estimated in this manner are within 9% of the bar stress values estimated based on strain gauges for all specimens except for 14-e (Appendix F).

Table 4.2 shows the bar stresses obtained from test results and bar stresses calculated based on ACI 408R-03 (Equation 2.4) and ACI 318-19 (Equation 2.6). The ACI 408R-03 descriptive equation is intended to be a best fit of the available data, whereas the ACI 318-19 design equation is necessarily more conservative for use in design. For Equation 2.4, $(c\omega + K_{tr,408})/d_b$ was taken as not greater than 4 as recommended in ACI 408R-03. Table 4.2 shows calculated bar stresses from Equation 2.6 with $(c_b + K_{tr})/d_b$ taken as either not greater than 2.5 or not greater than 4. The 2.5 limit is from ACI 318-19, but increasing the limit to 4, like Equation 2.4, provides a better fit to the experimental data in this study (COV of 0.13 compared with 0.20 in Table 4.2). This is examined further in Section 4.4.1.

Table 4.2: Bar stresses at failure [a, b]

Spec. ID	Beam Moment at Lap-Splice Center, kip-in.	f_s [c] Bar Stress at Failure, ksi	Calculated Bar Stress [d]					
			ACI 408R-03 [e], ksi	Test/ Calc.	ACI 318-19 [f], ksi $\left(\frac{c_b+K_{tr}}{d_b}\right) \leq 4.0$	Test/ Calc.	ACI 318-19 [f], ksi $\left(\frac{c_b+K_{tr}}{d_b}\right) \leq 2.5$	Test/ Calc.
14-a	6,440	53.8	63.0	0.85	62.3	0.86	62.3	0.86
14-b	6,570	54.9	65.2	0.84	60.1	0.91	60.1	0.91
14-c	7,160	60.2	66.1	0.91	57.7	1.04	46.2	1.30
14-d	6,270	52.0	58.6	0.89	58.1	0.90	58.1	0.90
14-e	6,440	53.4	64.6	0.83	50.3	1.06	46.7	1.14
14-f	8,660	73.2	102.4	0.71	95.3	0.77	95.3	0.77
14-g	12,760	109.3	111.8	0.98	88.5	1.23	75.9	1.44
18-a	15,540	67.0	76.7	0.87	67.3	1.00	67.3	1.00
18-b	15,340	66.6	77.7	0.86	65.4	1.02	65.4	1.02
18-c	14,590	61.4	71.8	0.86	63.4	0.97	63.4	0.97
18-d	14,930	62.9	74.4	0.85	58.1	1.08	58.1	1.08
			Mean:	0.86	Mean:	0.99	Mean:	1.04
			Coefficient of Variation:	0.07	Coefficient of Variation:	0.13	Coefficient of Variation:	0.20

[a] 1 ksi = 6.9 MPa

[b] 1 kip-in. = 0.113 kN-m

[c] Obtained from beam moment at failure using moment-curvature analysis per Section 4.4

[d] Minimum lap splice length requirements are neglected

[e] Equation 2.4

[f] Equation 2.6 with $\psi_g \geq \left[\left(1 + 0.15\frac{(f_s - 60\text{ ksi})}{20\text{ ksi}}\right), 1.0\right]$ or $\left[\left(1 + 0.15\frac{(f_s - 410\text{ MPa})}{140\text{ MPa}}\right), 1.0\right]$ and $\sqrt{f'_c} \leq 100$ psi (0.690 MPa)

Table 4.2 shows ratios of test/calculated (T/C) bar stresses. Equation 2.4, based on ACI 408R-03, provided the best fit of the data in terms of scatter, with a coefficient of variation (COV) of 0.07 compared with COVs of 0.13 and 0.20 for Equation 2.6 (based on ACI 318-19). Table 4.2 shows that 14-f had a very low test/calculated bar stress ratio, regardless of which equation was used to calculate bar stress. This outlier will be discussed further in Section 4.4.2.

The T/C values in Table 4.2 were also frequently less than 1.0. All T/C values were less than 1.0 for Equation 2.4, with a mean of 0.86, and 5 of the 11 specimens had T/C less than 1.0 based on Equation 2.6 and $(c_b + K_{tr})/d_b \leq 2.5$. This indicates that current ACI 318 design provisions are not safe for use in

design of large-bar lap splices without modification. Bar size effects are examined further in Sections 4.4.3 and 4.4.4.

4.4.1 ACI 318-19 Limit on $(c_b + K_{tr})/d_b$

The ACI 408 Database (2021) was used to further investigate the effect of increasing the limit on $(c_b + K_{tr})/d_b$ in Equations 2.5 and 2.6. For this comparison, all bottom-cast lap-splice specimens in the ACI 408 database were included, except for those with a lap splice length less than 12 in. (300 mm). Here Equation 2.6 is used with $\psi_g \geq \left[\left(1 + 0.15\frac{(f_s - 60\text{ ksi})}{20\text{ ksi}}\right), 1.0\right]$ or $\left[\left(1 + 0.15\frac{(f_s - 410\text{ MPa})}{140\text{ MPa}}\right), 1.0\right]$, $\sqrt{f'_c} \leq 100$ psi (0.690 MPa), and $\psi_s = 1.0$ for all bar sizes as recommended in ACI 408R-03.

Figure 4.11a shows calculated bar stress at failure from Equation 2.6 versus bar stress at failure from tests. There is no limit applied to the $(c_b + K_{tr})/d_b$ term in this plot. The black dashed trendline is based on specimens with $2.5 \leq (c_b + K_{tr})/d_b \leq 4$ and the solid grey trendline is based on those with $(c_b + K_{tr})/d_b < 2.5$. These two lines have similar slopes in Figure 4.11a. The slopes of the trendlines, which were forced to intersect the origin, were 1.14 for data with $2.5 \leq (c_b + K_{tr})/d_b \leq 4$ and 1.17 for data with $(c_b + K_{tr})/d_b < 2.5$. The scatter for these groups differed somewhat, with COV of 0.15 and 0.23 for the populations with $2.5 \leq (c_b + K_{tr})/d_b \leq 4$ and $(c_b + K_{tr})/d_b < 2.5$, respectively. As expected, the solid black trendline that is based on tests with $(c_b + K_{tr})/d_b > 4$ has a much lower slope (0.83), and most (72%) of these results have test/calculated stress values below 1. It therefore appears that the limit on $(c_b + K_{tr})/d_b$ in the ACI 318-19 equation could increase from 2.5 to 4 without resulting in lower expected strengths *than are already obtained for specimens* with $(c_b + K_{tr})/d_b < 2.5$. This is demonstrated in Figure 4.11b, as the slope of the solid black trendline increases to 1.08 when a limit of 4 is applied. Further analysis shows that with $(c_b + K_{tr})/d_b \leq 3.7$, the solid black trendline would have a slope equal to that of the trendline for $2.5 \leq (c_b + K_{tr})/d_b \leq 4$ (1.14), and that with $(c_b + K_{tr})/d_b \leq 3.5$, the solid black trendline would have a slope equal to that of the trendline for $(c_b + K_{tr})/d_b < 2.5$ (1.17). ACI 318-19 could, therefore, be modified to allow $(c_b + K_{tr})/d_b$ values up to 3.5 while maintaining similar ratios of

test-to-calculated bar stresses for all $(c_b + K_{tr})/d_b$ values. For simplicity and consistency with ACI 408R-03, a limit of 4 is applied to $(c_b + K_{tr})/d_b$ for the rest of Chapter 4.

Although not a focus of this study, there is considerable debate as to whether the relatively high percentage of cases with T/C below 1.0 is desirable (ACI 408R-03). Considering only specimens with $(c_b + K_{tr})/d_b$ < 2.5, 15 percent of specimens in Figure 4-11 have T/C < 1.0.

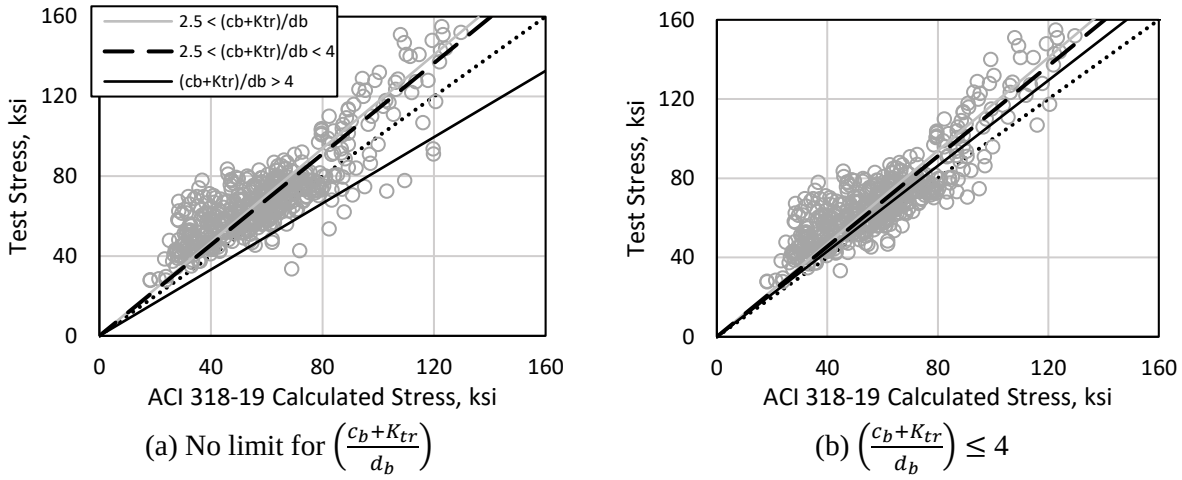

(a) No limit for $\left(\frac{c_b+K_{tr}}{d_b}\right)$ (b) $\left(\frac{c_b+K_{tr}}{d_b}\right) \leq 4$

Figure 4.11: ACI 408 Database (2021) bottom-cast specimens with $\ell_s \geq 12$ in. (300 mm). Bar stress at failure versus bar stress calculated based on Equation 2.6 (ACI 318-19) (1 ksi = 6.895 MPa)

4.4.2 Long Unconfined Lap Splices

The low T/C bar stress ratio for 14-f in Table 4.2 is an outlier from the other data in this study. Specimen 14-f had ℓ_s/d_b = 72 and had a bar stress of 73.2 ksi (505 MPa) at failure, corresponding to T/C of 0.71 and 0.77 when compared with Equations 2.4 and 2.6, respectively. For comparison, 14-g with ℓ_s/d_b = 36 and transverse reinforcement had a bar stress at failure of 109.3 ksi (754 MPa) and T/C of 0.98 and 1.23 when compared with Equations 2.4 and 2.6 (with $(c_b + K_{tr})/d_b \leq 4$), respectively. To understand whether the result for 14-f was an anomaly or evidence of a problem with long and unconfined lap splices, the literature was reviewed to identify other tests of long and unconfined lap splices.

Seliem et al. (2009) tested several beam-splice specimens. The study focused on bar sizes No. 5, 8, and 11 (No. 16, 25, and 36 mm), high bar stresses, and normal-strength concrete. Seliem et al. (2009) concluded that the presence of stirrups in the lap-splice region led to higher strengths at failure, as expected, but also that increasing unconfined splice lengths as a method to achieve a high bar stresses may not be as efficient as adding transverse reinforcement. Furthermore, a closer look at their results shows that specimens 11-5-XC0-2 and 11-8-XC0-2, which had No. 11 (36 mm) bars and $\ell_s/d_b = 56$ and 65 and were the only two specimens in the study with bars larger than No. 8 (25 mm) and $\ell_s/d_b \geq 50$, had bar stresses at failure between 70 and 80 ksi (480 and 550 MPa) and T/C less than 1.0 (0.78 and 0.76, respectively) based on Equation 2.4. This implies there may be a value of ℓ_s/d_b beyond which increases in unconfined lap splice length do not provide increased bond strength.

Results from Richter (2012), described in Section 2.5.2 and shown in Figure 2.9, support this interpretation. Their tests showed that increases in unconfined lap splice length beyond $\ell_s/d_b = 60$ produced little increase in bar stress at failure. Results from Frosch, Fleet, and Glucksman (2020) further demonstrate that increasing the length of long unconfined lap splices does not produce an increase in bar stress at failure. Specimens U-80-5, U-100-5, and U-120-5, which had No. 5 (16 mm) bars, the same concrete, and lap splice lengths of 80, 100, and 120 times the bar diameter, exhibited bar stresses at failure of 102.2, 103.7, and 103.5 ksi (705, 715, and 714 MPa). These results imply that $\ell_s/d_b = 80$ may be beyond the limit at which increases in unconfined lap splice length can be expected to provide increases in strength.

Given the results from this study, Seliem et al. (2009), Richter (2012), and Frosch, Fleet, and Glucksman (2020), it seems appropriate to limit the unconfined lap splice length to approximately $60d_b$. However, a limit of $50d_b$ is recommended regardless of bar size because (1) there are few data available with lap splices longer than $50d_b$, and (2) the 11 test results in the ACI 408 Database (2021) that had unconfined bars with a lap splice length between 50 and $60d_b$ had a mean T/C of 0.90 based on Equation 2.4. For comparison, the mean T/C for specimens in the ACI 408 Database (2021) with bottom-cast

unconfined lap splices with lap splice lengths shorter than $50d_b$ is 1.01. The authors therefore recommend prohibiting unconfined lap splices based on a calculated development length $\ell_d > 50d_b$.

4.4.3 Effects of Bar Size

The results in Table 4.2 show that the mean test/calculated values were 0.86 and near 1.0 based on Equations 2.4 and 2.6 (from ACI 408R-03 and ACI 318-19), respectively. The ACI 408 Database (2021) was used to examine how these results compare with a broader set of test results with smaller bar sizes to identify whether there is an effect of bar size. Equation 2.4 (ACI 408R-03) is a "descriptive" equation designed to produce T/C near 1.0, whereas Equation 2.6 (ACI 318-19) is a design equation that should produce T/C greater than 1.0.

These comparisons are based on bottom-cast specimens from the ACI 408 Database (2021) with $\ell_s \geq 12\text{ in.}\,(300\text{ mm})$ and, for unconfined lap splices, $\ell_s \leq 50d_b$ (see Section 4.4.2 for rationale). For comparisons against Equation 2.4, the dataset was further limited to $\ell_s \geq 16d_b$ as recommended in ACI 408R-03. Thus, 14-e and 14-f from the current study are not included in comparisons against Equation 2.4 in this section.

Figure 4.12 shows bar stress at failure from tests (see Section 4.4) versus bar stress calculated with Equation 2.4 for specimens from the ACI 408 Database (2021) and this study (circles and triangles, respectively). The dashed line represents a T/C of 1.0. Equation 2.4 provides an accurate estimation of bond strength, with a mean T/C of 1.02 and a COV of 0.12 for the specimens from the ACI 408 Database (2021). Conversely, the nine selected tests from this study in Figure 4.12 had a mean T/C of 0.88. The mean T/C for specimens from the current study (0.88) is considerably less than the mean T/C for the entire database (1.02). These differences are also statistically significant based on a two-tailed Student's t-Test assuming equal variances, with p less than 0.001, where p values less than 0.05 are taken as evidence of statistical significance.

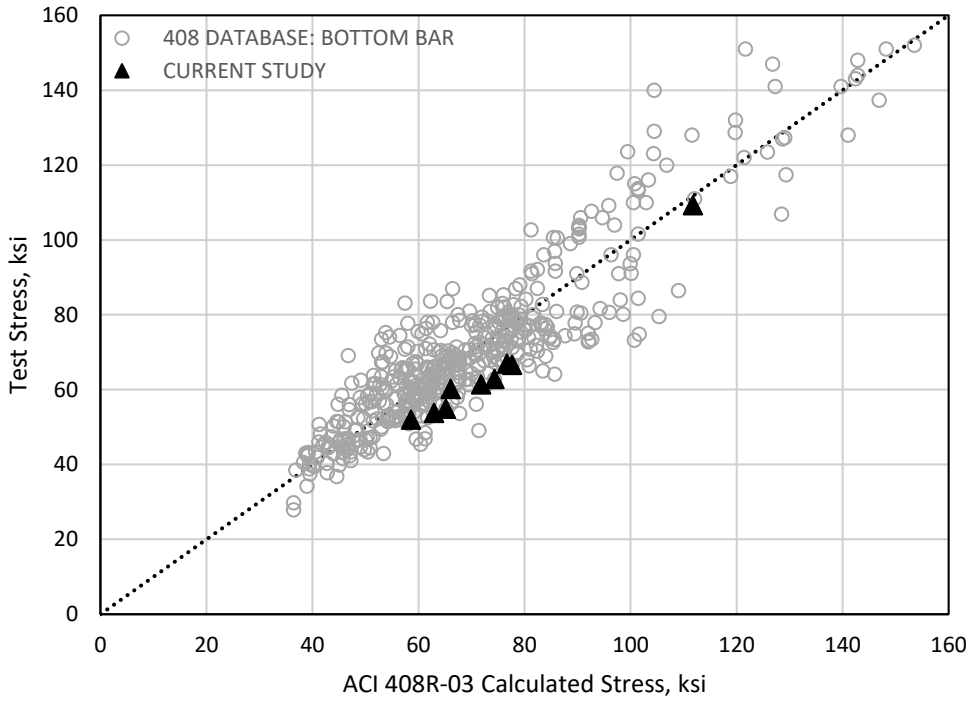

Figure 4.12: Test versus calculated bar stress for Equation 2.4 (ACI 408R-03) (1 ksi = 6.895 MPa)

Figure 4.13 shows T/C based on Equation 2.4 (ACI 408R-03) versus six key variables: bar stress at failure, concrete compressive strength, lap splice length to bar diameter ratio, confinement term $(c\omega + K_{tr,408})/d_b$, minimum clear cover divided by d_b, and $K_{tr,408}/d_b$ for the 24 specimens that the authors are aware of that meet the following criteria: bottom-cast lap-spliced bars larger than No. 11 (36 mm), $\ell_s \geq 16d_b$, $\ell_s \geq 12$ in. (300 mm), and if unconfined $\ell_s \leq 50d_b$. While not included in the ACI 408 Database (2021) because they had threaded bars, specimens from Hassan, Lucier, and Rizkalla (2012) are included here to supplement the sparse data.

Figure 4.13 shows that 21 of 24 specimens with large bars had T/C less than 1.0 (mean = 0.87 and COV = 0.14), indicating that the low T/C values in Table 4.2 are not anomalies among tests with large bars. This is evidence of a large-bar size effect that is not captured by Equation 2.4.

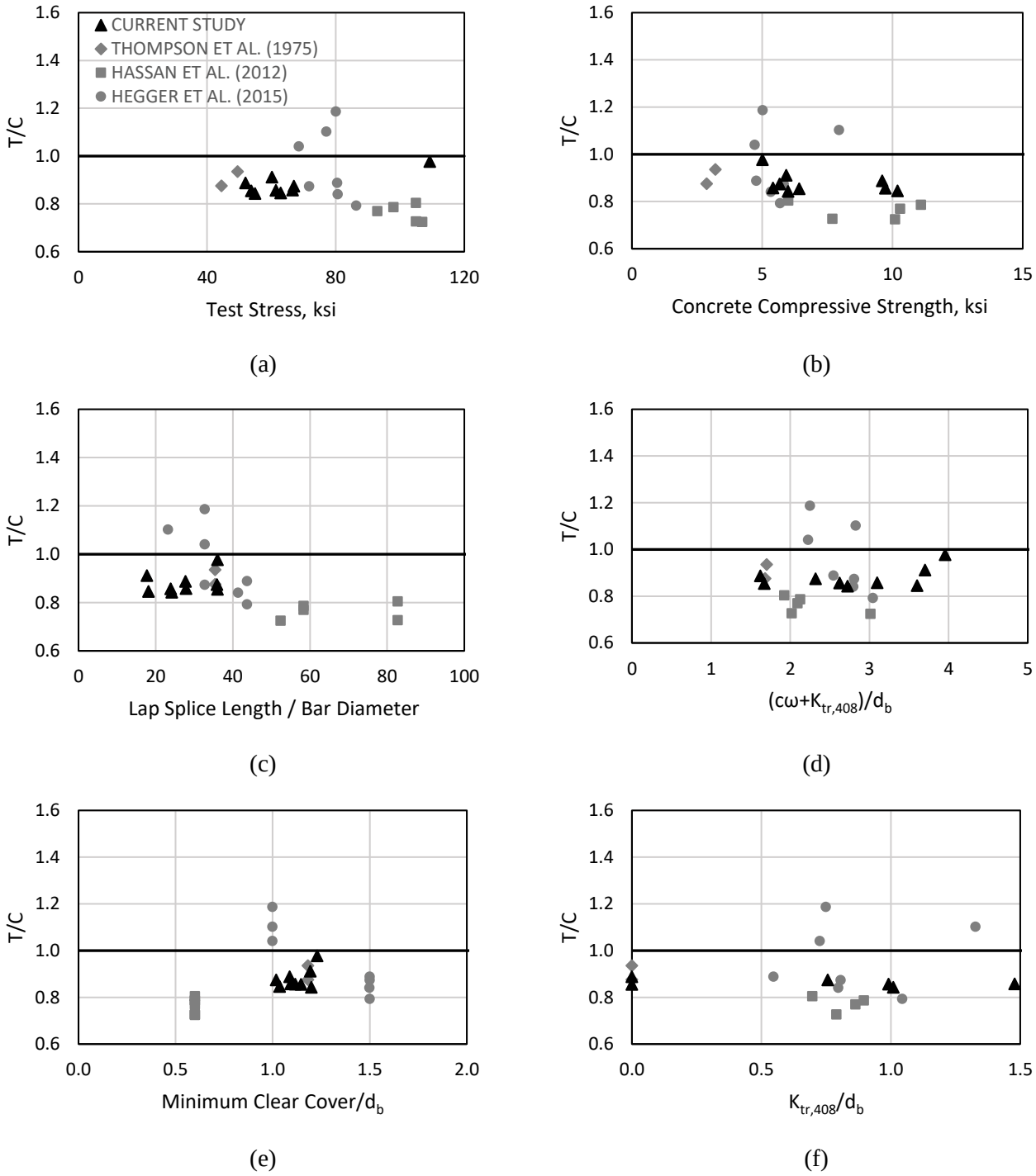

Figure 4.13: Test-to-calculated bar stress ratios for large-bar specimens based on Equation 2.4 (ACI 408R-03) (1 ksi = 6.895 MPa)

Figure 4.13 shows no clear trend between T/C and bar stress at failure, concrete compressive strength, or confinement term $(c\omega + K_{tr,408})/d_b$. There does appear to be a downward trend between T/C and ℓ_s/d_b, with T/C less than or equal to 0.80 for specimens with ℓ_s/d_b > 50 and the three T/C over 1.0 being for specimens with lap splices shorter than $35d_b$. Figures 4.13(e) and (f) also show that specimens with minimum clear cover less than d_b and $K_{tr,408}/d_b$ less than 0.5 tended to have low T/C values. The available data therefore do not support permitting lap splices of large bars with small amounts of clear cover or transverse reinforcement. It is recommended that large-bar lap splices have clear cover not less than d_b and $K_{tr,408}/d_b$ not less than 0.5.

Figures 4.14 and 4.15 are corollaries to Figures 4.12 and 4.13, except with bar stresses calculated using Equation 2.6 based on ACI 318-19. Again, Equation 2.6 is used with $\psi_g \geq \left[\left(1 + 0.15\frac{(f_s - 60\text{ ksi})}{20\text{ ksi}}\right), 1.0\right]$ or $\left[\left(1 + 0.15\frac{(f_s - 410\text{ MPa})}{140\text{ MPa}}\right), 1.0\right]$, $\sqrt{f'_c} \leq 100$ psi (0.690 MPa), $(c_b + K_{tr})/d_b \leq 4$, and $\psi_s = 1.0$ for all bar sizes as recommended in ACI 408R-03. The mean T/C for specimens from the ACI 408 Database (2021) is 1.22, with a COV of 0.21. The large bar tests included in Figure 4.15 have a mean T/C of 1.05 and a COV of 0.11. As with the comparison against Equation 2.4, these differences are statistically significant based on a two-tailed Student's t-test assuming equal variances (p < 0.001). It therefore appears there is a large-bar size effect that is not captured by Equation 2.6.

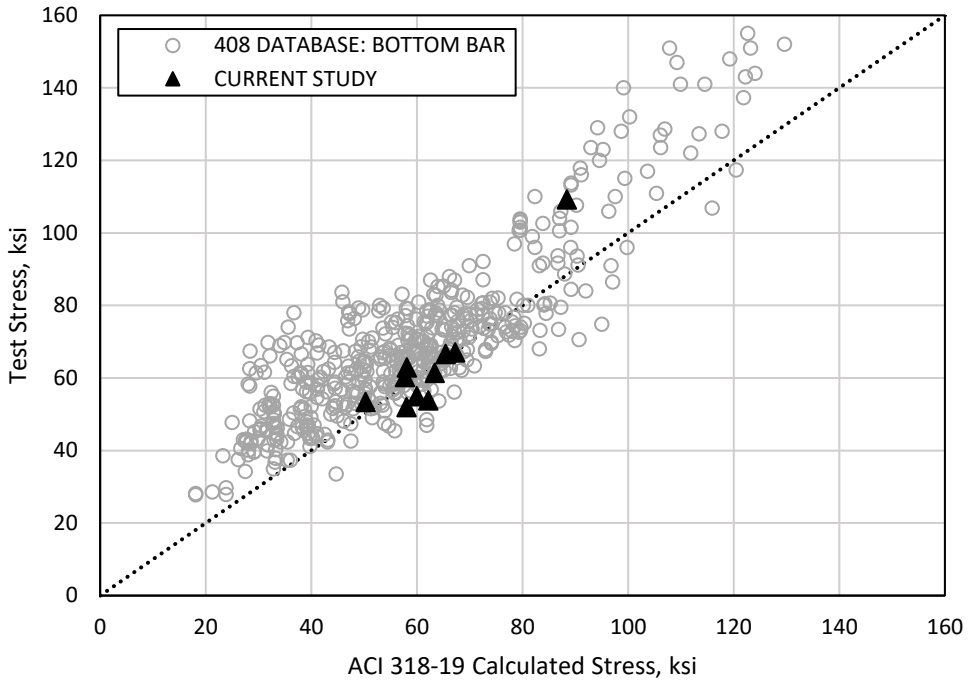

Figure 4.14: Test versus calculated bar stress for Equation 2.6 (ACI 318-19) (1 ksi = 6.895 MPa)

Figure 4.15 includes 25 specimens that meet the following criteria: bottom-cast lap-spliced bars larger than No. 11 (36 mm), $\ell_s \geq 12$ in. (300 mm), and if unconfined $\ell_s \leq 50d_b$. Each data cluster is shifted up when compared to Figure 4.13, as ACI 318-19 is a design equation and, thus, more conservative than ACI 408R-03. The scatter is also larger for ACI 318-19. Figure 4.15 shows that ACI 318-19 tends to have higher T/C for high bar stresses and long lap splice lengths (note that unconfined lap splices longer than $50d_b$ are excluded from this figure). Figure 4.15 also shows that the lowest T/C values are for specimens with no transverse reinforcement ($K_{tr} = 0$). Again, it is recommended that large-bar lap splices be required to have a clear cover not less than d_b and K_{tr}/d_b not less than 0.5 until additional data are available to justify their safe use.

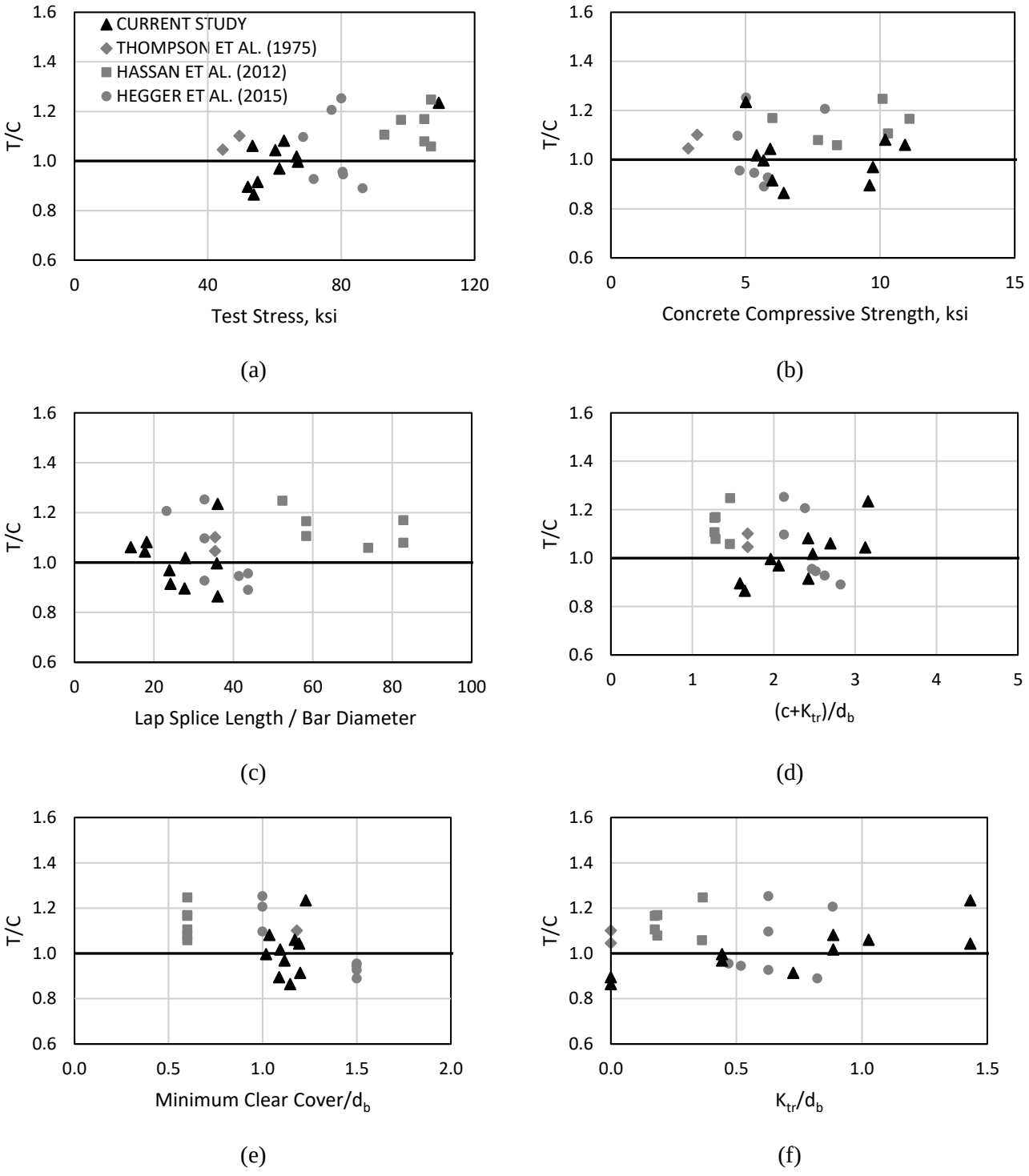

Figure 4.15: Test-to-calculated bar stress ratios for large-bar specimens based on Equation 2.6 (ACI 318-19) (1 ksi = 6.895 MPa)

To further demonstrate the trend between T/C and bar size, Figures 4.16 and 4.17 show bar stress at failure versus bar stress calculated with Equations 2.4 and 2.6 (based on ACI 408R-03 and ACI 318-19), respectively. These plots contain the same specimens used in Figures 4.12 and 4.14, but trends are shown for groups of specimens with No. 10 (32 mm) or smaller bars and specimens with No. 11 (36 mm) or larger bars (circles show results for "smaller" bars while the squares and triangles show results for "larger" bars).

It is evident in Figure 4.16 that T/C values are larger for the smaller bars than for larger bars, with the slope for the data with No. 10 (32 mm) or smaller bars being 1.04 and the slope for the data with No. 11 (36 mm) or larger bars being 0.95. If a similar trendline were applied to only tests with bars larger than No. 11 (36 mm) (total of 19 specimens), the slope would be 0.90.

The mean T/C for Equation 2.4 (ACI 408R-03) for bars No. 10 (32 mm) or smaller is 1.04 (COV = 0.12), while the mean for bars No. 11 (36 mm) or larger is 0.95 (COV is 0.11). These differences are statistically significant, with a *p*-value less than 0.001 (8.1E-11) when comparing test/calculated for specimens with No. 10 (32 mm) or smaller bars against specimens with No. 11 (36 mm) or larger bars. A size effect is evident.

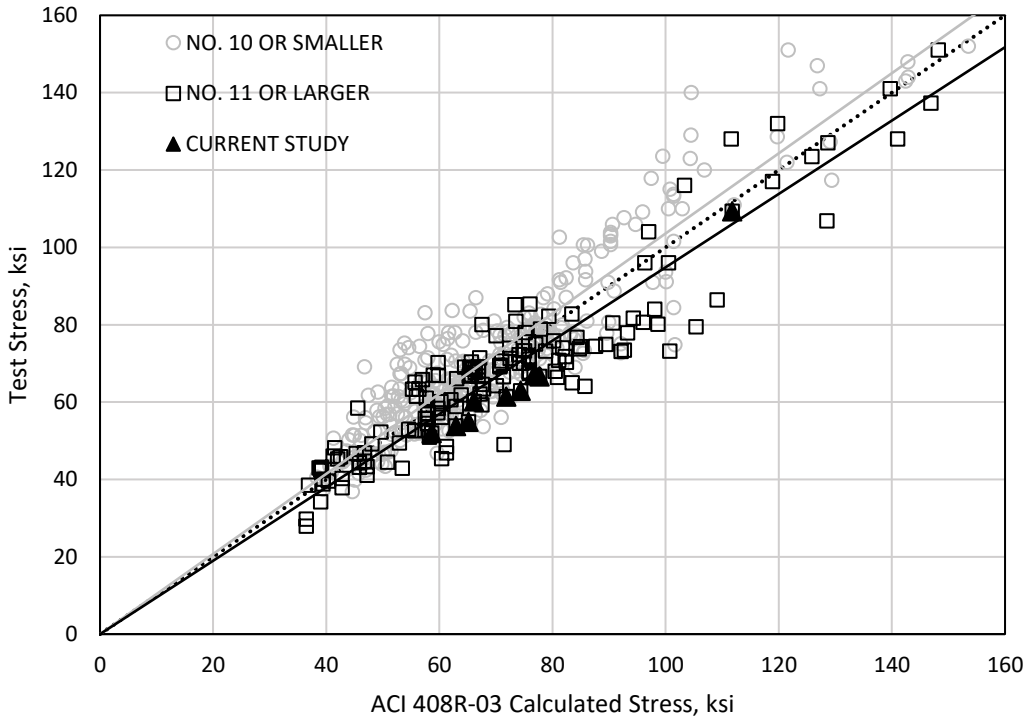

Figure 4.16: Test versus calculated bar stress by bar size for Equation 2.4 (ACI 408R-03) (1 ksi = 6.895 MPa)

Figure 4.17 shows similar trends as Figure 4.16, but with the ACI 318-19 expression for development length (Equation 2.6). Again, Equation 2.6 is used with $\psi_g \geq \left[\left(1 + 0.15\frac{(f_s - 60\text{ ksi})}{20\text{ ksi}}\right), 1.0\right]$ or $\left[\left(1 + 0.15\frac{(f_s - 410\text{ MPa})}{140\text{ MPa}}\right), 1.0\right]$, $\sqrt{f'_c} \leq 100$ psi (0.690 MPa), $(c_b + K_{tr})/d_b \leq 4$, and $\psi_s = 1.0$ for all bar sizes as recommended in ACI 408R-03. Although both trendlines have slopes greater than 1.0, the slope of the grey trendline (1.17 for No. 10 (32 mm) or smaller bars) is higher than that of the black trendline (1.10 for No. 11 (36 mm) or larger bars). These differences are also statistically significant, with a *p*-value of 0.036 when comparing "smaller" bars versus "larger" bars.

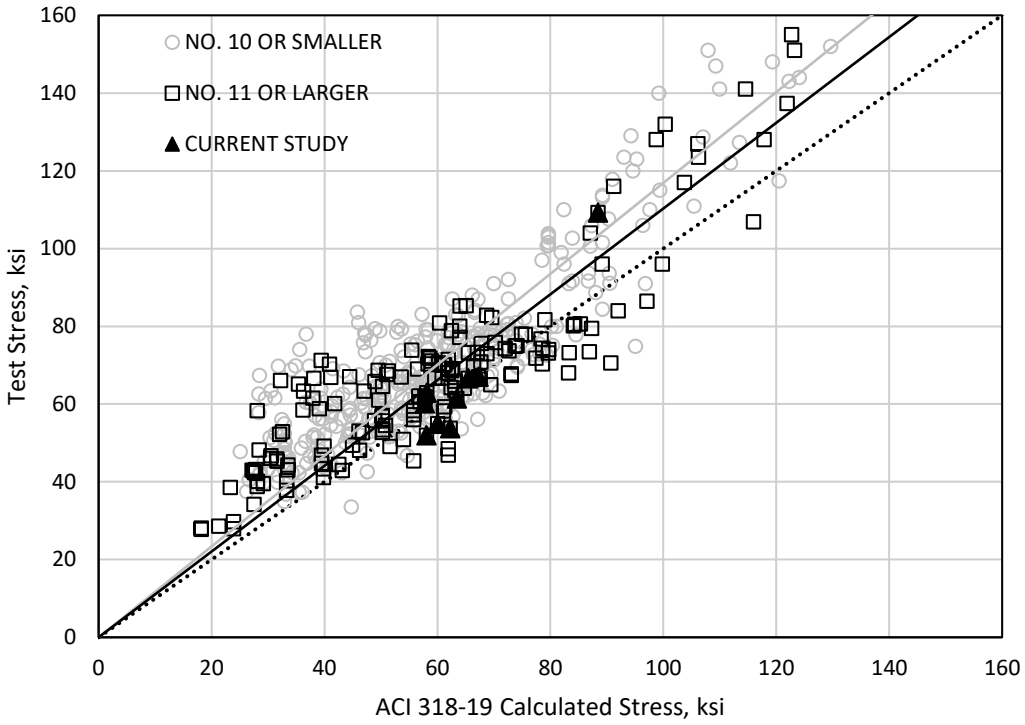

Figure 4.17: Test versus calculated bar stress by bar size for Equation 2.6 (ACI 318-19) (1 ksi = 6.895 MPa)

Table 4.3 shows results that complement Figures 4.16 and 4.17 based on data from the ACI 408 Database (2021) and this study. Results are split into four different bar size groups in Table 4.3: bars smaller than No. 7 (22 mm), No. 7 to No. 10 (19 to 32 mm) bars, No. 11 (36 mm) bars, and bars larger than No. 11 (36 mm). A mean, minimum, and maximum T/C is reported for each bar size group. Specimens with and without transverse reinforcement throughout the lap splice (confined and unconfined) were considered separately. Equation 2.6 is based on a design equation, so relatively few specimens should have T/C below 1.0 since the tests are considered representative of conditions in practice. Equation 2.4, which has been used here with a phi-factor of 1.0, provides mean values much nearer to 1.0 as expected. Additional safety factors would need to be applied for Equation 2.4 to be used for design.

For application of Equation 2.6 in Table 4.3, $\psi_s = 1.0$ based on ACI 408R-03 recommendations. If $\psi_s = 0.8$ were indeed applied to the Table 4.3 bar group "smaller than No. 7 (19 mm)", the mean T/C would drop from 1.32 to 1.08 for unconfined specimens (with 32% below 1.0) and from 1.17 to 1.00 for confined specimens (with 44% below 1.0). This supports the ACI 408R-03 recommendation to set $\psi_s = 1.0$ for Equation 2.6 (ACI 318-19), as having nearly half of specimens with T/C below 1.0 is not satisfactory for a design equation.

Table 4.3: Test to calculated bar stress ratios based on current equations

Type	Bar Size Group [a]	Equation 2.4 (ACI 408R-03) [b]					Equation 2.6 (ACI 318-19) [c,d,e]				
		Count	Mean	T/C <1.0	Min.	Max.	Count	Mean	T/C <1.0	Min.	Max.
Unconfined	Smaller than No. 7	25	1.06	32%	0.92	1.24	28	1.32	7%	0.88	1.70
	No. 7 to No. 10	75	1.01	49%	0.74	1.27	90	1.25	16%	0.79	2.37
	No. 11	60	0.97	67%	0.69	1.28	64	1.19	22%	0.76	1.84
	Larger than No. 11	4	0.89	100%	0.85	0.93	4	0.98	50%	0.86	1.10
Confined	Smaller than No. 7	41	1.11	12%	0.83	1.45	43	1.17	9%	0.92	1.45
	No. 7 to No. 10	174	1.03	47%	0.78	1.48	190	1.23	15%	0.75	2.21
	No. 11	74	0.97	62%	0.73	1.16	80	1.22	14%	0.88	2.08
	Larger than No. 11	14	0.92	79%	0.79	1.19	15	1.04	47%	0.89	1.25

[a] No. 7, 10, and 11 bars in U.S. have diameters of approximately 22, 32, and 36 mm

[b] 467 specimens from the ACI 408 Database (2021) and this study that were bottom-cast and had $\ell_s \geq 12$ in. (300 mm), $\ell_s \geq 16d_b$, and for unconfined specimens $\ell_s \leq 50d_b$

[c] 514 specimens from ACI 408 Database (2021) and this study that were bottom-cast and had $\ell_s \geq 12$ in. (300 mm) and for unconfined specimens $\ell_s \leq 50d_b$

[d] $\psi_g \geq \left[\left(1 + 0.15\frac{(f_s - 60\text{ ksi})}{20\text{ ksi}}\right), 1.0\right]$ or $\left[\left(1 + 0.15\frac{(f_s - 410\text{ MPa})}{140\text{ MPa}}\right), 1.0\right]$, $\sqrt{f'_c} \leq 100$ psi (0.690 MPa), $\left(\frac{c_b + K_{tr}}{d_b}\right) \leq 4$, and $\psi_s = 1.0$ for all bar sizes

[e] if $\psi_s = 0.8$ for specimens with bars smaller than No. 7, mean T/C = 1.08 for unconfined specimens (with 32% below 1.0) and 1.00 for confined specimens (with 44% below 1.0).

Table 4.3 shows a clear trend associated with bar size for both Equations 2.4 and 2.6. The mean T/C decreases in almost all cases as the bar size increases for both unconfined and confined specimens. Likewise, the percentage of tests with T/C less than 1.0 increases with bar size in almost all cases, except for the comparison between confined specimens with No. 7 to No. 10 (22 to 32 mm) bars and specimens with No. 11 (36 mm) bars using Equation 2.6 (15 and 14% of specimens had test/calculated below 1.0).

Even though Table 4.3 reports results from only four unconfined and 14 confined (15 for ACI 318-19) specimens that contained bars larger than No. 11 (36 mm), the evidence of a trend between T/C and bar size within the broader database is evident in Table 4.3.

4.4.4 Accounting for Effects of Bar Size in Design

Section 4.4.3 shows that T/C for the ACI 318-19 and ACI 408R-03 development length equations decreases as bar size increases. This finding builds on observations of a possible size effect in Thompson et al. (1979), Ichinose et al. (2004), and Hegger et al. (2015).

There are many possible methods of adjusting development and lap splice equations to account for bar size; two are described in this section: (1) a bar size factor can be added to the numerator of Equations 2.3 and 2.5 (see Section 4.4.4.1) or (2) the exponent on bar diameter can be increased (see Section 4.4.4.2). Both methods (1) and (2) can allow for T/C to be independent of bar size.

4.4.4.1 Large-Bar Size Factor

ACI 408R-03 and ACI 318-19 development and lap splice length equations can be made independent of bar size by adding a bar size factor in the numerator of Equations 2.3 and 2.5 as shown in Equations 4.2 and 4.3. This is a relatively simple change, as the ACI 318-19 equation already has $\psi_s = 0.8$ for bars that are No. 6 (19 mm) and smaller, so it would only require a modification of ψ_s. It is proposed to define this factor as shown in Equation 4.4. There are zero tests in the database with No. 10 (32 mm) bars, so some judgement is necessary here. It is proposed to assign $\psi_s = 1.0$ to No. 10 (32 mm) bars, although it could be argued that $\psi_s = 1.15$ would be appropriate until data are available.

$$\ell_d = \left(\frac{\left(\frac{f_y}{\varphi f_c'^{1/4}} - 2400\omega \right) \alpha\beta\lambda\psi_s}{76.3\left(\frac{c_{\omega}\omega + K_{tr,408}}{d_b} \right)} \right) d_b \qquad \text{Equation 4.2}$$

$$\ell_d = \left(\frac{3}{40} \frac{f_y}{\lambda \sqrt{f'_c}} \frac{\psi_t \psi_e \psi_s \psi_g}{\left(\frac{c_b + K_{tr}}{d_b} \right)} \right) d_b \qquad \text{Equation 4.3}$$

$$\psi_s = \begin{cases} 1.0 \text{ for No. } 10 \text{ (32 mm) and smaller bars} \\ 1.15 \text{ for No. } 11 \text{ (36 mm) bars} \\ 1.25 \text{ for No. } 14 \text{ (43 mm) and larger bars} \end{cases} \qquad \text{Equation 4.4}$$

Table 4.4 is a repeat of Table 4.3, but with ψ_s defined according to Equation 4.4 included in both Equations 4.2 and 4.3. Table 4.4 shows that this modification produces similar mean T/C across bar sizes for Equation 4.2, with mean T/C between 1.01 and 1.11 for both unconfined and confined bars of all sizes. Also, the percent of specimens with T/C below 1.0 are no longer correlated with bar size in Table 4.4. The results in Table 4.4 for Equation 4.3 also show somewhat improved consistency in mean T/C across bar sizes. It is believed that, based on the available data, defining ψ_s according to Equation 4.4 provides a reasonable correction for both Equations 4.2 and 4.3 without penalizing any group of bar sizes.

Figures 4.18 and 4.19 are similar to Figures 4.16 and 4.17 except they include the large-bar size factor (Equation 4.4). Figure 4.18 shows the overall improved T/C trends; the slope for the data with No. 10 (32 mm) or smaller bars is still 1.04 and the slope for the updated data with No. 11 (36 mm) or larger bars is now 1.05. Use of the Equation 4.4 bar size factor, therefore, causes the ACI 408R-03 equation to have similar T/C for all bar sizes. Figure 4.19 shows a similar outcome for the ACI 318-19 equation; the slope for the data with No. 10 (32 mm) or smaller bars is still 1.17 and the slope for the updated data with No. 11 (36 mm) or larger bars is now 1.24.

Table 4.4: Test to calculated bar stress at failure with proposed size effect factor

Type	Bar Size Group [a]	Equation 2.4 (ACI 408R-03) [b]					Equation 2.6 (ACI 318-19) [c,d]				
		Count	Mean	T/C <1.0	Min.	Max.	Count	Mean	T/C <1.0	Min.	Max.
Unconfined	Smaller than No. 7	25	1.06	32%	0.92	1.24	28	1.32	7%	0.88	1.70
	No. 7 to No. 10	75	1.01	49%	0.74	1.27	90	1.25	16%	0.79	2.37
	No. 11	60	1.05	30%	0.75	1.39	64	1.36	12%	0.85	2.12
	Larger than No. 11	4	1.08	25%	0.95	1.38	4	1.22	0%	1.06	1.38
Confined	Smaller than No. 7	41	1.11	12%	0.83	1.45	43	1.17	9%	0.92	1.45
	No. 7 to No. 10	174	1.03	47%	0.78	1.48	190	1.23	15%	0.75	2.21
	No. 11	74	1.07	24%	0.80	1.28	80	1.38	3%	0.96	2.39
	Larger than No. 11	14	1.08	36%	0.95	1.38	15	1.25	0%	1.03	1.52

[a] No. 7, 10, and 11 bars in U.S. have diameters of approximately 22, 32, and 36 mm

[b] 467 specimens from the ACI 408 Database (2021) and this study that were bottom-cast and had $\ell_s \geq$ 12 in. (300 mm), $\ell_s \geq 16d_b$, and for unconfined specimens $\ell_s \leq 50d_b$

[c] 514 specimens from ACI 408 Database (2021) and this study that were bottom-cast and had $\ell_s \geq$ 12 in. (300 mm) and for unconfined specimens $\ell_s \leq 50d_b$

[d] $\psi_g \geq \left[\left(1 + 0.15\frac{(f_s - 60\text{ ksi})}{20\text{ ksi}}\right), 1.0\right]$ or $\left[\left(1 + 0.15\frac{(f_s - 410\text{ MPa})}{140\text{ MPa}}\right), 1.0\right]$, $\sqrt{f'_c} \leq$ 100 psi (0.690 MPa), $(c_b + K_{tr})/d_b \leq 4$, and $\psi_s = 1.0$ for all bar sizes

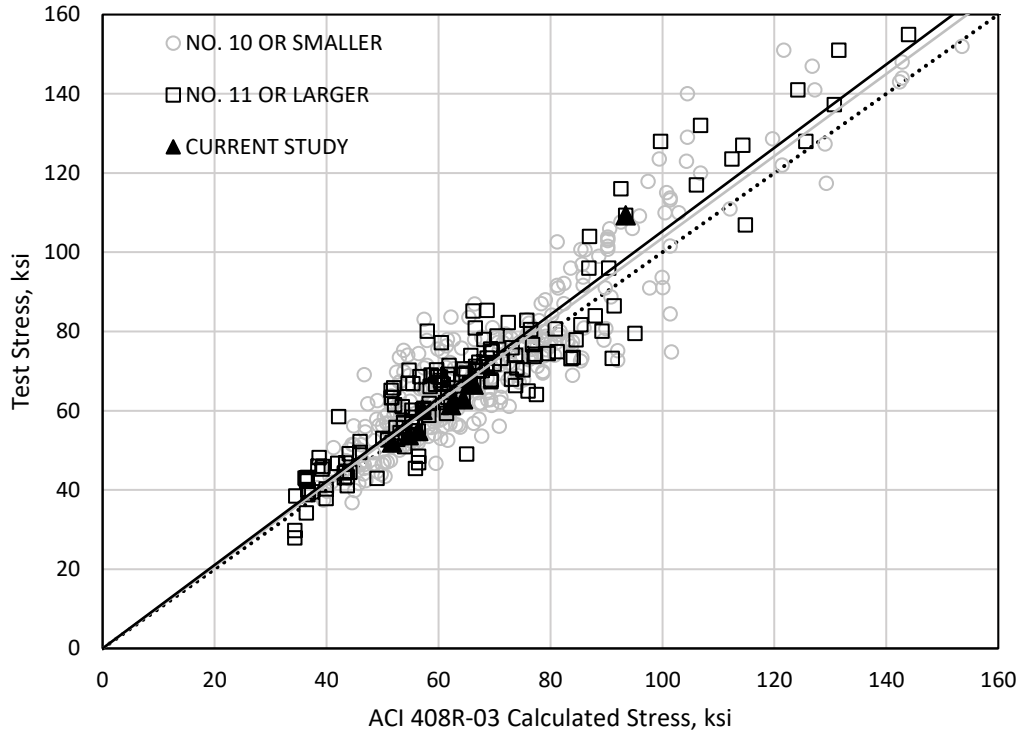

Figure 4.18: Test versus calculated bar stress by bar size for Equations 4.2 and 4.4 (1 ksi = 6.895 MPa)

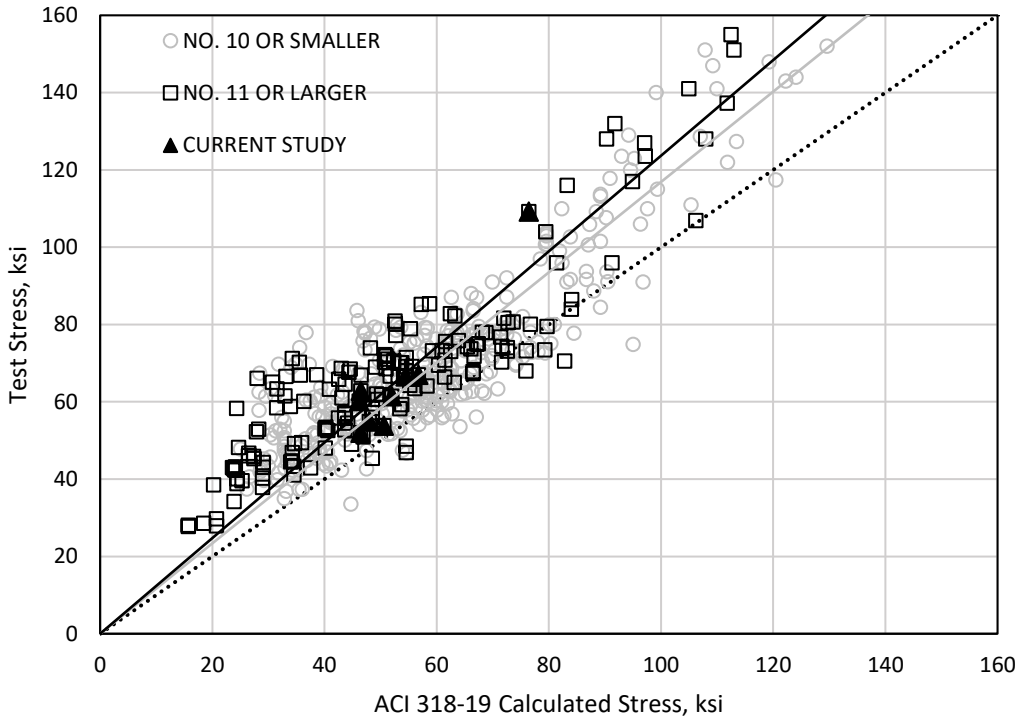

Figure 4.19: Test versus calculated bar stress by bar size for Equations 4.3 and 4.4 (1 ksi = 6.895 MPa)

4.4.4.2 Modified Exponent for Bar Diameter

Use of a modified exponent on bar diameter is examined as a means of accounting for effects of bar size. The concept is based on recommendations in Ichinose et al. (2004), which reported tests from short lap-splice specimens with large diameter bars. They found that changing the exponent on bar diameter by 0.2 or 0.3 produced a more accurate estimate of bond strength with a similar level of conservatism across bar sizes.

Using the same test data shown in Figures 4.18 and 4.19, the authors found that changing the exponent on bar diameter is a viable solution for adjusting both the ACI 408R-03 and ACI 318-19 equations to produce similar T/C values across all bar sizes. Using exponents of 1.35 and 1.25 on bar diameter in Equations 4.5 and 4.6 provides results with mean T/C and percent of T/C below 1.0 showing no clear

correlation with bar size. For this comparison, ψ_s is taken as 1.0 for all bar sizes and, thus, is not shown in Equations 4.5 and 4.6.

$$\ell_d = \left(\frac{\left(\frac{f_y}{\varphi f'^{1/4}_c} - 2400\omega \right) \alpha\beta\lambda}{76.3\left(\frac{c\omega + K_{tr,408}}{d_b} \right)} \right)_{\geq} d_b^{1.35} \qquad \text{Equation 4.5}$$

$$\ell_d = \left(\frac{3}{40} \frac{f_y}{\lambda\sqrt{f'_c}} \frac{\psi_t \psi_e \psi_g}{\left(\frac{c_b + K_{tr}}{d_b} \right)} \right)_{\geq} d_b^{1.25} \qquad \text{Equation 4.6}$$

The results in Table 4.5 are based on the same test data as Tables 4.3 and 4.4, but with $d_b^{1.35}$ and $d_b^{1.25}$ replacing bar diameter in equations from ACI 408R-03 (Equation 4.5) and ACI 318-19 (Equation 4.6). Table 4.5 shows mean ratios between 0.98 and 1.04 for both unconfined and confined bars of all sizes when calculated by Equation 4.5. The bar diameter exponent results in no clear trend between T/C and bar size. The results in Table 4.5 for Equation 4.6 also show less correlation between T/C and bar size.

Figures 4.20 and 4.21 are similar to Figures 4.16 and 4.17, respectively, except they are based on Equations 4.5 and 4.6, which include bar diameter exponents greater than 1.0. Figure 4.20 shows improved T/C trends for both small and large bars (No. 10 (32 mm) or smaller and No. 11 (36 mm) or larger). The slope for the data with No. 10 (32 mm) or smaller bars is now 1.02 and the slope for the updated data with No. 11 (36 mm) or larger bars is now 1.03. A bar diameter exponent of 1.35 therefore causes the ACI 408R-03 equation to have similar T/C for all bar sizes. Figure 4.21 shows a similar trend for the modified ACI 318-19 equation; the slope for the data with No. 10 (32 mm) or smaller bars is now 1.15 and the slope for the data with No. 11 (36 mm) or larger bars is now 1.18.

Table 4.5: Test to calculated bar stress at failure with proposed size effect exponent

Type	Bar Size Group [a]	Equation 2.4 (ACI 408R-03) [b]					Equation 2.6 (ACI 318-19) [c,d]				
		Count	Mean	T/C <1.0	Min.	Max.	Count	Mean	T/C <1.0	Min.	Max.
Unconfined	Smaller than No. 7	25	0.99	60%	0.81	1.17	28	1.22	11%	0.76	1.58
	No. 7 to No. 10	75	1.01	49%	0.74	1.27	90	1.25	16%	0.79	2.37
	No. 11	60	1.03	37%	0.74	1.36	64	1.29	17%	0.81	2.01
	Larger than No. 11	4	0.98	75%	0.94	1.03	4	1.11	25%	0.97	1.26
Confined	Smaller than No. 7	41	1.04	32%	0.78	1.37	43	1.11	21%	0.87	1.37
	No. 7 to No. 10	174	1.03	49%	0.78	1.48	190	1.24	15%	0.75	2.30
	No. 11	74	1.04	31%	0.78	1.25	80	1.31	7%	0.93	2.27
	Larger than No. 11	14	1.04	50%	0.88	1.30	15	1.17	14%	0.96	1.36

[a] No. 7, 10, and 11 bars in U.S. have diameters of approximately 22, 32, and 36 mm

[b] 467 specimens from the ACI 408 Database (2021) and this study that were bottom-cast and had $\ell_s \geq$ 12 in. (300 mm), $\ell_s \geq 16d_b$, and for unconfined specimens $\ell_s \leq 50d_b$

[c] 514 specimens from ACI 408 Database (2021) and this study that were bottom-cast and had $\ell_s \geq$ 12 in. (300 mm) and for unconfined specimens $\ell_s \leq 50d_b$

[d] $\psi_g \geq \left[\left(1 + 0.15\frac{(f_s - 60\text{ ksi})}{20\text{ ksi}}\right), 1.0\right]$ or $\left[\left(1 + 0.15\frac{(f_s - 410\text{ MPa})}{140\text{ MPa}}\right), 1.0\right]$, $\sqrt{f'_c} \leq 100$ psi (0.690 MPa), $(c_b + K_{tr})/d_b \leq 4$, and $\psi_s = 1.0$ for all bar sizes

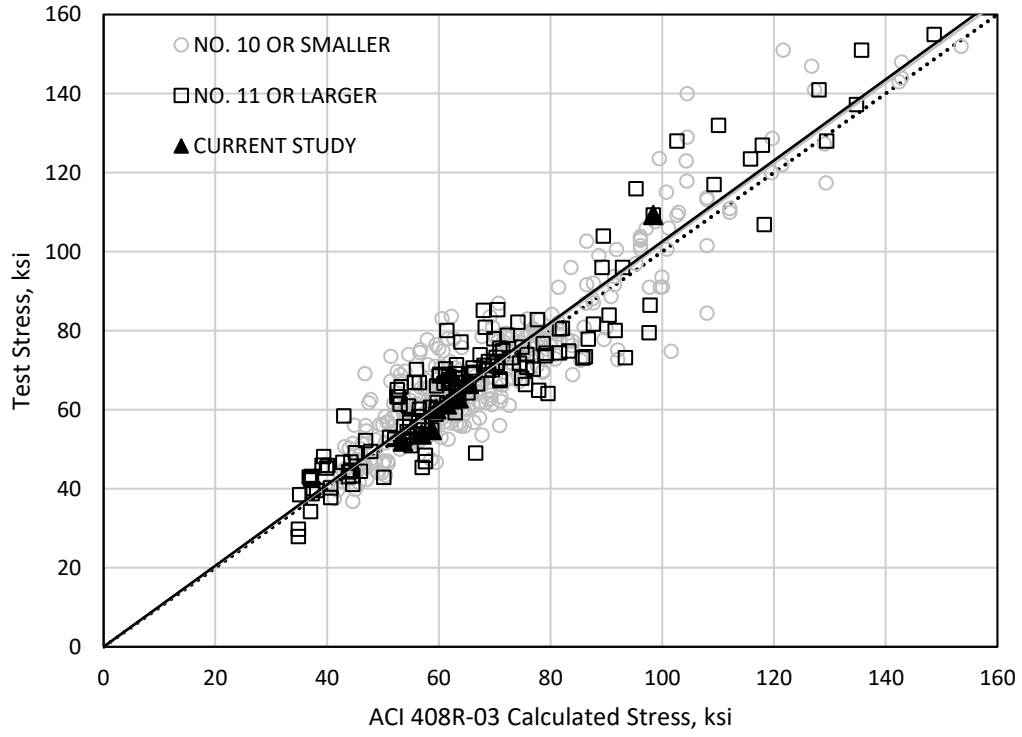

Figure 4.20: Test versus calculated bar stress by bar size for Equation 4.5 (1 ksi = 6.895 MPa)

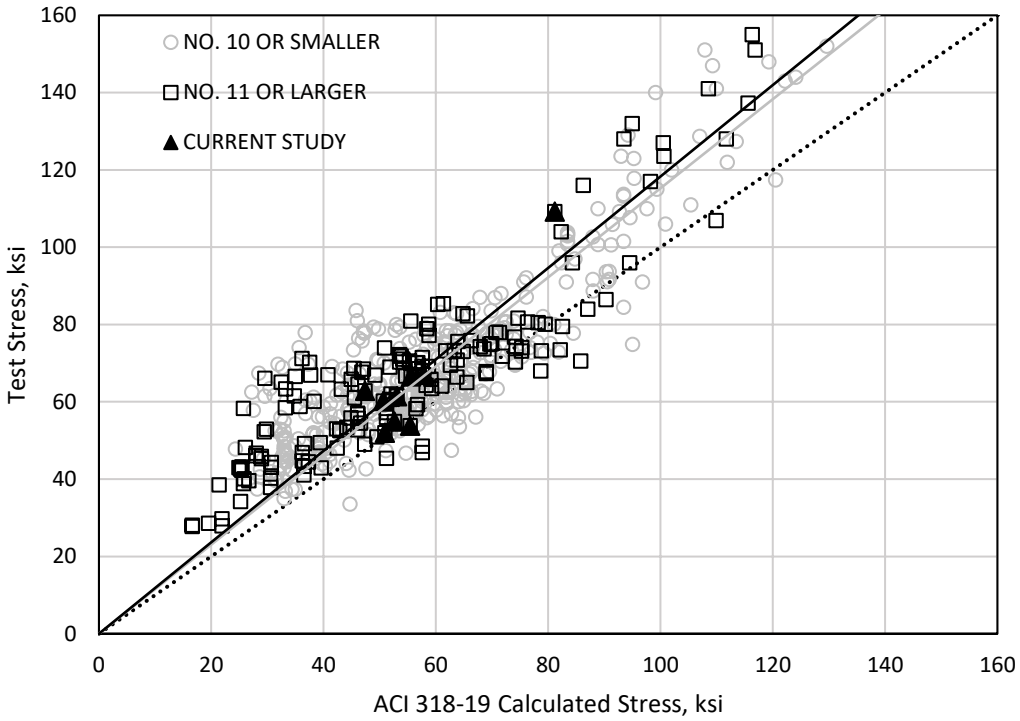

Figure 4.21: Test versus calculated bar stress by bar size for Equation 4.6 (1 ksi = 6.895 MPa)

4.4.5 Plausible Explanations for Effects of Bar Size

The linear fracture mechanics size effect might explain the trends between T/C and bar size (Ichinose et al. 2004).

It might also be expected that larger bars, which have larger deformations and longer lap splices than smaller bars, will induce wider splitting cracks and cause yielding of transverse (confining) reinforcement that might compromise bond strength. However, there was no evidence of either wider cracks or transverse reinforcement yielding in this study.

Another potential explanation for the observed effect of bar size is related to the bar prying action that causes unconfined lap-spliced bars to push the cover off at failure (Figures 4.4c, E-1, and E-4). In beam tests, lap splices are subjected to bending as well as tension. Although generally negligible, bending/prying of the lapped bars does tend to induce tension in the concrete cover perpendicular to the plane containing

the lapped bars that could, in theory, reduce the effectiveness of the cover for resisting bond-splitting failures. Data obtained with the optical sensors described in Section 3.5 were used to explore whether bar prying/bending could produce tension in the concrete cover large enough to affect bond strength. The analysis, described in Appendix G, demonstrates that bar bending/prying can produce concrete stresses large enough to compromise the splitting resistance of the concrete cover for No. 14 (43 mm) and No. 18 (57 mm) bars. Because of the larger bar diameter, bending of a No. 18 (57 mm) bar induces concrete splitting stresses that are approximately twenty times larger than a No. 9 (29 mm) bar and eight times larger than a No. 11 (36 mm) bar. So, while prying appears negligible for No. 11 (36 mm) and smaller bars, it may be non-negligible for the larger bars considered in this study.

The size effect described by fracture mechanics and bar bending may, together, explain the lower bond strengths observed for No. 14 and 18 (43 and 57 mm) bars in this study.

CHAPTER 5 – CONCLUSIONS AND RECOMMENDATIONS

Eleven large-scale beam specimens were tested to measure the strength of lap-spliced No. 14 and 18 (43 and 57 mm) bars. Specimens had bottom and side clear cover to the lap-spliced bars of approximately 1.15 times the longitudinal bar diameter, varied amounts of transverse reinforcement, nominal concrete compressive strengths of 5 or 10 ksi (34 or 69 MPa), and target bar stresses at splice failure of 60 to 100 ksi (420 to 690 MPa) for No. 14 (43 mm) bars and 60 ksi (420 MPa) for No. 18 (57 mm) bars. Test results justify the following conclusions:

1. Lap splices of No. 14 (43 mm) bars can develop bar stresses up to 100 ksi (690 MPa) and lap splices of No. 18 (57 mm) bars can develop bar stresses of at least 60 ksi (420 MPa). These limits reflect the scope of the test matrix, as there was no indication that higher bar stresses cannot be attained.
2. Equations for development length in both ACI 408R-03 and ACI 318-19 (Equations 2.3 and 2.5) become less conservative as bar size increases, and that these differences are statistically significant. The mean test/calculated value of 0.86 obtained with Equation 2.3 for the tests described in this report is considerably less than the mean test/calculated value of 1.02 obtained with Equation 2.3 for the ACI 408 Database (2021). Bar size effects were also observed within the ACI 408 Database (2021) when comparisons were made between groups of specimens with No. 6 (19 mm) and smaller bars, No. 7 to No. 10 (22 to 32 mm) bars, No. 11 (36 mm) bars, and bars larger than No. 11 (36 mm). This trend is evident for both unconfined and confined specimens, although it is more pronounced for unconfined specimens, particularly for Equation 2.5 (ACI 318-19).
3. Two alternatives are proposed for modifying ACI 408R-03 and ACI 318-19 development length equations to obtain similar ratios of test-to-calculated bar stresses across all bar sizes.
    a. *Bar size factor in numerator of development length equation*: Adding a 1.15 factor for No. 11 (36 mm) bars and a 1.25 factor for bars larger than No. 11 (36 mm) to the numerator of

development length Equations 2.3 and 2.5 produces similar mean test/calculated values across bar sizes, with mean ratios between 1.01 and 1.11 for both unconfined and confined bars (ACI 408R-03). This also causes the percentage of specimens with test/calculated values below 1.0 to no longer be correlated with bar size (Section 4.4.4.1). See conclusion 7 for discussion of small bar factor ψ_s.

b. *Exponent on bar diameter*: Multiplying Equation 2.3 (ACI 408R-03) by $d_b^{0.35}$ and Equation 2.5 (ACI 318-19) by $d_b^{0.25}$ results in similar ratios of test-to-calculated bar stresses across all bar sizes (Section 4.4.4.2). This recommendation is similar to that in Ichinose et al. (2004).

4. Transverse reinforcement should be required throughout lap splices on No. 14 and 18 (43 and 57 mm) bars, regardless of bar stress (as recommended by Ferguson and Krishnaswamy (1971)). Even small quantities of confinement ($K_{tr}/d_b = 0.5$) appeared to reduce the size effect.
5. A minimum clear cover of one bar diameter should be required for large-bar lap splices. There is insufficient evidence that lap splices of No. 14 and 18 (43 and 57 mm) bars are functional with less cover. A minimum clear spacing of two bar diameters is also recommended within a lap splice.
6. An unconfined lap splice with a length of $72d_b$ (14-f) failed at a much lower force than expected. A review of prior work indicates there may be a limit beyond which increases in the length of unconfined lap splices do not produce increased bond strengths. Based on this prior work, a review of the ACI 408 Database (2021), and the result obtained for 14-f, it is recommended that development length ℓ_d be limited to $50d_b$ when designing unconfined lap splices (and thus unconfined lap splices classified as Class B in ACI 319-19 should not be longer than $65d_b$).
7. Analyses support the ACI 408-03 recommendation that the ψ_s term in the numerator of the ACI 318-19 development length equation be taken as 1.0 for No. 6 (19 mm) and smaller bars. When $\psi_s = 1.0$, ACI 318-19 has similar test-calculated values for No. 3 to No. 9 (10 to 29 mm) bars, with a mean test/calculated of 1.23 based on the ACI 408 Database (2021). When $\psi_s = 0.8$, a mean

test/calculated of 1.04 is obtained for No. 6 (19 mm) and smaller bars. This is insufficiently conservative for a design equation.

8. Analyses of the ACI 408 Database (2021) show that increasing the limit on $\left(\frac{c_b+K_{tr}}{d_b}\right)$ in the ACI 318-19 development length provisions from 2.5 to 3.5 results in similar mean ratios of test-to-calculated bar stresses for all amounts of confinement.
9. Test results reported herein support prior observations that lap splices fail before yielding of the transverse reinforcement confining a lap splice.
10. The size effect described by fracture mechanics might adequately explain the observed trends. It was also shown that the greater bending stiffness of large bars might contribute to the lower observed bond strengths. This is because large bars have substantially larger moments of inertia than smaller bars and thus bending/prying of large bars might induce non-negligible tensile stresses in the concrete normal to the plane containing the lap-spliced bars.

CHAPTER 6 – REFERENCES

ACI Committee 318 (1995). *Building Code Requirements for Structural Concrete (ACI 318-95) and Commentary (ACI 318R-95)*, American Concrete Institute, Farmington Hills, MI, 370 pp.

ACI Committee 318 (2019). *Building Code Requirements for Reinforced Concrete (ACI 318-19) and Commentary (ACI 318R-19)*, American Concrete Institute, Farmington Hills, MI, 629 pp.

ACI Committee 408 (2003). *Bond and Development of Straight Reinforcing Bars in Tension (ACI 408R-03)*, American Concrete Institute, Farmington Hills, MI, 49 pp.

ACI Committee 408 (2021). *Tension Lap Splice Database*, American Concrete Institute, Farmington Hills, MI. [Available from ACI Store at concrete.org]

ASTM A370-21 (2021). *Standard Test Methods and Definitions for Mechanical Testing of Steel Products*, ASTM International, West Conshohocken, PA, 50 pp.

ASTM A1035/A1035M-20 (2020). *Standard Specification for Deformed and Plain, Low-Carbon, Chromium, Steel Bars for Concrete Reinforcement*, ASTM International, West Conshohocken, PA, 7 pp.

ASTM C33/C33M-18 (2018). *Standard Specification for Concrete Aggregates*, ASTM International, West Conshohocken, PA, 8 pp.

ASTM C39/C39M-21 (2021). Sta*ndard Test Method for Compressive Strength of Cylindrical Concrete Specimens*, ASTM International, West Conshohocken, PA, 8 pp.

ASTM C138/C138M-17a (2017). *Standard Test Method for Density (Unit Weight), Yield, and Air Content (Gravimetric) of Concrete*, ASTM International, West Conshohocken, PA, 6 pp.

ASTM C143/C143M-20 (2020). *Standard Test Method for Slump of Hydraulic-Cement Concrete*, ASTM International, West Conshohocken, PA, 4 pp.

ASTM C150/C150M-21 (2021). *Standard Specification for Portland Cement*, ASTM International, West Conshohocken, PA, 9 pp.

ASTM C172/C172M-17 (2017). *Standard Practice for Sampling Freshly Mixed Concrete*, ASTM International, West Conshohocken, PA, 2017, 3 pp.

ASTM C192/C192M-19 (2019). *Standard Practice for Making and Curing Concrete Test Specimens in the Laboratory*, ASTM International, West Conshohocken, PA, 2019, 8 pp.

ASTM C494/C494M-19 (2019). *Standard Specification for Chemical Admixtures for Concrete*, ASTM International, West Conshohocken, PA, 15 pp.

ASTM C1017/C1017M-13e1 (2013). *Standard Specification for Chemical Admixtures for Use in Producing Flowing Concrete*, ASTM International, West Conshohocken, PA, 9 pp.

ASTM C1064/C1064M-17 (2017). *Standard Test Method for Temperature of Freshly Mixed Hydraulic-Cement Concrete*, ASTM International, West Conshohocken, PA, 3 pp.

ASTM C1602/C1602M-18 (2018). *Standard Specification for Mixing Water Used in the Production of Hydraulic Cement Concrete*, ASTM International, West Conshohocken, PA, 5 pp.

ASTM E8/E8M-21 (2021). *Standard Test Methods for Tension Testing of Metallic Materials*, ASTM International, West Conshohocken, PA, 30 pp.

Briggs, M., Miller, S., Darwin, D., and Browning, J., (2007). *Bond Behavior of Grade 100 ASTM A 1035 Reinforcing Steel in Beam-Splice Specimens*, SL Report 07-1, University of Kansas Center for Research, Lawrence, KS, 92 pp.

CEB-FIP (2010). *Model Code for Concrete Structures*, International Federation for Structural Concrete (fib), Lausanne, Switzerland, 432 pp.

Darwin, D., Tholen, M. L., Idun, E. K., and Zuo, J., (1996a). "Splice Strength of High Relative Rib Area Reinforcing Bars," *ACI Structural Journal*, 93(1), 95-107.

Darwin, D., Zuo, J., Tholen, M. L., and Idun, E. K., (1996b). "Development Length Criteria for Conventional and High Relative Rib Area Reinforcing Bars," *ACI Structural Journal*, 93(3), 347-359.

Darwin, D., and Dolan, C., (2021). *Design of Concrete Structures*, 16th Edition, McGraw Hill, 864 pp.

Ferguson, P. M., and Krishnaswamy, C. N., (1971). *Tensile Lap Splices Part 2: Design Recommendations for Retaining Wall Splices and Large Bar Splices*, Report No. 113-3. TX: The Texas Highway Department, 67 pp.

Ferguson, P. M., and Thompson, J. N., (1965). "Development Length for Large High Strength Reinforcing Bars," *ACI Journal Proceedings*, 62(1), 71-94.

Frosch, R., Fleet, E., and Glucksman, R., (2020). *Development and Splice Lengths for High-Strength Reinforcement, Volume I: General Bar Development*, Charles Pankow Foundation, 358 pp.

Glucksman, R., (2018). *Bond Strength of ASTM A615 Grade 100 Reinforcement for Beams*, Master's Thesis, Lyles School of Civil Engineering, Purdue University, West Lafayette, IN., 226 pp.

Hassan, T. K., Lucier, G. W., and Rizkalla, S. H., (2012). "Splice Strength of Large Diameter, High Strength Steel Reinforcing Bars," *Construction and Building Materials*, 26, 216-225.

Hegger, J., Schnell, J., Empelmann, M., Schoening, J., Schäfer, M., Oettel, V., (2015). *Weiterentwicklung von Bemessungs- und Konstruktionsregeln bei großen Stabdurchmessern (>Ø 32 mm, B500)*. Final report, Research Project 16992 N/1, German Federation of Industrial Research Associations (AiF).Ichinose, T., Kanayama, Y., Inoue, Y., and Bolander Jr., J. E., (2004). "Size Effect on Bond Strength of Deformed Bars," *Construction and Building Materials*, 18(7), 549-558.

Orangun, C. O., Jirsa, J. O., and Breen, J. E., (1977), "Reevaluation of Test Data on Development Length and Splices," *ACI Journal Proceedings*, 74(3), 114-122.

Richter, B. P., (2012), *A New Perspective on the Tensile Strength of Lap Splices in Reinforced Concrete Members*, Master's Thesis, Lyles School of Civil Engineering, Purdue University, West Lafayette, IN., 187 pp.

Seliem, H. M., Hosny, A., Rizkalla, S., Zia, P., Briggs, M., Miller, S., Darwin, D., Browning, J., Glass, G. M., Hoyt, K., Donnelly, K., and Jirsa, J. O., (2009). "Bond Characteristics of ASTM A1035 Steel Reinforcing Bars," *ACI Structural Journal*, 106(4), 530-539.

Thompson, M. A., Jirsa, J. O., Breen, J. E., and Meinheit, D. F., (1979). "Behavior of Multiple Lap Splices in Wide Sections," *ACI Journal Proceedings*, 76(2), 227-248.

Zuo, J., and Darwin, D., (1998). *Bond Strength of High Relative Rib Area Reinforcing Bars*, SM Report No. 46, University of Kansas Center for Research, Lawrence, KS., 332 pp.

Zuo, J., and Darwin, D., (2000). "Splice Strength of Conventional and High Relative Rib Area Bars in Normal and High-Strength Concrete," *ACI Structural Journal*, 97(4), 630-641.

APPENDIX A: SPECIMEN DRAWINGS

Figures A.1 through A.11 show profile (elevation) and plan views for each of the 11 specimens in this study. Cross-section drawings are shown in Figures A.12 through A.22. The drawings show the lap-spliced bars at the bottom of the beam, as they were for concrete placement. Specimens were then inverted and tested with the lap splice at the top of the specimens for convenience (Section 3.4). Values of K_{tr}/d_b in Figures A.1 through A.11 are the target value set during initial design.

The drawings show the nominal specimen dimensions. Relevant as-built dimensions are in Table A.1. As-built dimensions were measured at multiple places throughout the lap splice region after testing was complete, then averaged. Measurements of clear cover were taken from the concrete face to the non-deformed bar edge (in between bar deformations). As-built beam cross-section height (*h*) and width (*b*), lap splice length (ℓ_s), and transverse reinforcement spacing (*S1*) were within 0.25 in. (6 mm) of the nominal dimensions, so nominal dimensions are used throughout except for development length calculations.

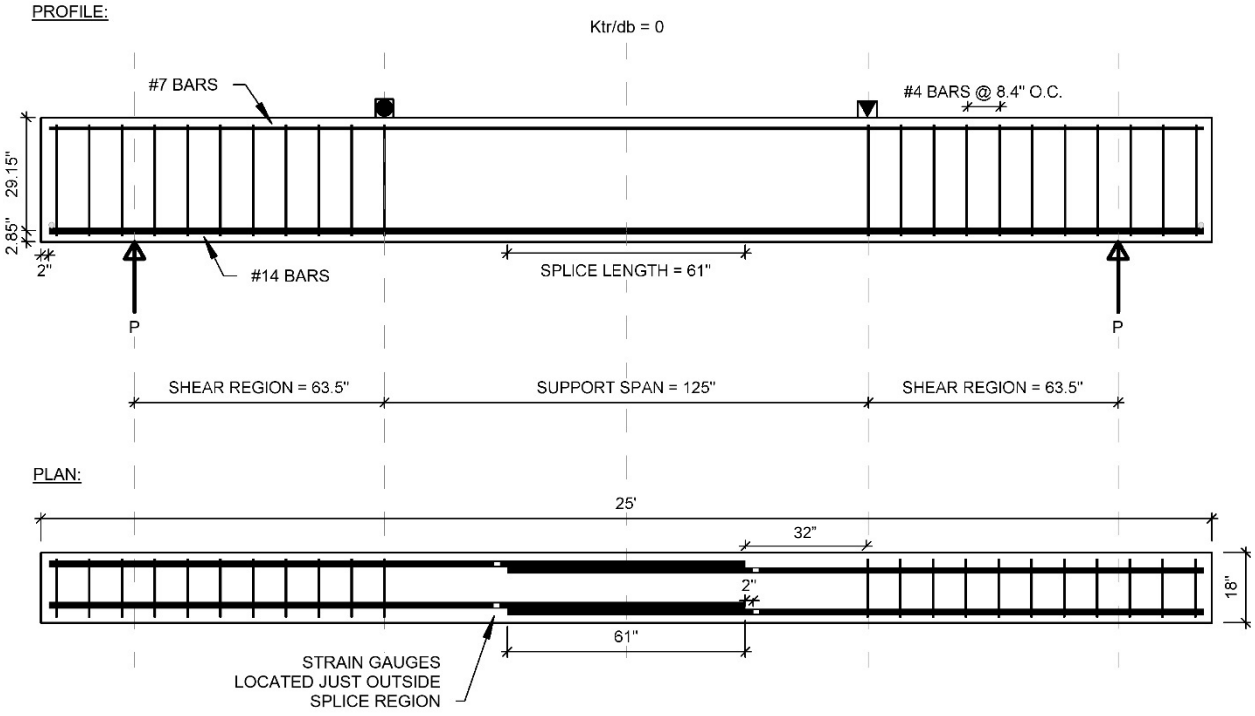

Figure A.1: Profile and plan of 14-a (1 in. = 25.4 mm)

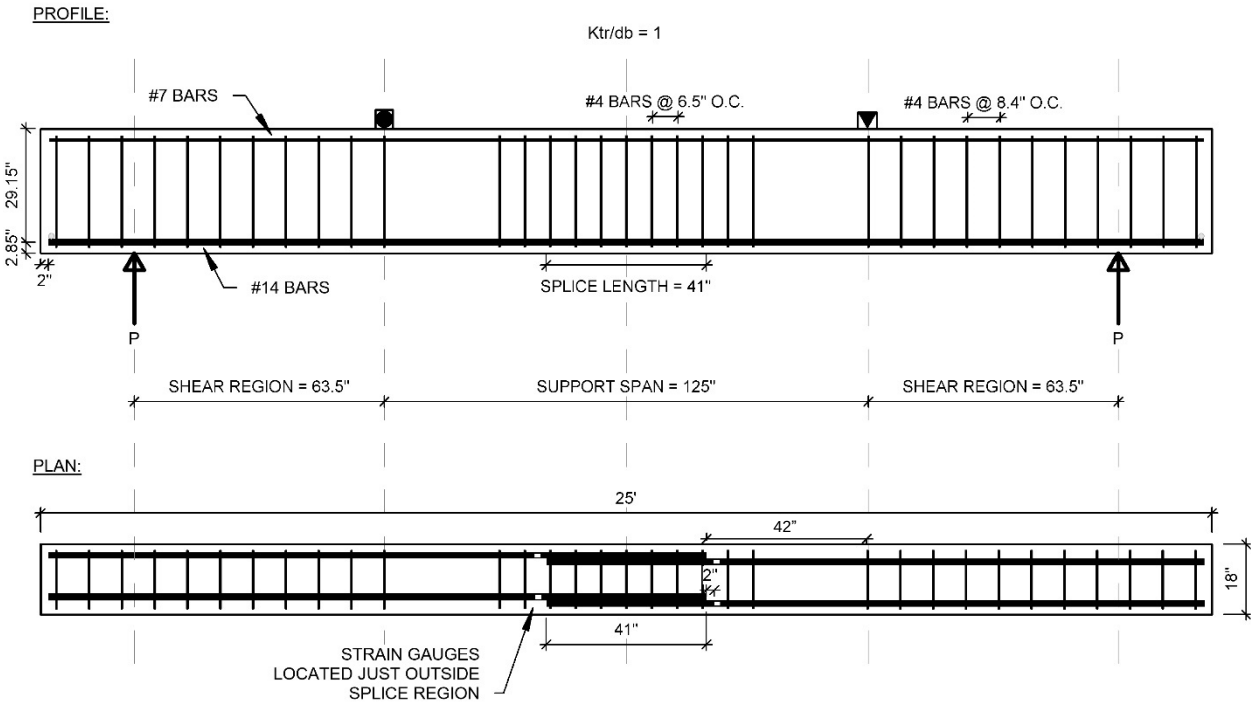

Figure A.2: Profile and plan of 14-b (1 in. = 25.4 mm)

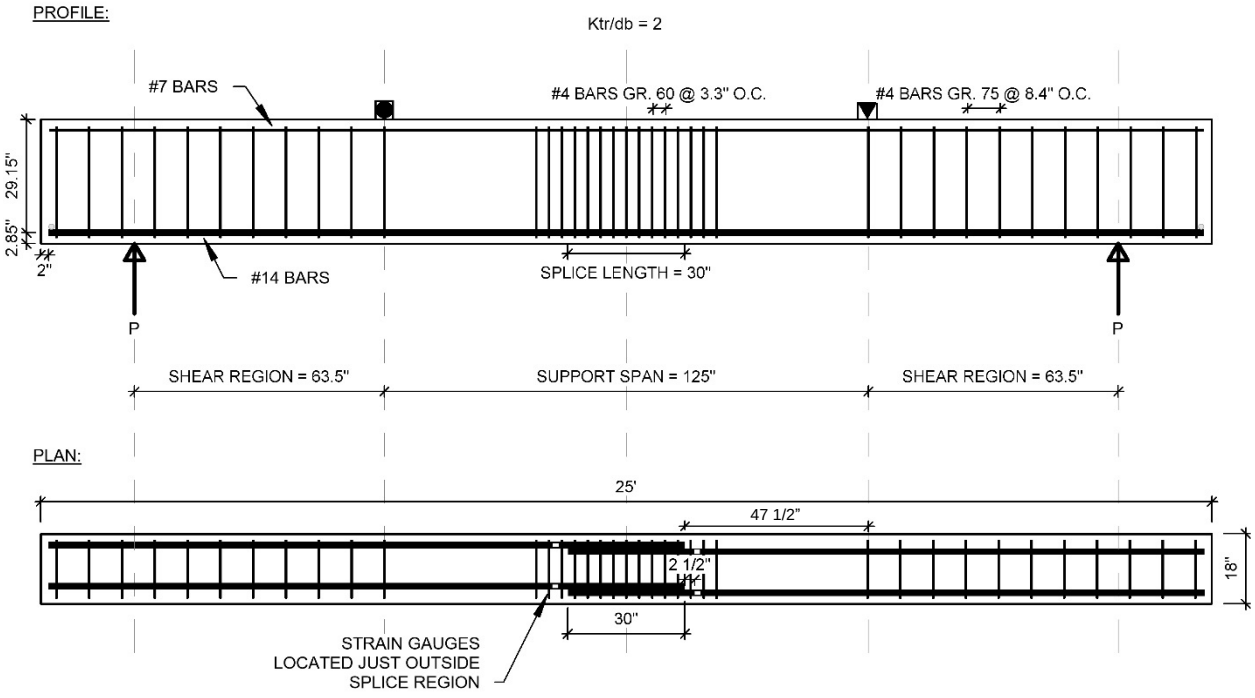

Figure A.3: Profile and plan of 14-c (1 in. = 25.4 mm)

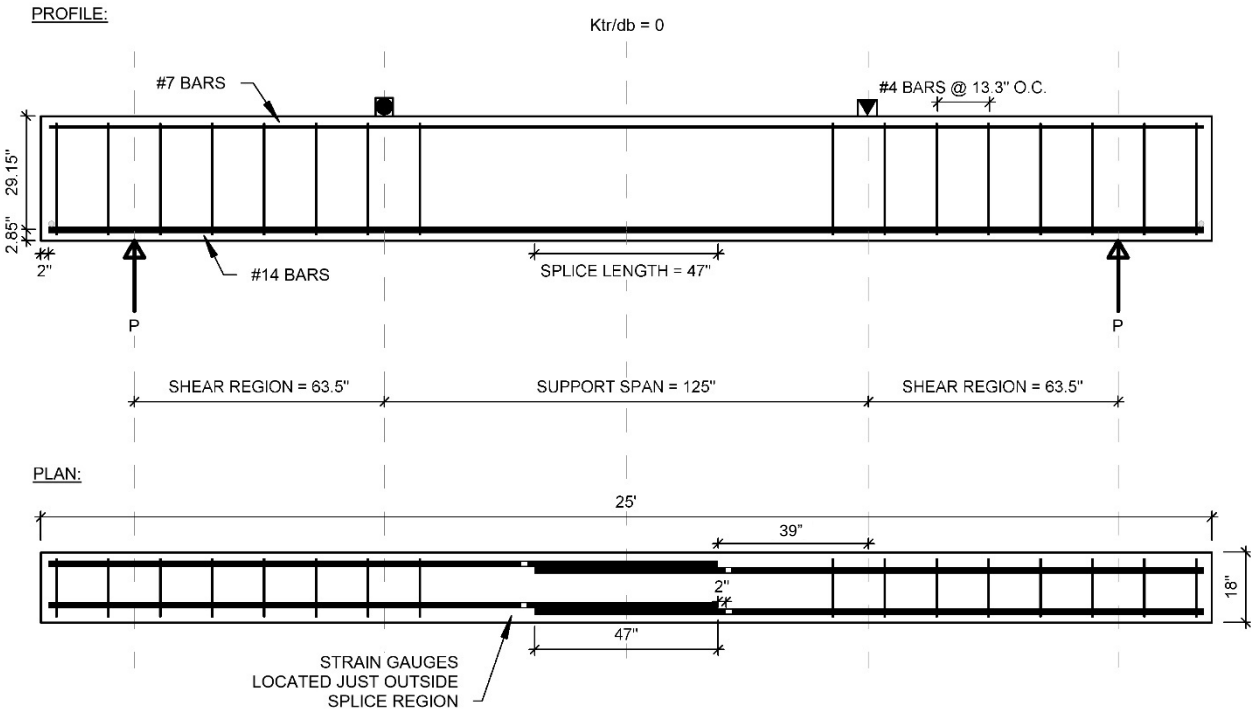

Figure A.4: Profile and plan of 14-d (1 in. = 25.4 mm)

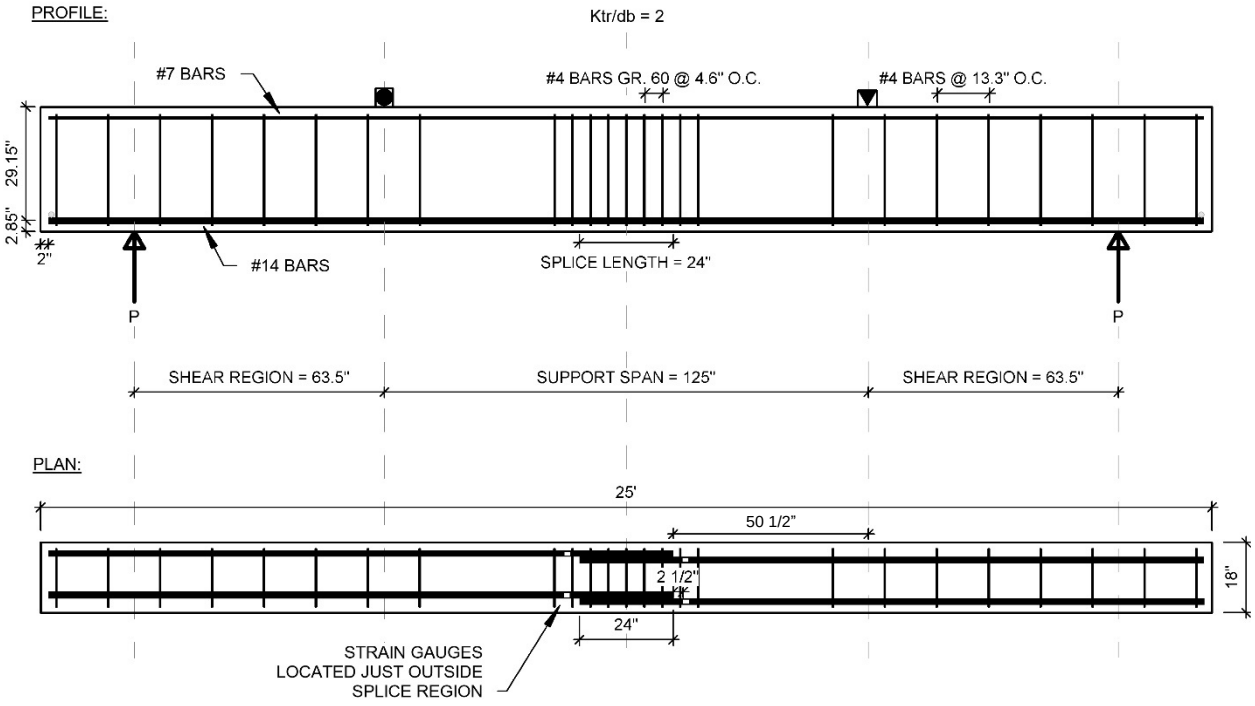

Figure A.5: Profile and plan of 14-e (1 in. = 25.4 mm)

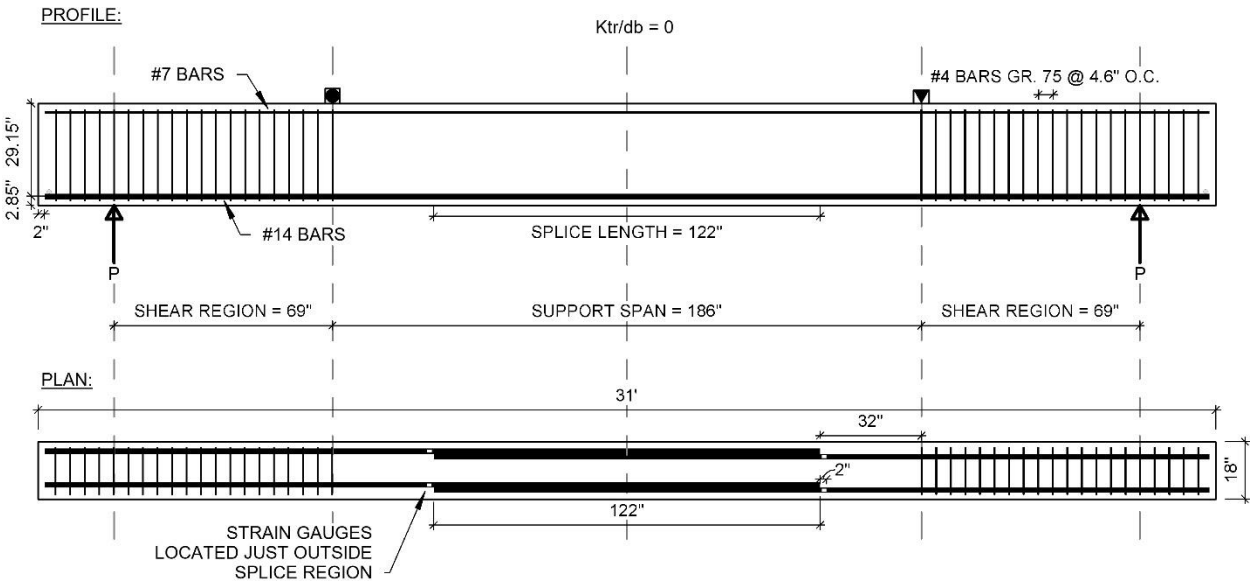

Figure A.6: Profile and plan of 14-f (1 in. = 25.4 mm)

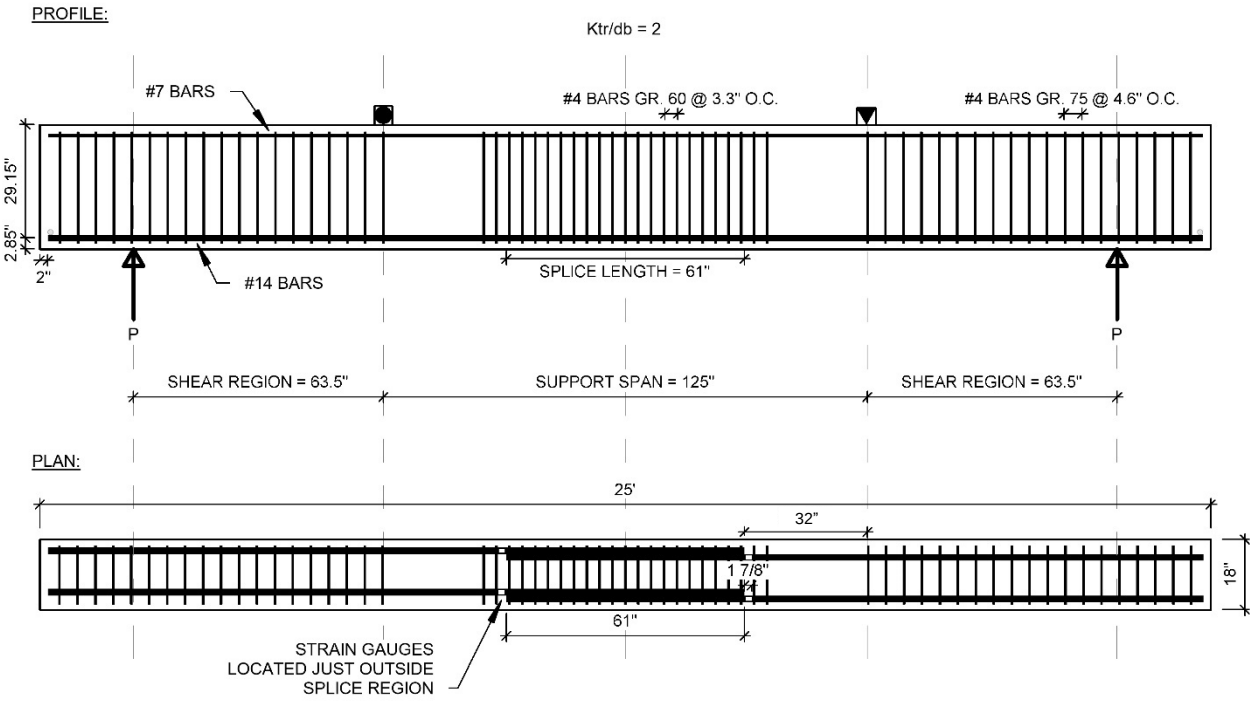

Figure A.7: Profile and plan of 14-g (1 in. = 25.4 mm)

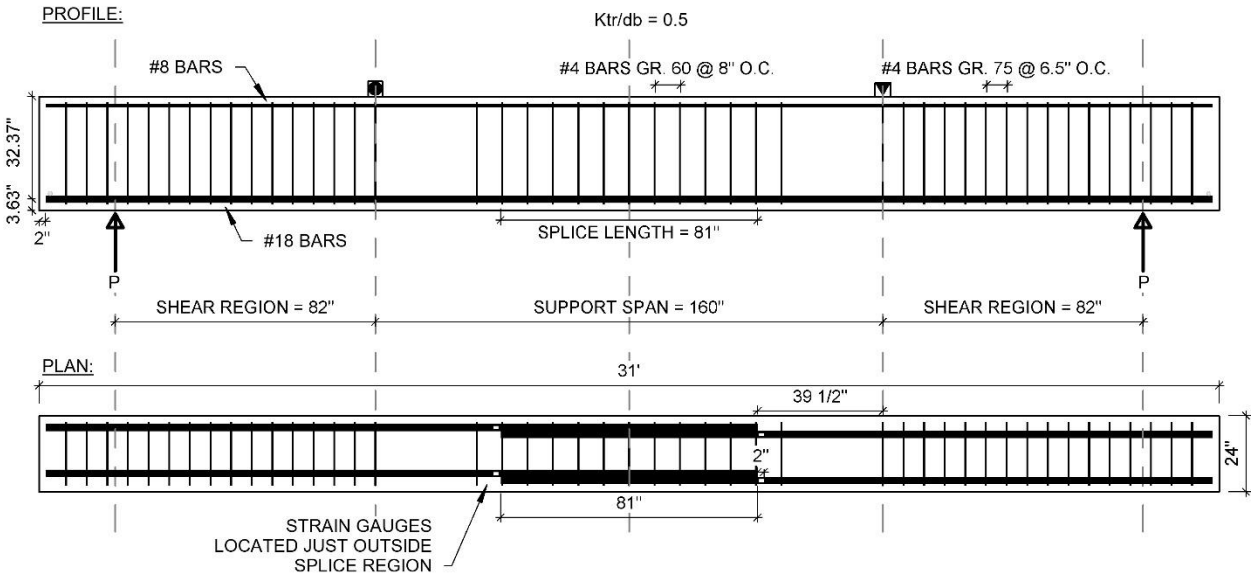

Figure A.8: Profile and plan of 18-a (1 in. = 25.4 mm)

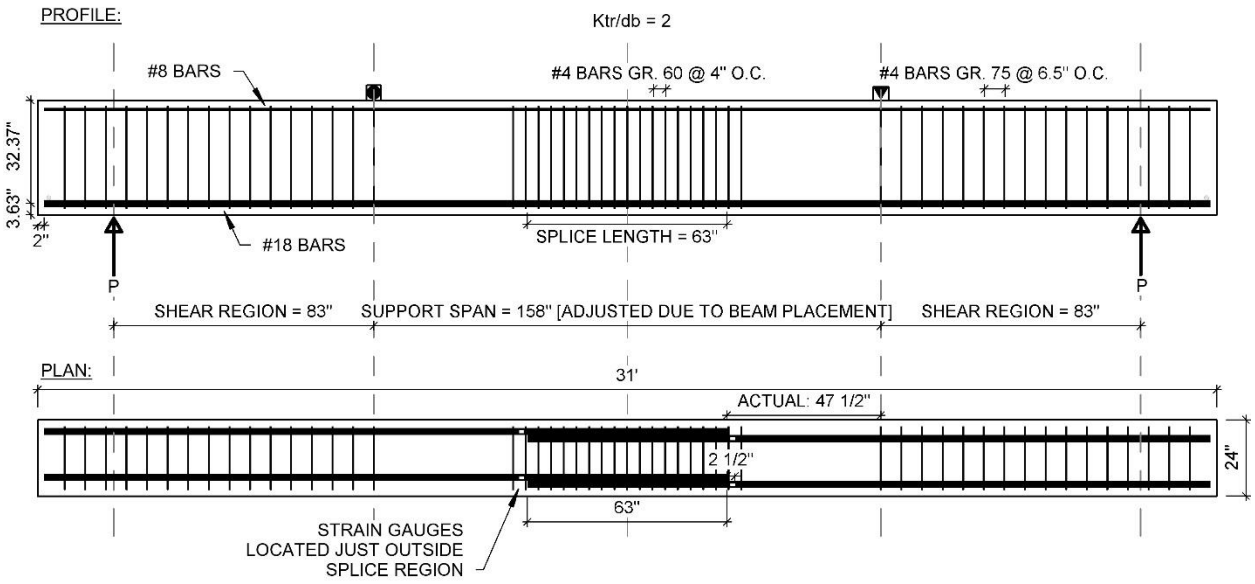

Figure A.9: Profile and plan of 18-b (1 in. = 25.4 mm)

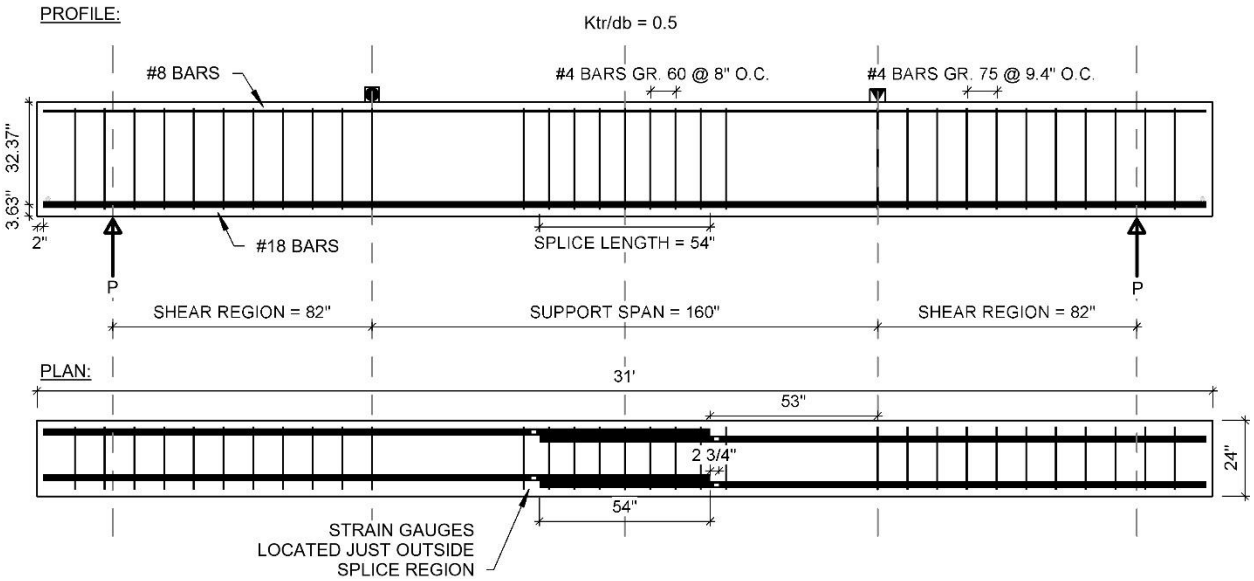

Figure A.10: Profile and plan of 18-c (1 in. = 25.4 mm)

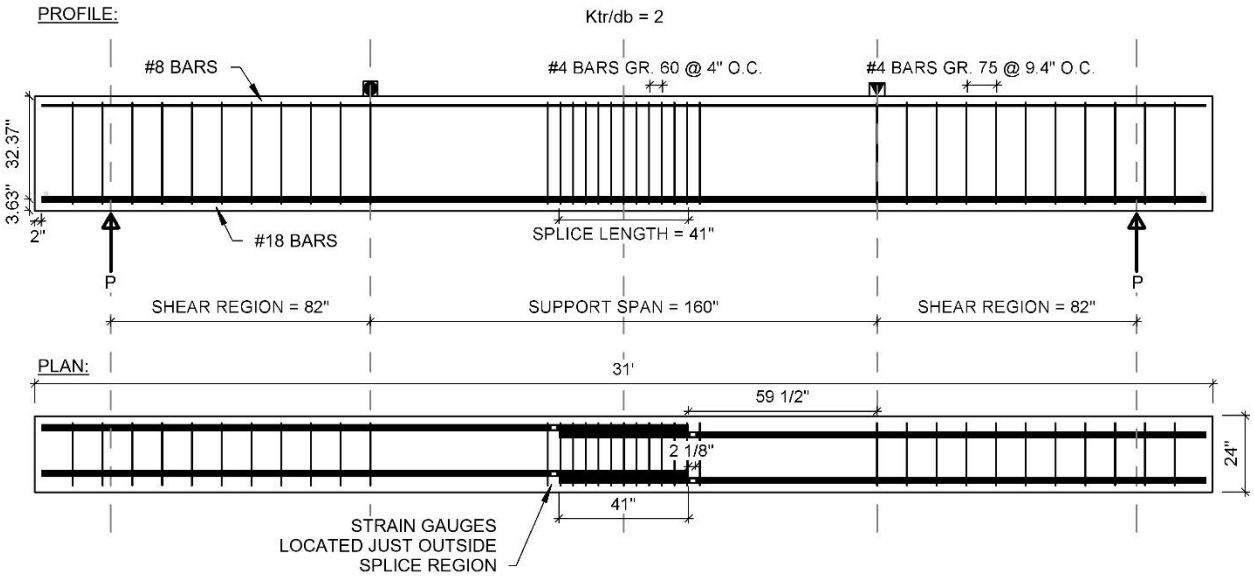

Figure A.11: Profile and plan of 18-d (1 in. = 25.4 mm)

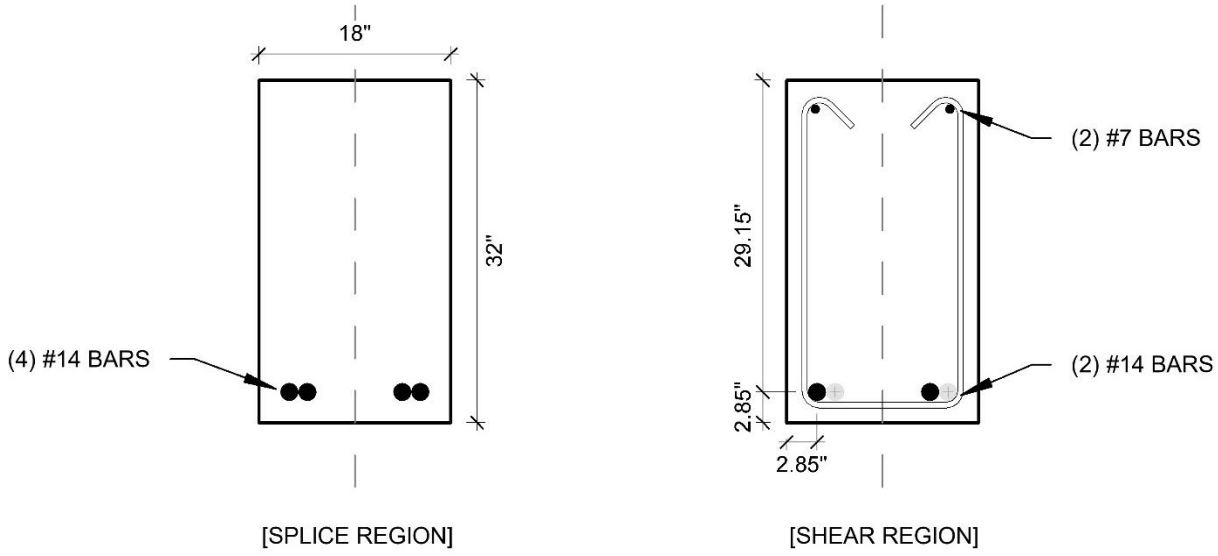

Figure A.12: Cross section of 14-a (1 in. = 25.4 mm)

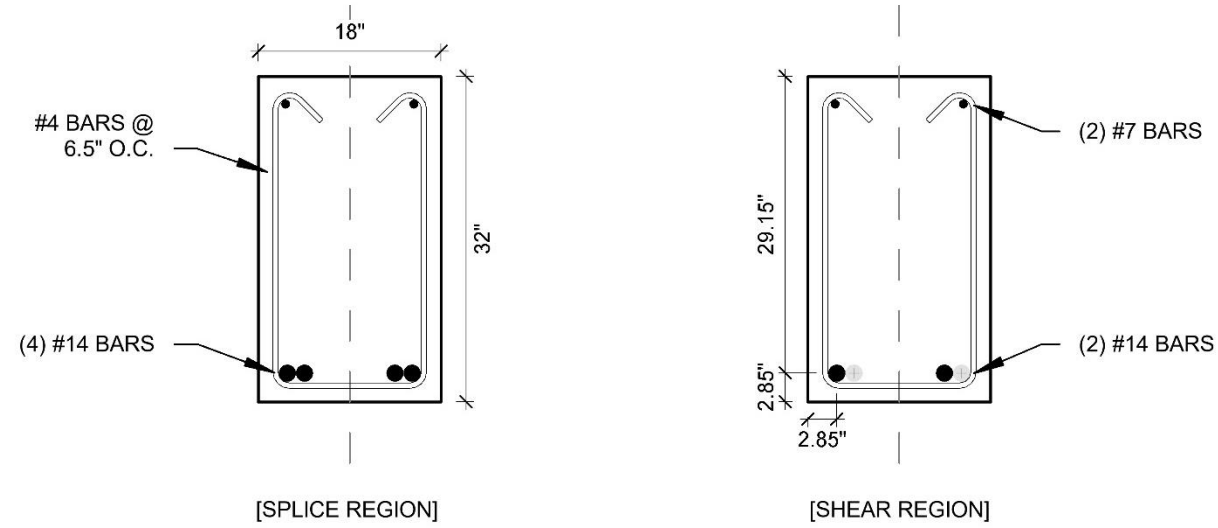

Figure A.13: Cross section of 14-b (1 in. = 25.4 mm)

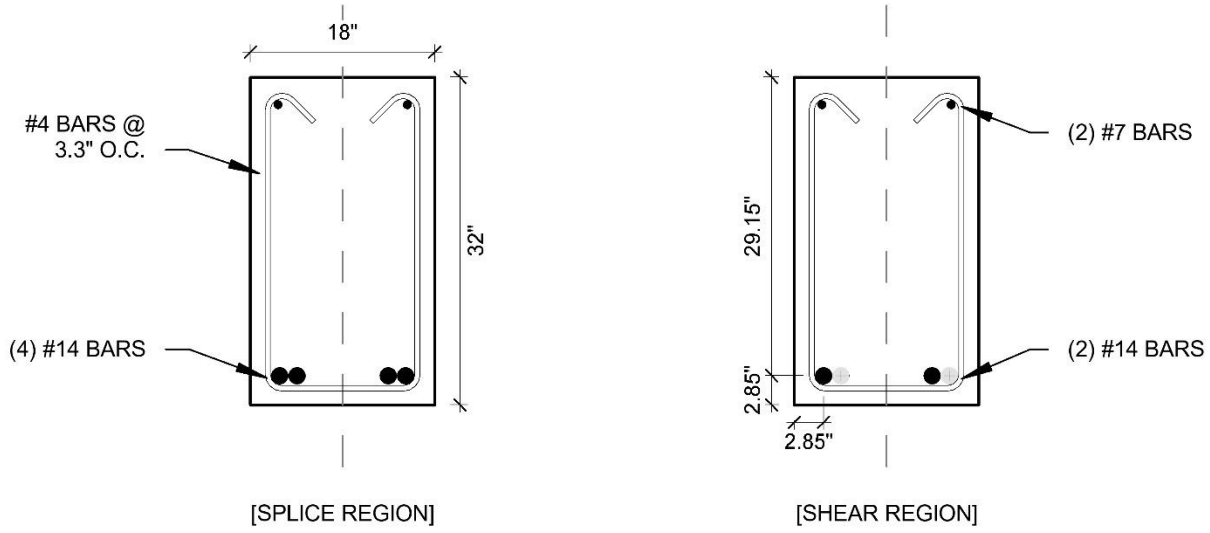

Figure A.14: Cross section of 14-c (1 in. = 25.4 mm)

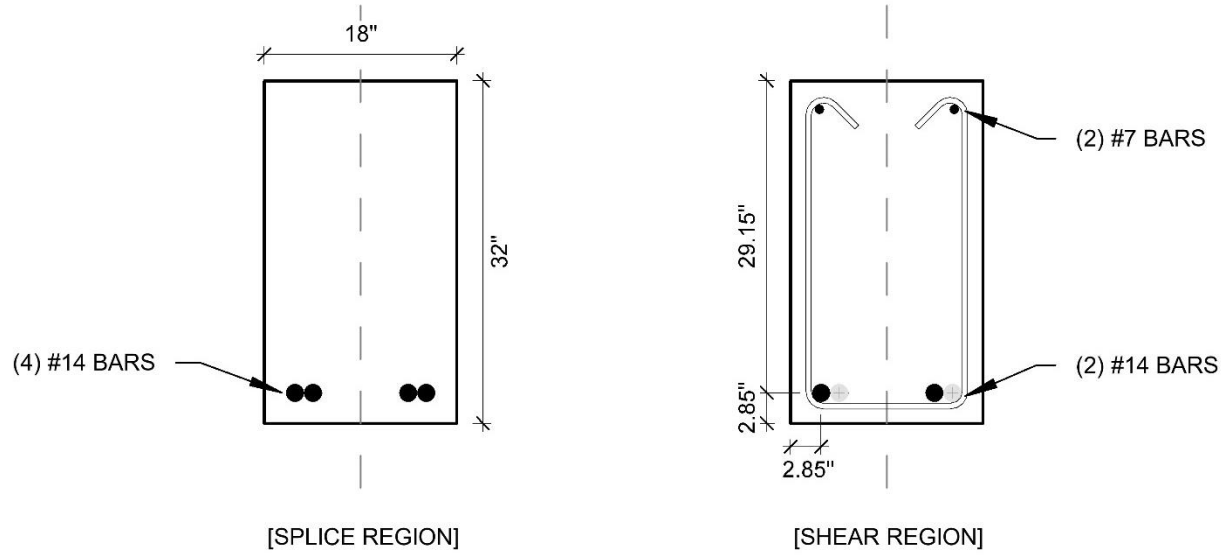

Figure A.15: Cross section of 14-d (1 in. = 25.4 mm)

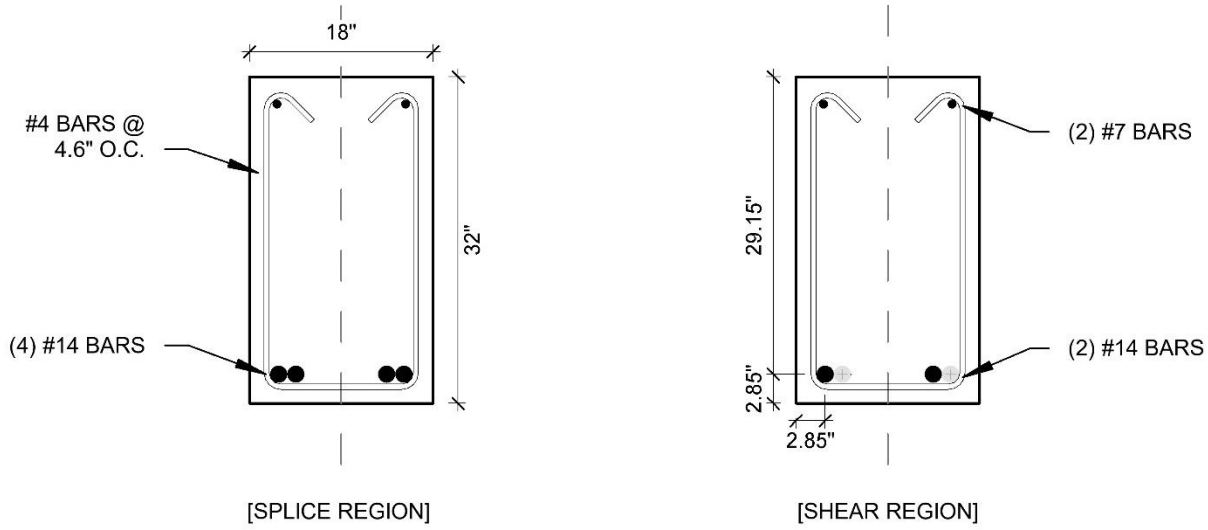

Figure A.16: Cross section of 14-e (1 in. = 25.4 mm)

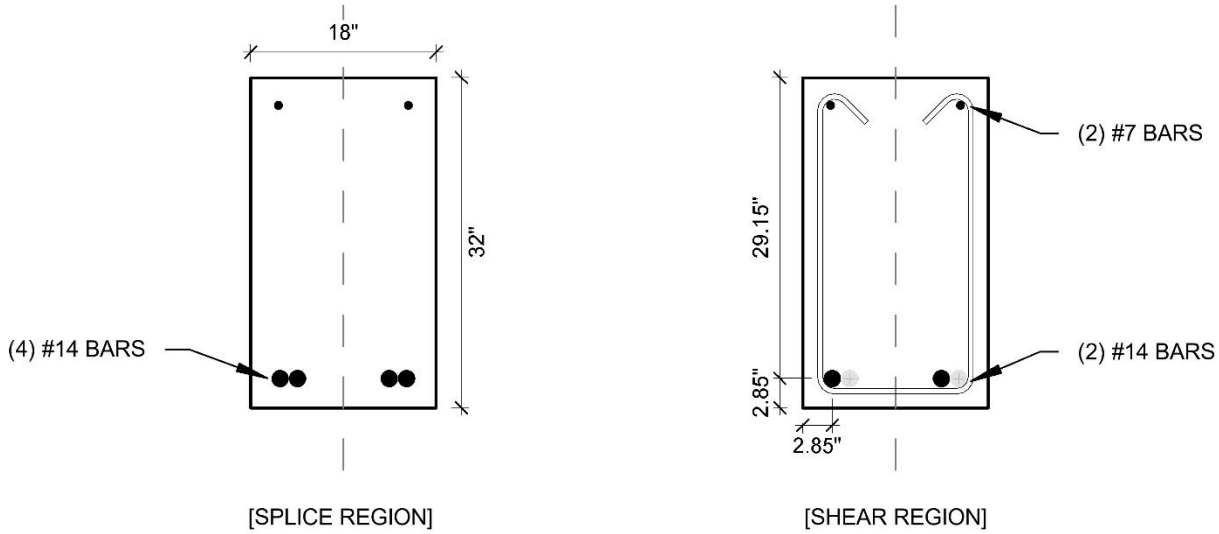

Figure A.17: Cross section of 14-f (1 in. = 25.4 mm)

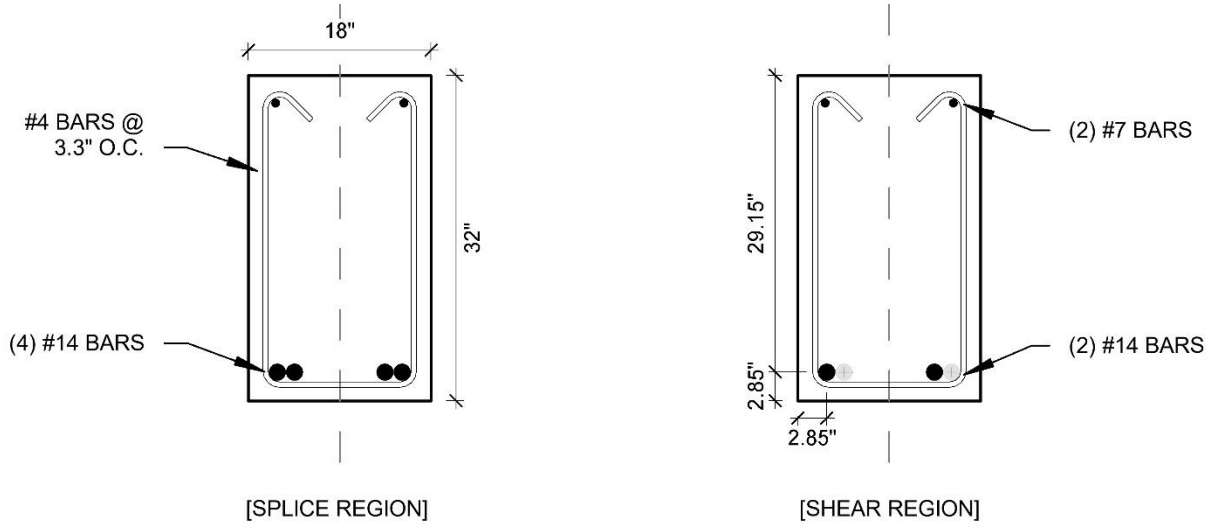

Figure A.18: Cross section of 14-g (1 in. = 25.4 mm)

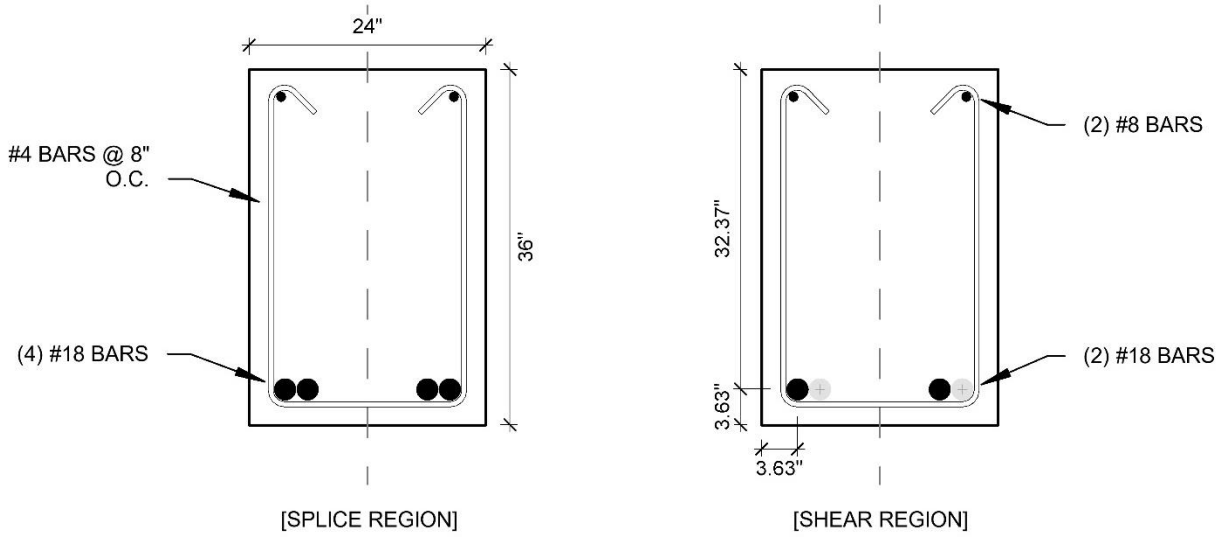

Figure A.19: Cross section of 18-a (1 in. = 25.4 mm)

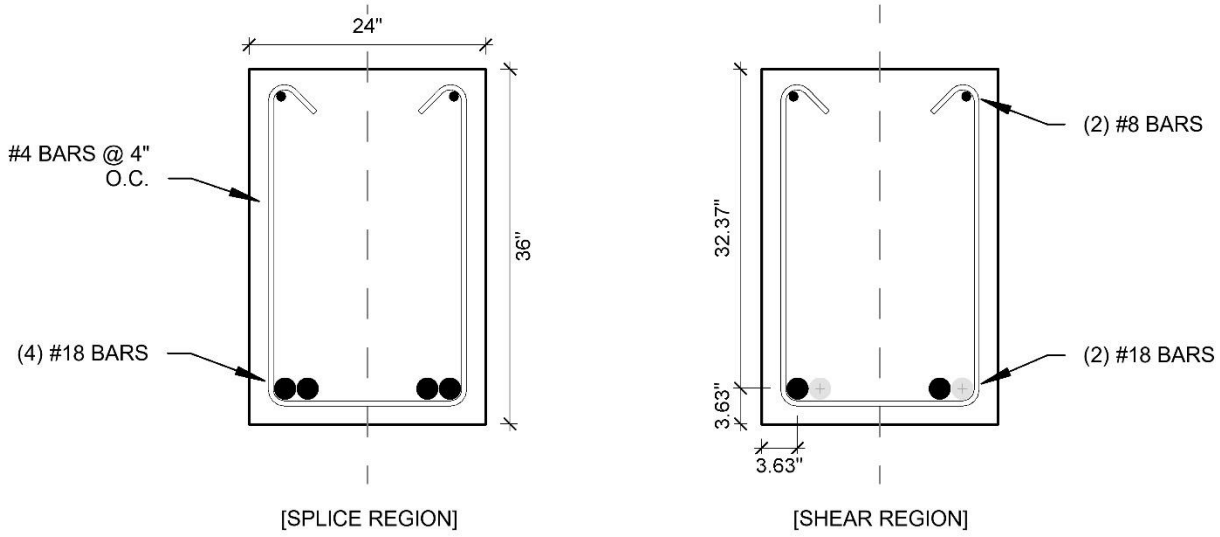

Figure A.20: Cross section of 18-b (1 in. = 25.4 mm)

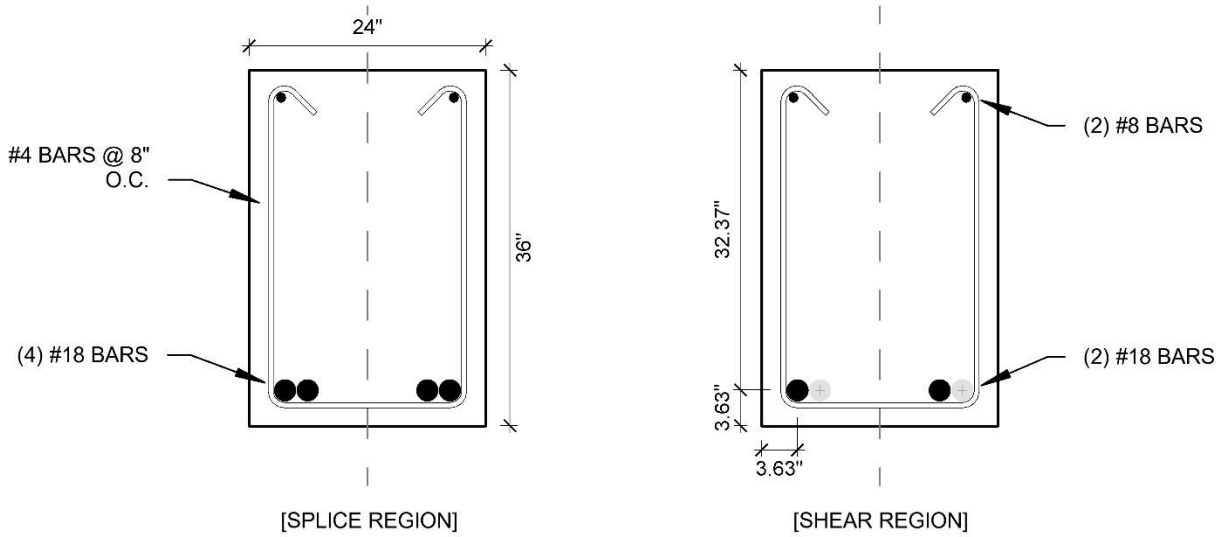

Figure A.21: Cross section of 18-c (1 in. = 25.4 mm)

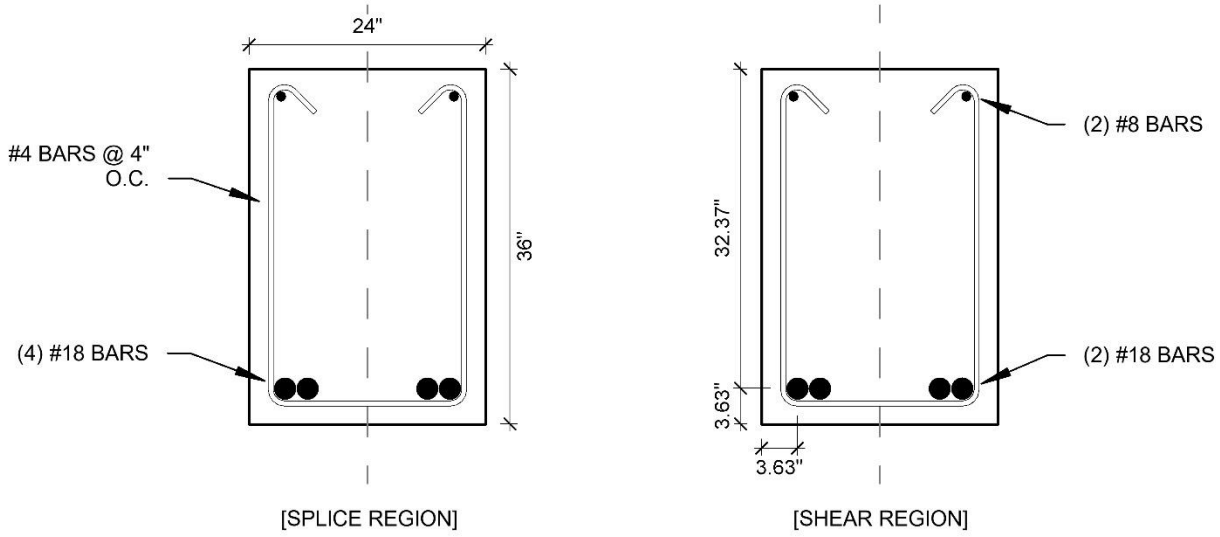

Figure A.22: Cross section of 18-d (1 in. = 25.4 mm)

Table A.1: As-built dimensions [a]

Specimen ID	*h*, in.	*b*, in.	c_{min}, in. (clear)	c_{max}, in. (clear)
14-a	32	18	1.94	2.26
14-b	32	18	2.03	2.21
14-c	32	18	2.02	2.40
14-d	32	18	1.84	2.25
14-e	32	18	1.98	2.34
14-f	32	18	2.01	2.35
14-g	32	18	2.08	2.28
18-a	36	24	2.30	2.95
18-b	36	24	2.47	2.86
18-c	36	24	2.52	2.75
18-d	36	24	2.34	2.89

[a] 1 in. = 25.4 mm

APPENDIX B: STRESS VERSUS STRAIN FOR REINFORCEMENT

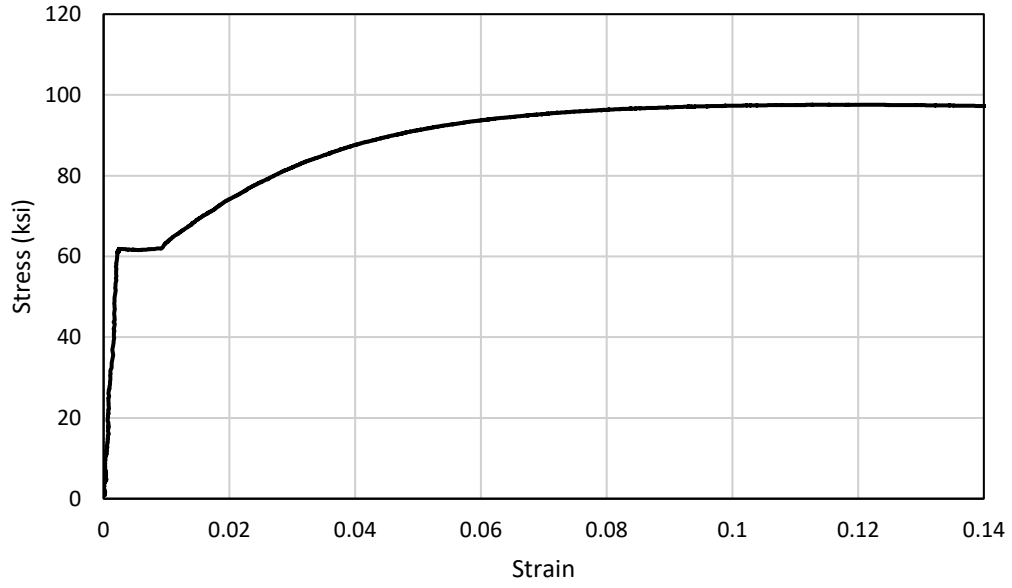

Figure B.1: Stress versus strain for No. 4 Grade 60 (13 mm, 420) transverse reinforcement, 14-a to 14-g (nominal area of specimen: 0.2 in^2 (130 mm^2), average sample yield stress: 62.2 ksi (429 MPa)) (1 ksi = 6.895 MPa)

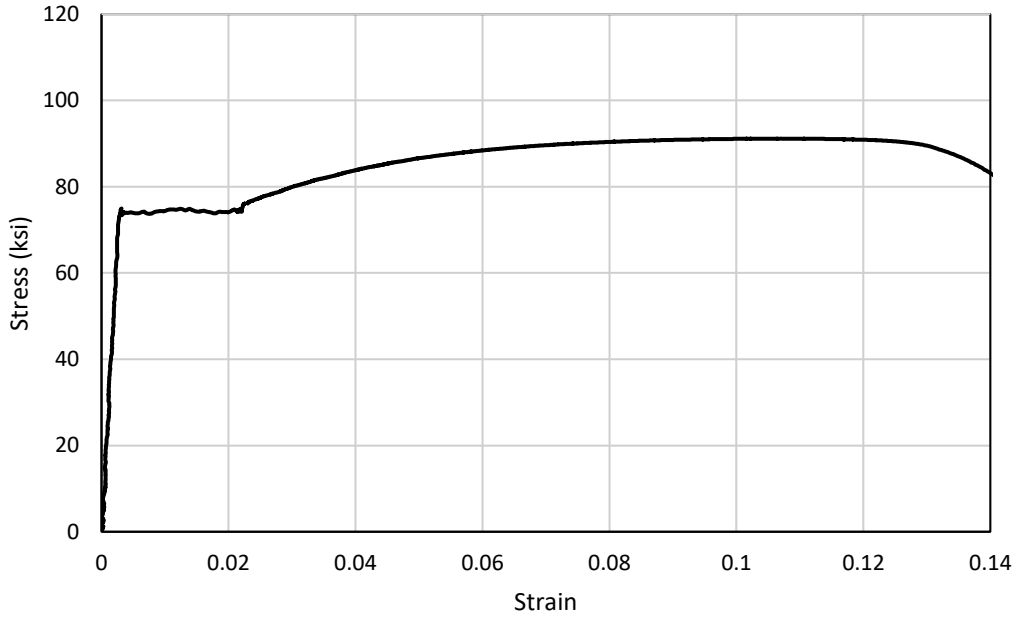

Figure B.2: Stress versus strain for No. 4 Grade 60 (13 mm, 420) transverse reinforcement, 18-a to 18-d (nominal area of specimen: 0.2 in^2 (130 mm^2), average sample yield stress: 74.0 ksi (510 MPa)) (1 ksi = 6.895 MPa)

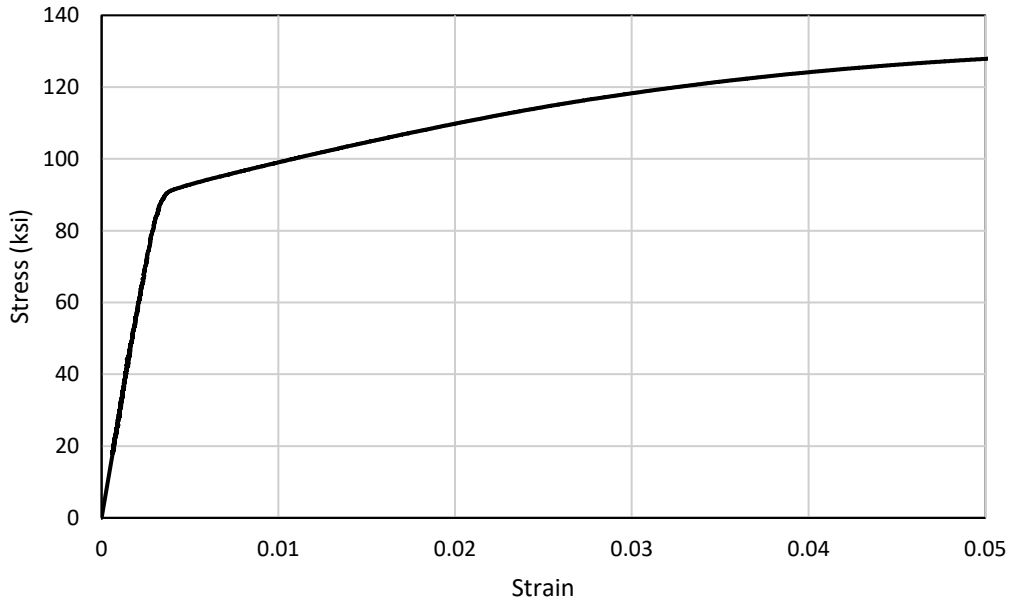

Figure B.3: Stress versus strain for No. 14 Grade 80 (43 mm, 550) longitudinal reinforcement, 14-a to 14-e (nominal area of specimen: 2.25 in^2 (1450 mm^2), average sample yield stress: 92.6 ksi (638 MPa)) (1 ksi = 6.895 MPa)

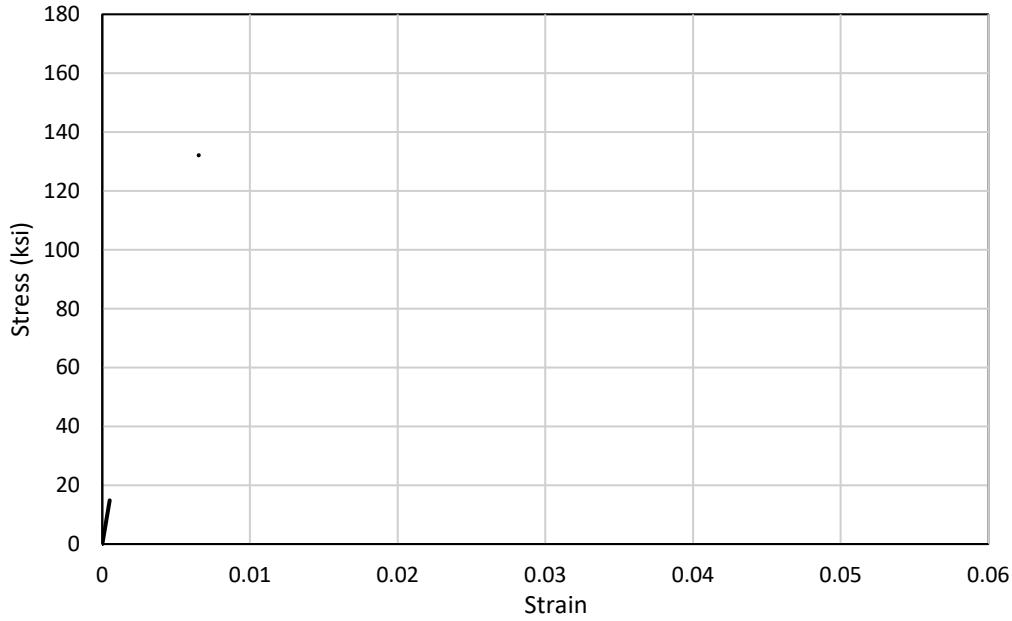

Figure B.4: Stress versus strain for No. 14 Grade 120 (43 mm, 830) longitudinal reinforcement, 14-f and 14-g (nominal area of specimen: 2.25 in^2 (1450 mm^2), average sample yield stress: 134.6 ksi (928 MPa)) (1 ksi = 6.895 MPa)

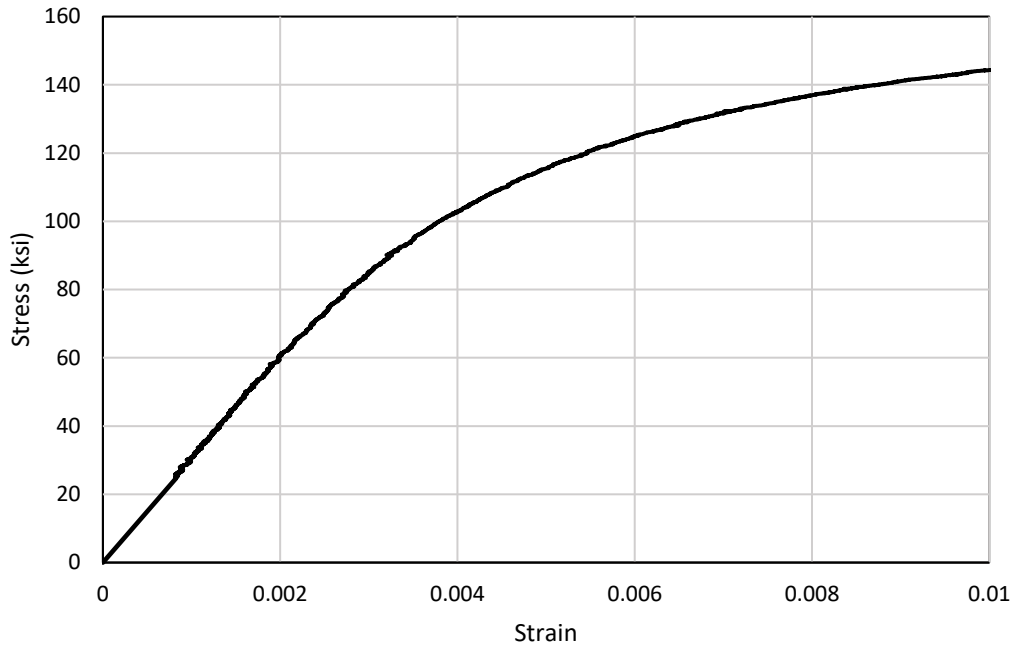

Figure B.5: Stress versus strain for No. 18 Grade 120 (57 mm, 830) longitudinal reinforcement, 18-g and 18-d (nominal area of specimen: 4.0 in^2 (2580 mm^2), average sample yield stress: 129.4 ksi (892 MPa)) (1 ksi = 6.895 MPa)

APPENDIX C: PLASTIC CONCRETE PROPERTIES

Table C.1 provides the plastic properties of each concrete batch used in this study. The unit weight, slump, and concrete temperature were determined in accordance with ASTM C138, C143, and C1064, respectively.

Table C.1: Specimen plastic concrete properties [a]

Specimen ID	Unit Weight, lb/ft^3	Slump, in.	Concrete Temperature, ˚F
14-a	147.9	6.50	73
14-b	147.6	4.25	60
14-c	146.9	5.75	60
14-d	149.4	6.50	62
14-e	150.7	9.50	69
14-f	145.4	8.00	70
14-g	146.7	6.00	62
18-a	147.8	3.75	68
18-b	147.7	4.25	71
18-c	151.8	6.50	79
18-d	151.8	6.00	83

[a] 1 lb/ft^3 = 16.02 kg/m^3, 1 in. = 25.4 mm, (˚F-32) x 5/9 = ˚C

APPENDIX D: APPLIED LOAD VERSUS DEFLECTION

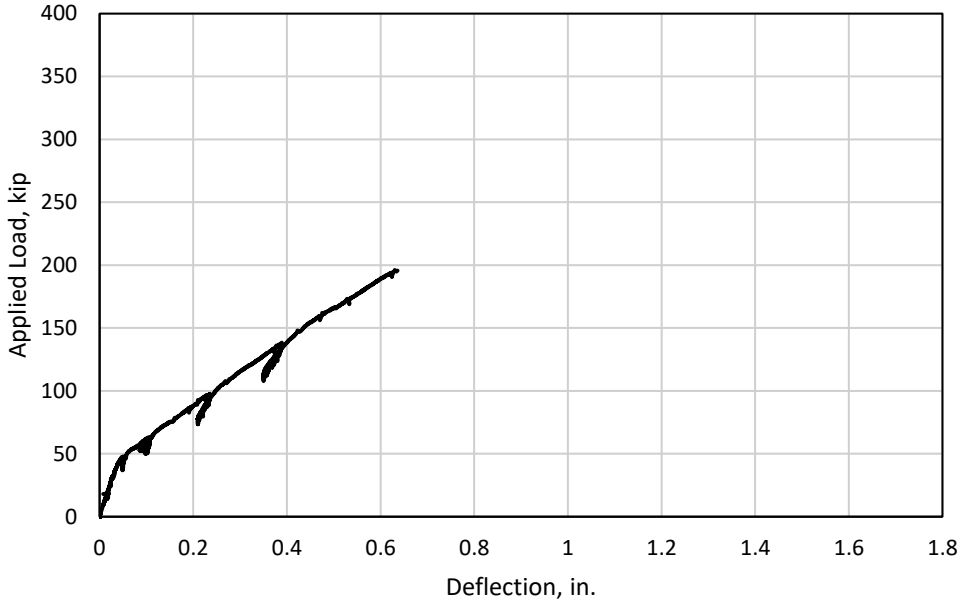

Figure D.1: Load-Deflection for 14-a (1 kip = 4.448 kN, 1 in. = 25.4 mm)

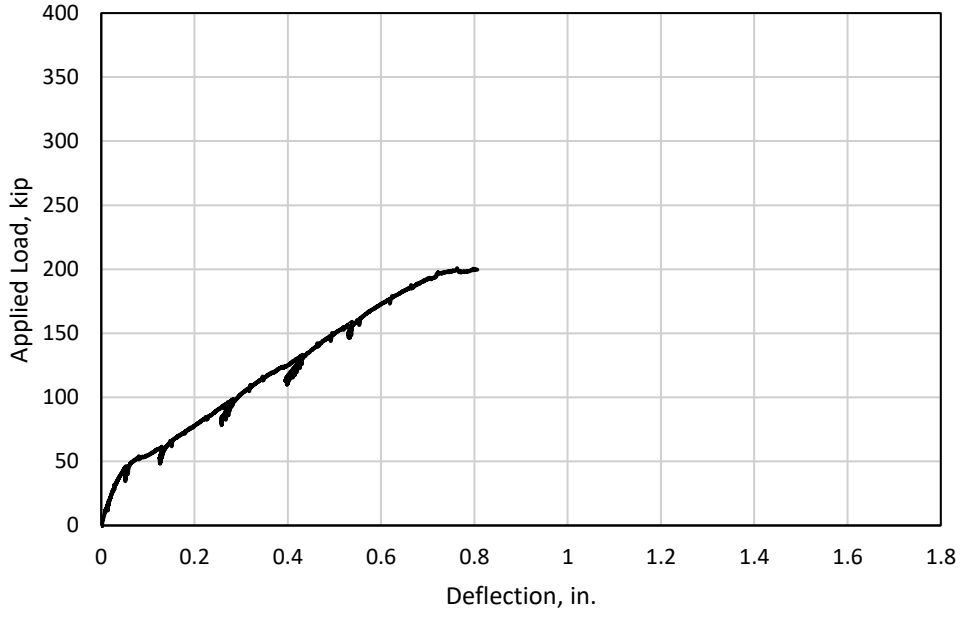

Figure D.2: Load-Deflection for 14-b (1 kip = 4.448 kN, 1 in. = 25.4 mm)

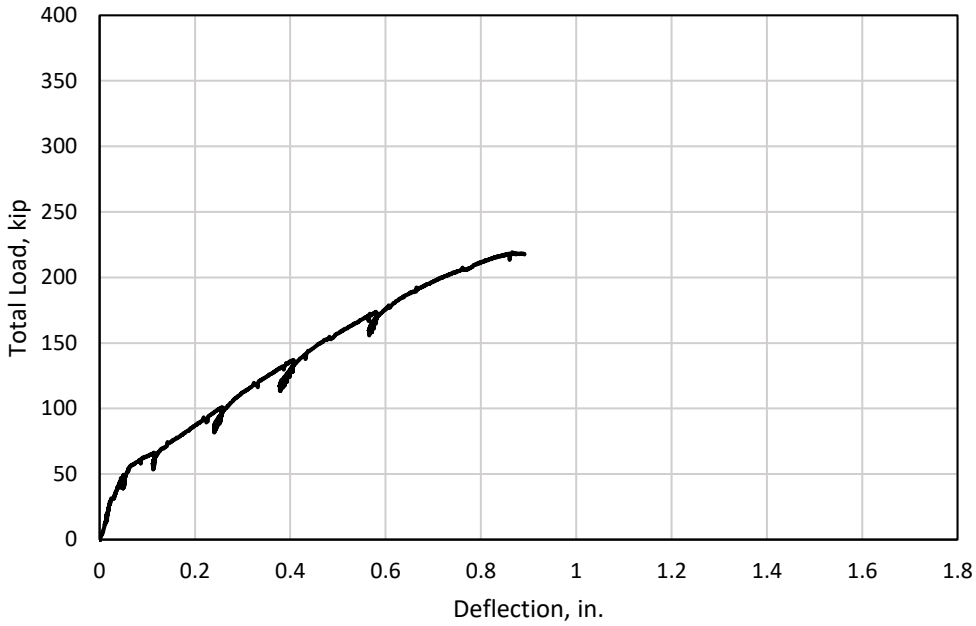

Figure D.3: Load-Deflection for 14-c (1 kip = 4.448 kN, 1 in. = 25.4 mm)

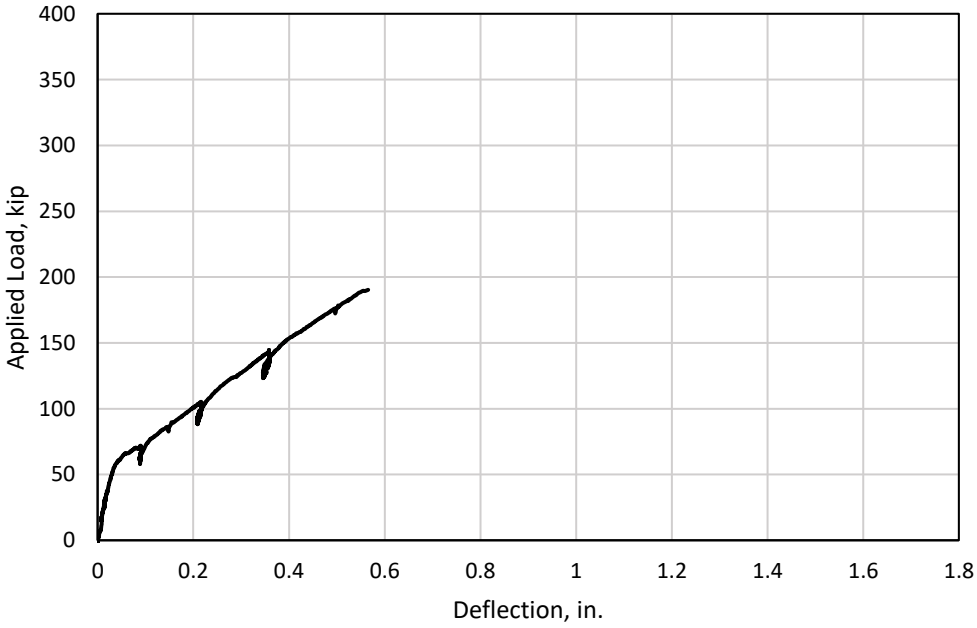

Figure D.4: Load-Deflection for 14-d (1 kip = 4.448 kN, 1 in. = 25.4 mm)

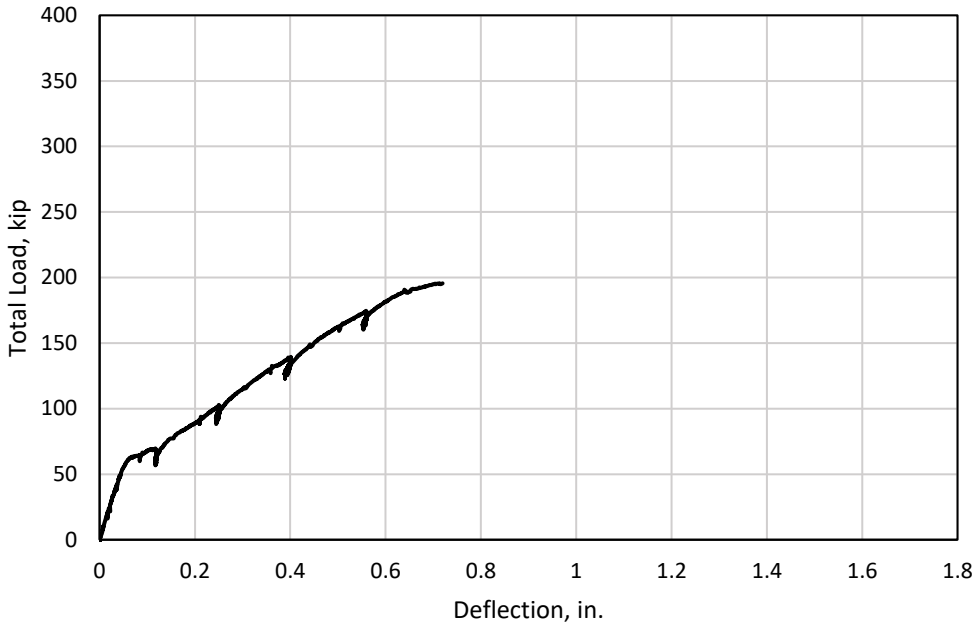

Figure D.5: Load-Deflection for 14-e (1 kip = 4.448 kN, 1 in. = 25.4 mm)

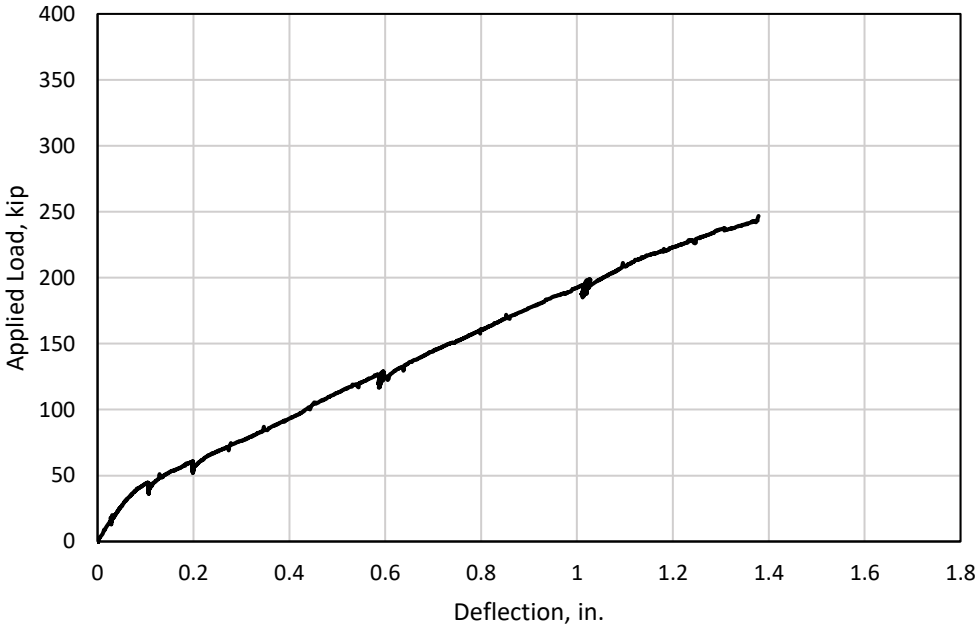

Figure D.6: Load-Deflection for 14-f (1 kip = 4.448 kN, 1 in. = 25.4 mm)

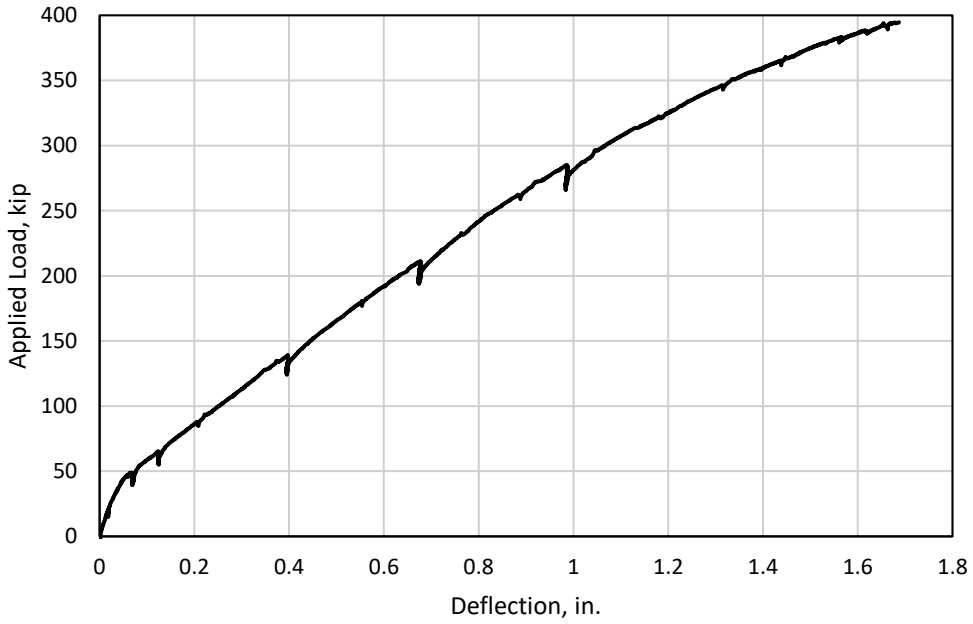

Figure D.7: Load-Deflection for 14-g (1 kip = 4.448 kN, 1 in. = 25.4 mm)

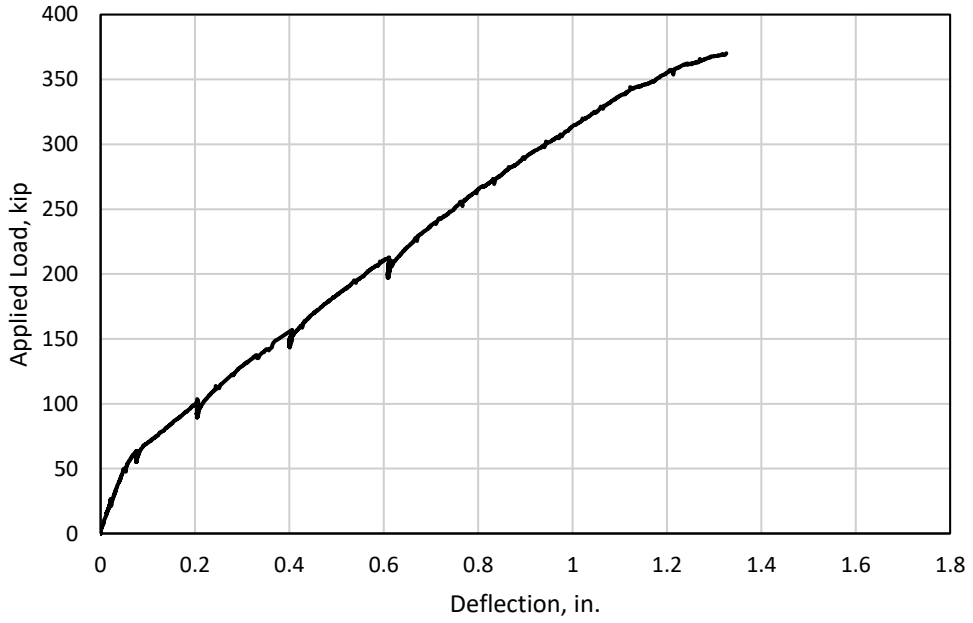

Figure D.8: Load-Deflection for 18-a (1 kip = 4.448 kN, 1 in. = 25.4 mm)

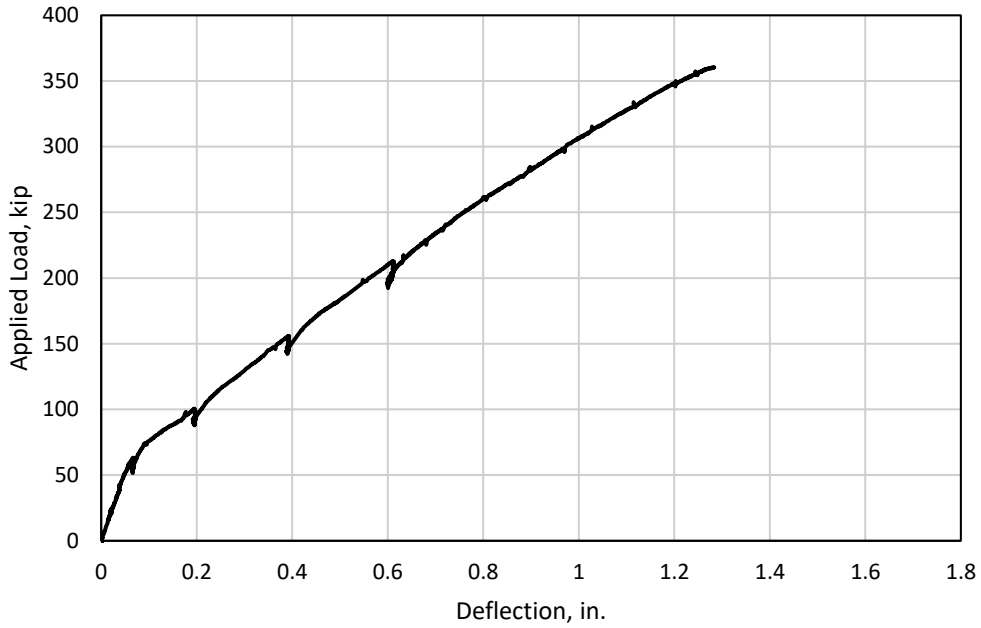

Figure D.9: Load-Deflection for 18-b (1 kip = 4.448 kN, 1 in. = 25.4 mm)

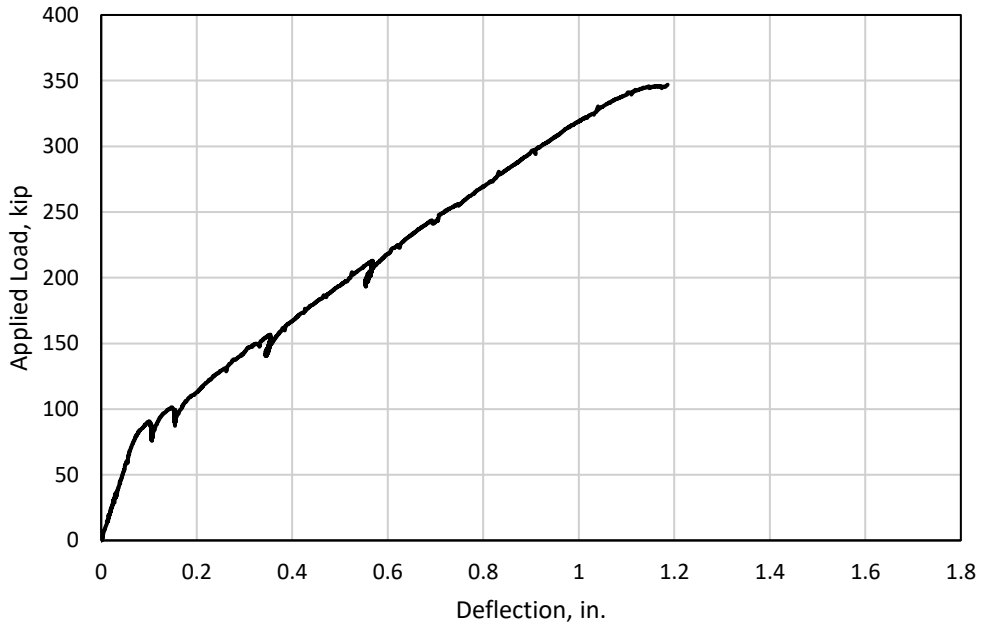

Figure D.10: Load-Deflection for 18-c (1 kip = 4.448 kN, 1 in. = 25.4 mm)

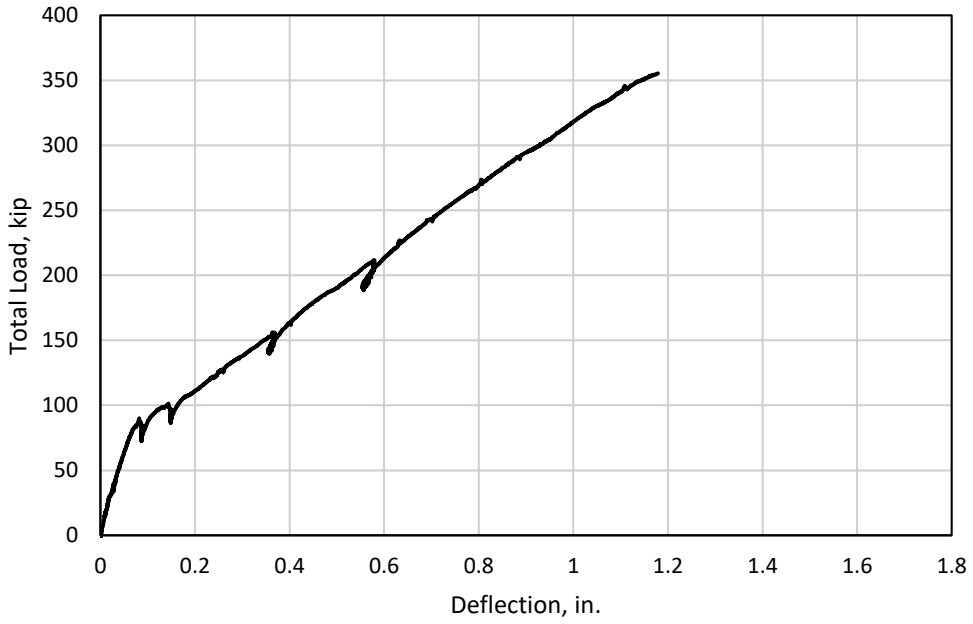

Figure D.11: Load-Deflection for 18-d (1 kip = 4.448 kN, 1 in. = 25.4 mm)

APPENDIX E: PHOTOS AND CRACK WIDTHS

Appendix E contains a photo of each specimen after failure. The dashed line near the center of each image represents the centerline of the lap splice, while the solid lines represent the ends.

Figure E.1: Photo of 14-a after failure

Figure E.2: Photo of 14-b after failure

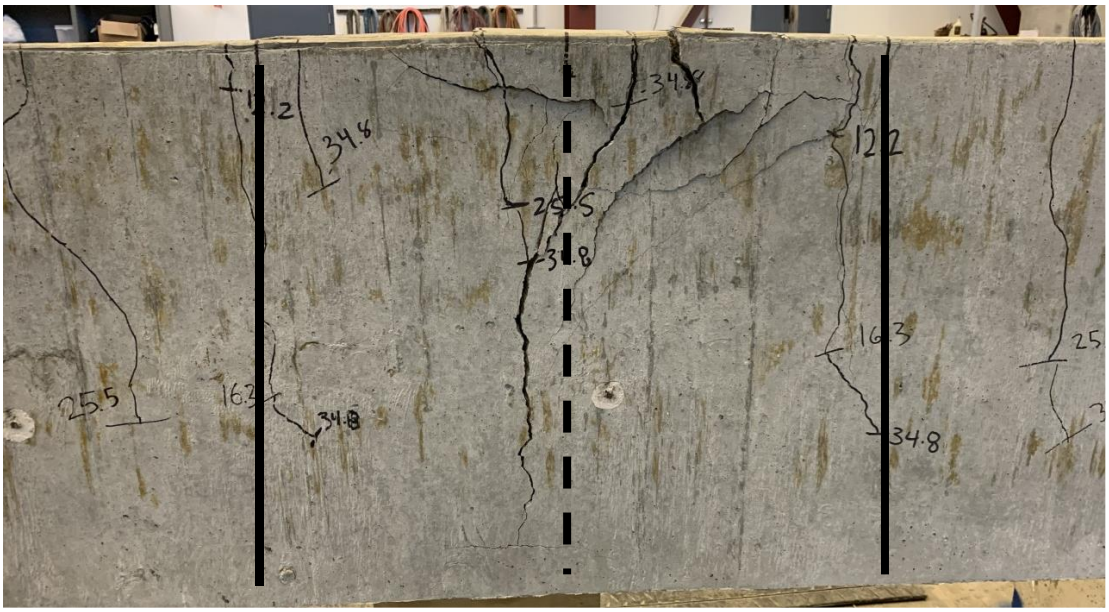

Figure E.3: Photo of 14-c after failure

Figure E.4: Photo of 14-d after failure

Figure E.5: Photo of 14-e after failure

Figure E.6: Photo of 14-f after failure

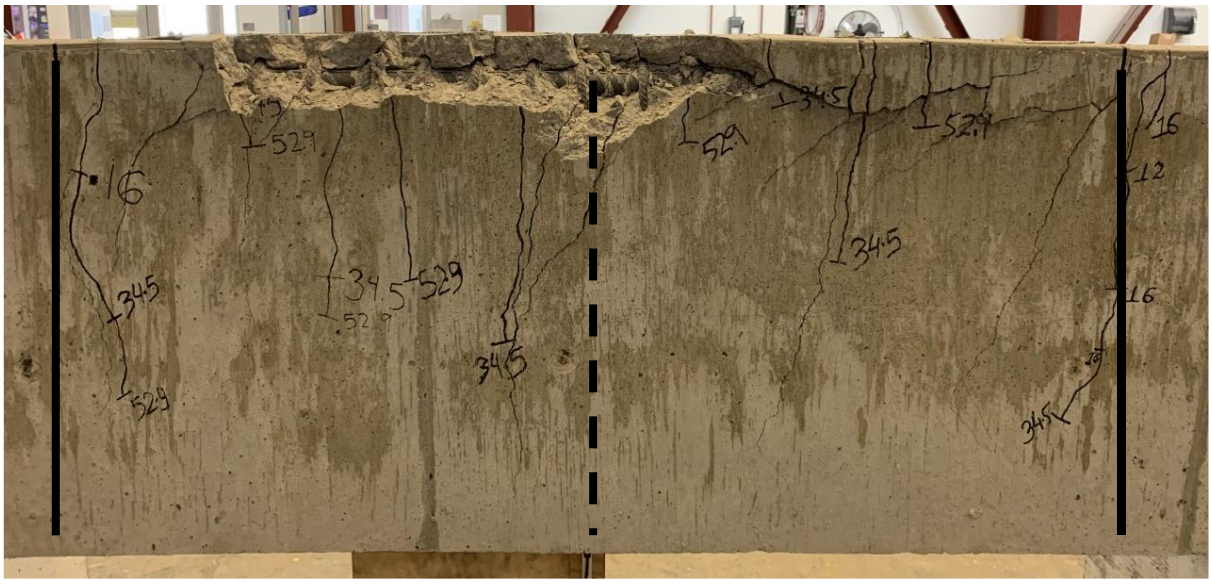

Figure E.7: Photo of 14-g after failure

Figure E.8: Photo of 18-a after failure

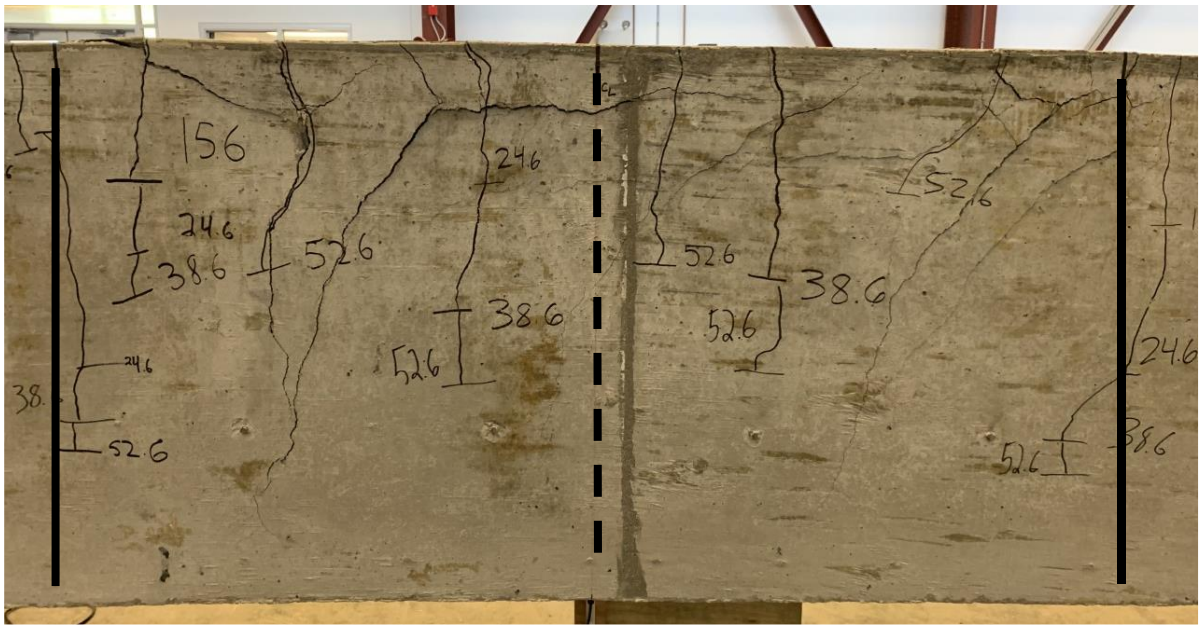

Figure E.9: Photo of 18-b after failure

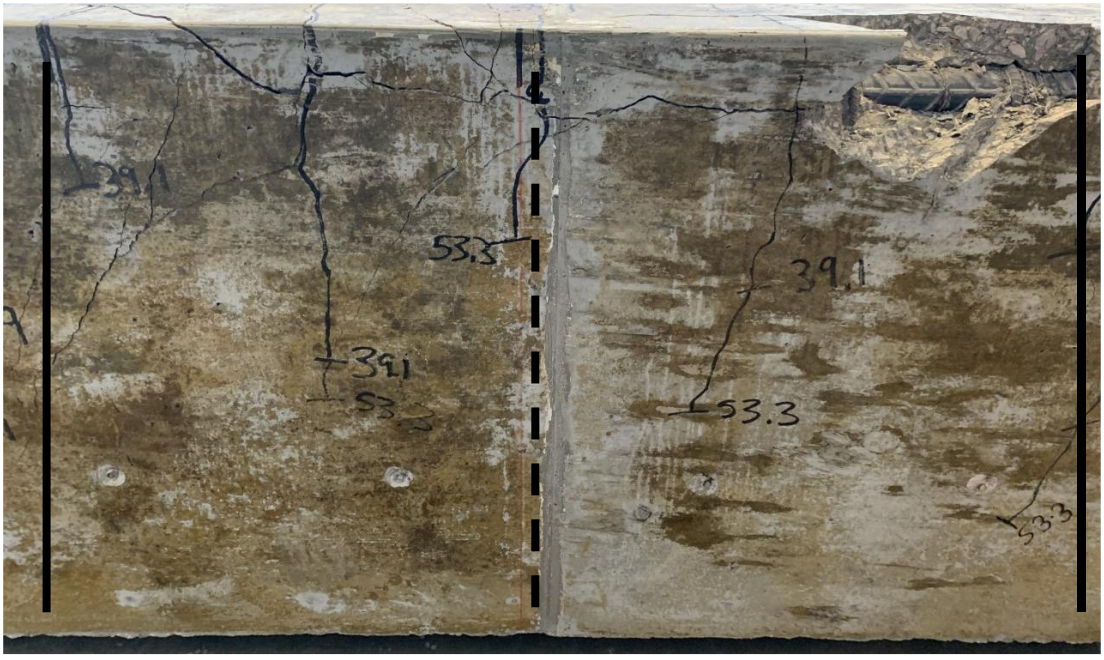

Figure E.10: Photo of 18-c after failure

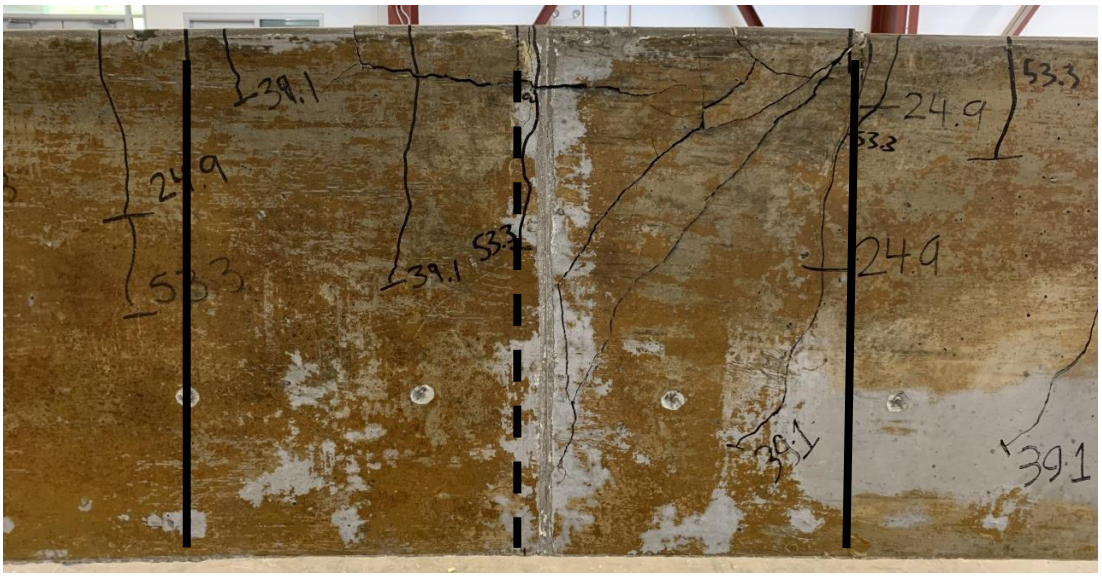

Figure E.11: Photo of 18-d after failure

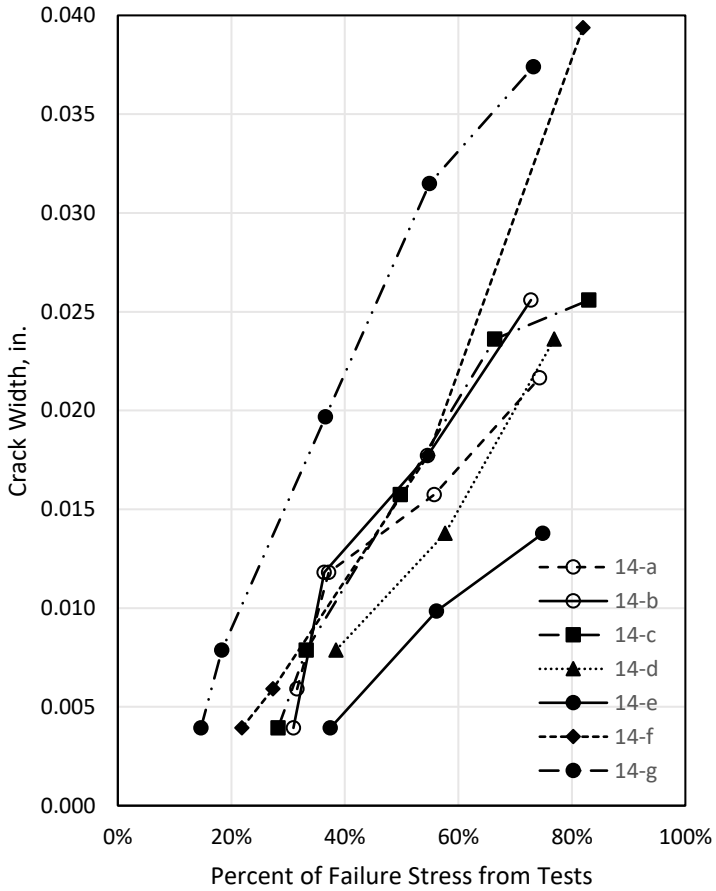

Figure E.12: Crack widths versus percent of bar stress at failure for specimens with No. 14 (43 mm) bars (1 in. = 25.4 mm)

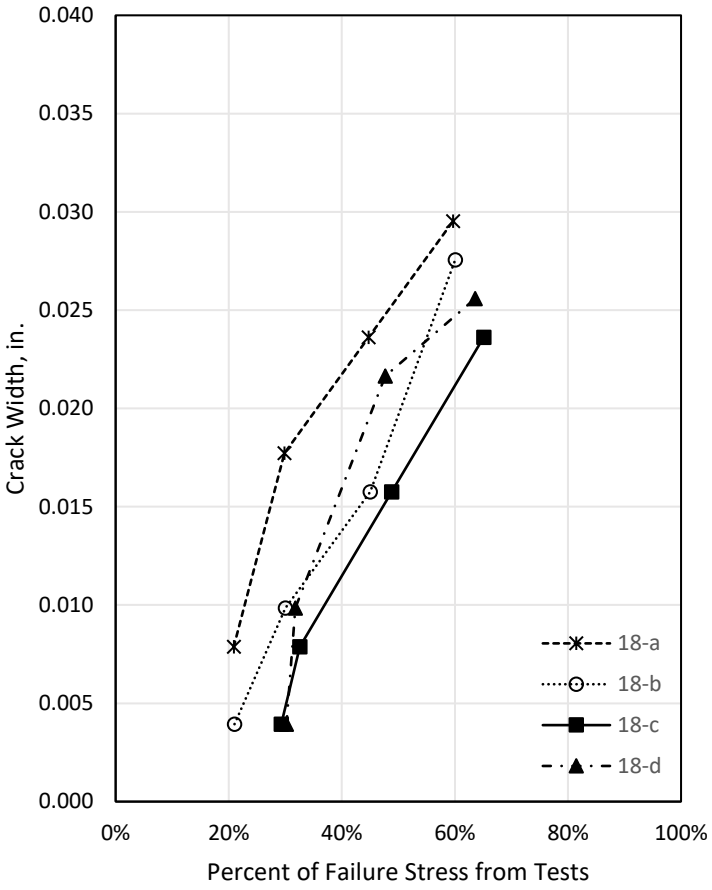

Figure E.13: Crack widths versus percent of bar stress at failure for specimens with No. 18 (57 mm) bars (1 in. = 25.4 mm)

Table E.1: Maximum crack widths for specimens with No. 14 (43 mm) bars [a]

Specimen ID	Bar Stress at Failure (ksi)	Approximate Bar Stress (ksi)	Maximum Crack Width (in.)	% of Bar Stress at Failure
14-a	53.8	17 (M_{cr})	0.006	32%
		20	0.012	37%
		30	0.016	56%
		40	0.022	74%
14-b	54.9	17 (M_{cr})	0.004	31%
		20	0.012	36%
		30	0.018	55%
		40	0.026	73%
14-c	60.2	17 (M_{cr})	0.004	28%
		20	0.008	33%
		30	0.016	50%
		40	0.024	66%
		50	0.026	83%
14-d	52.0	20 (M_{cr})	0.008	38%
		30	0.014	58%
		40	0.024	77%
14-e	53.4	20 (M_{cr})	0.004	37%
		30	0.010	56%
		40	0.014	75%
14-f	73.2	16 (M_{cr})	0.004	22%
		20	0.006	27%
		40	0.018	55%
		60	0.039	82%
14-g	109.3	16 (M_{cr})	0.004	15%
		20	0.008	18%
		40	0.020	37%
		60	0.031	55%
		80	0.037	73%

[a] 1 ksi = 6.895 MPa, 1 in. = 25.4 mm

Table E.2: Maximum crack widths for specimens with No. 18 (57 mm) bars [a]

Specimen ID	Bar Stress at Failure (ksi)	Approximate Bar Stress (ksi)	Maximum Crack Width (in.)	% of Bar Stress at Failure
18-a	67.0	14 (M_{cr})	0.008	21%
		20	0.018	30%
		30	0.024	45%
		40	0.030	60%
18-b	66.6	14 (M_{cr})	0.004	21%
		20	0.010	30%
		30	0.016	45%
		40	0.028	60%
18-c	61.4	18 (M_{cr})	0.004	29%
		20	0.008	33%
		30	0.016	49%
		40	0.024	65%
18-d	62.9	19 (M_{cr})	0.004	30%
		20	0.010	32%
		30	0.022	48%
		40	0.026	64%

[a] 1 ksi = 6.895 MPa, 1 in. = 25.4 mm

APPENDIX F: REINFORCEMENT STRAINS

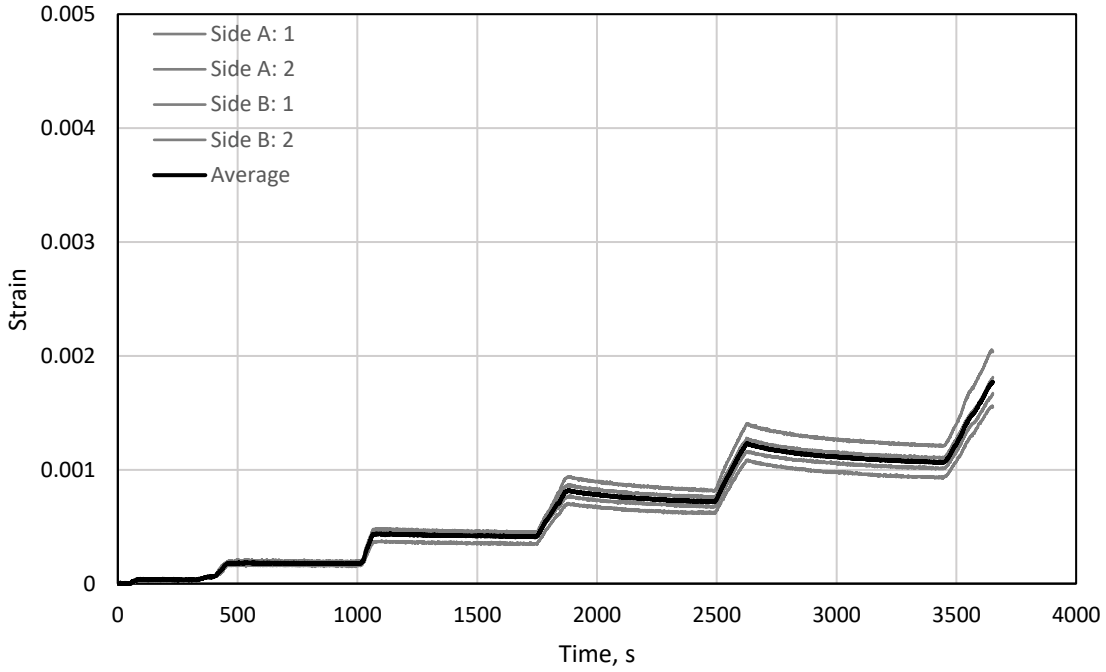

Figure F.1: Longitudinal bar strains for 14-a

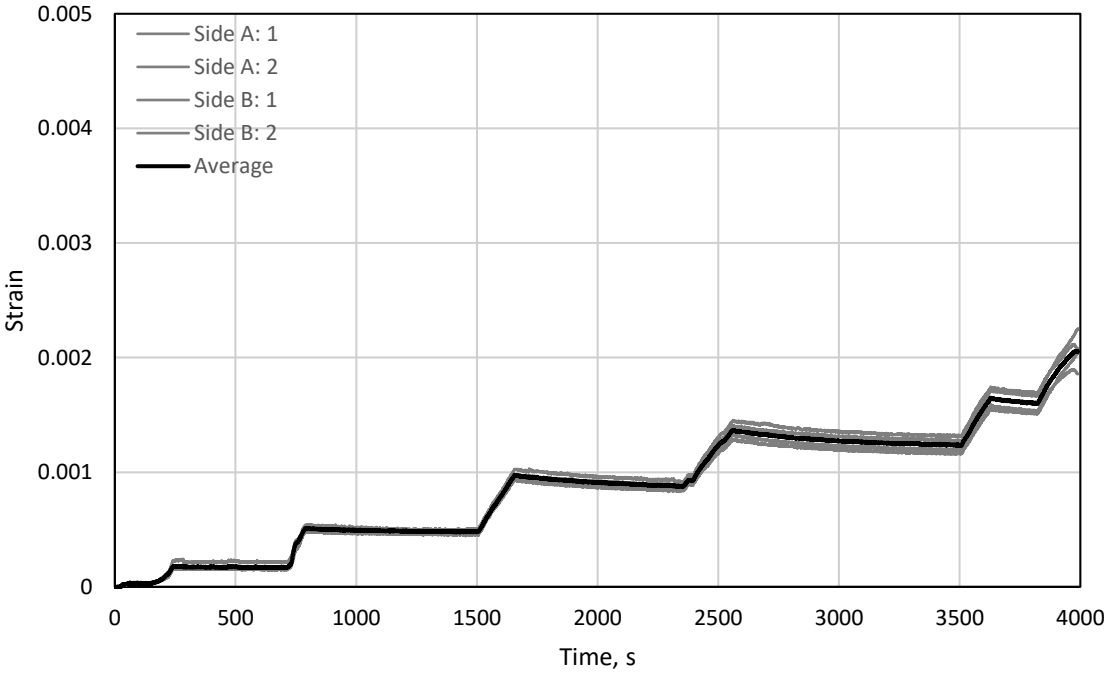

Figure F.2: Longitudinal bar strains for 14-b

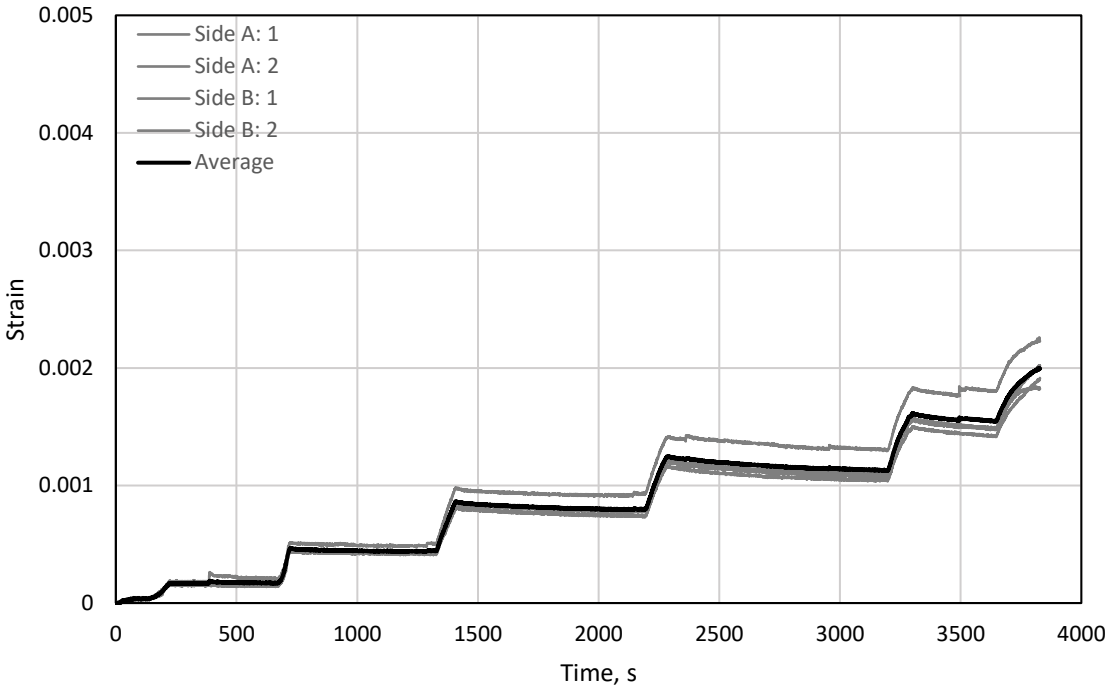

Figure F.3: Longitudinal bar strains for 14-c

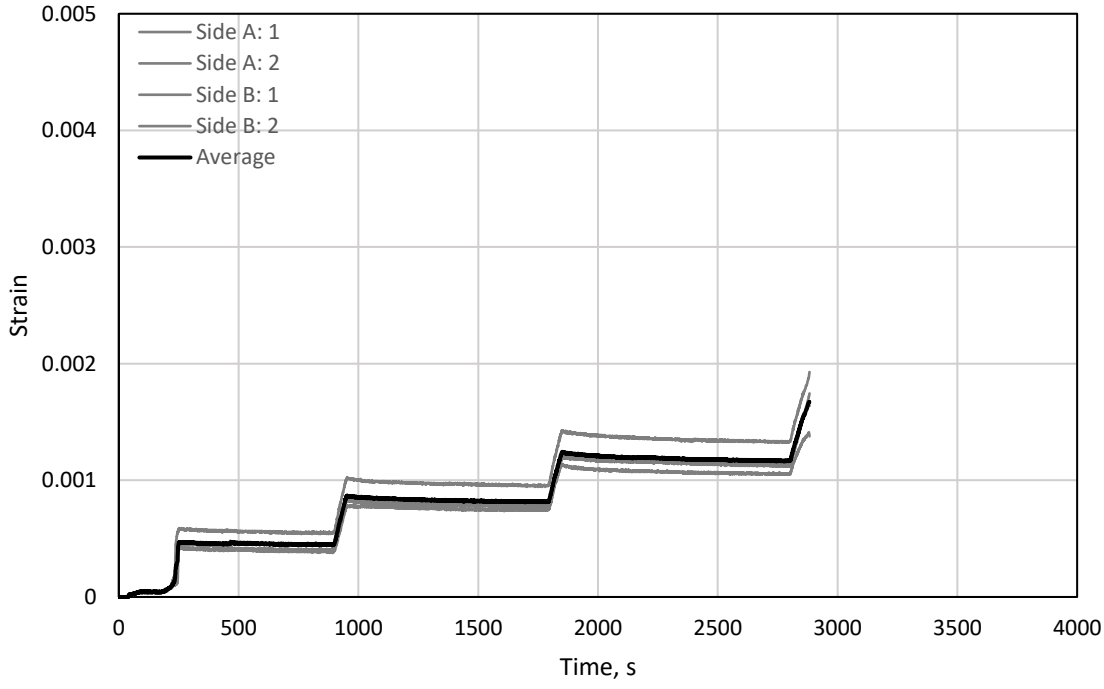

Figure F.4: Longitudinal bar strains for 14-d

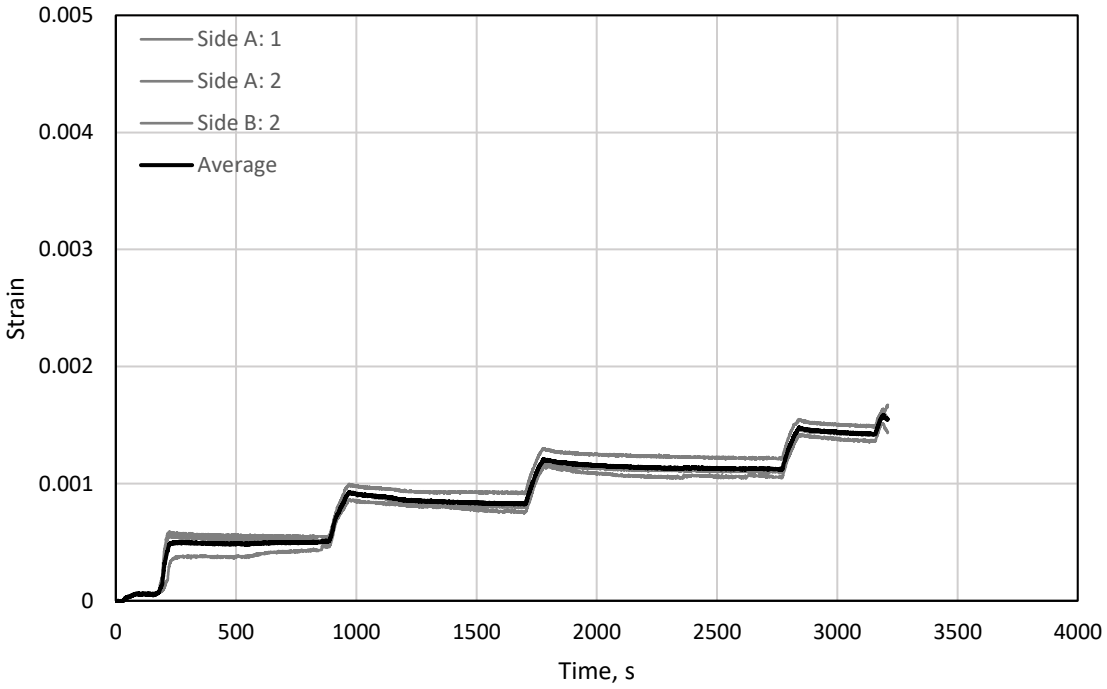

Figure F.5: Longitudinal bar strains for 14-e (Side B: 1, not recorded)

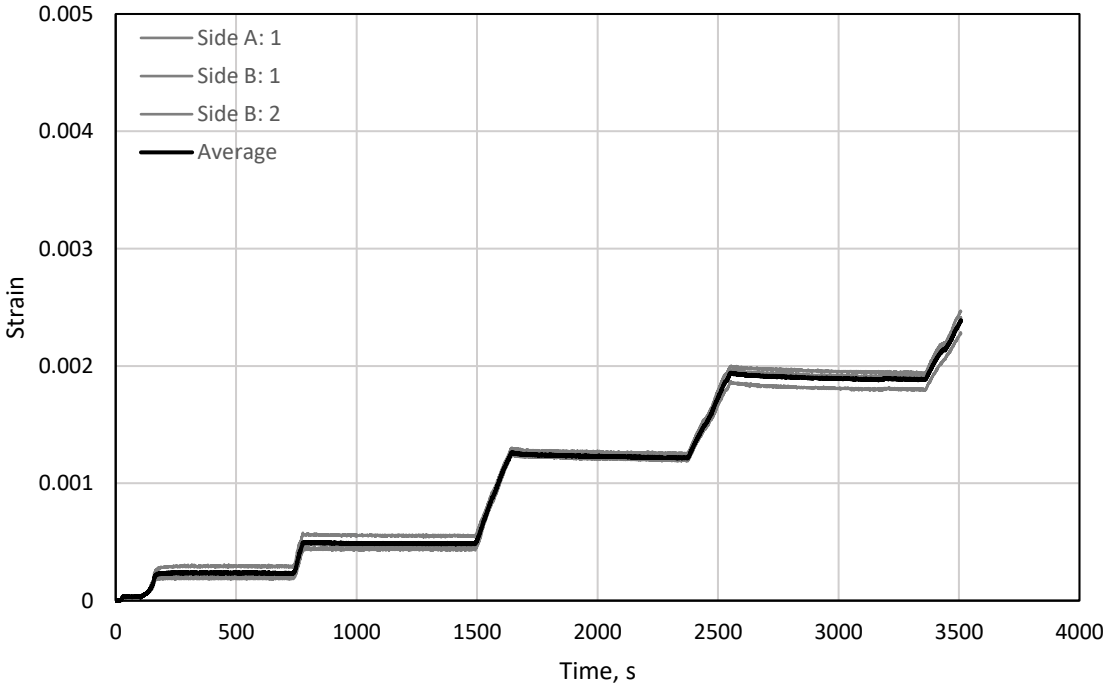

Figure F.6: Longitudinal bar strains for 14-f (Side A: 2, not recorded)

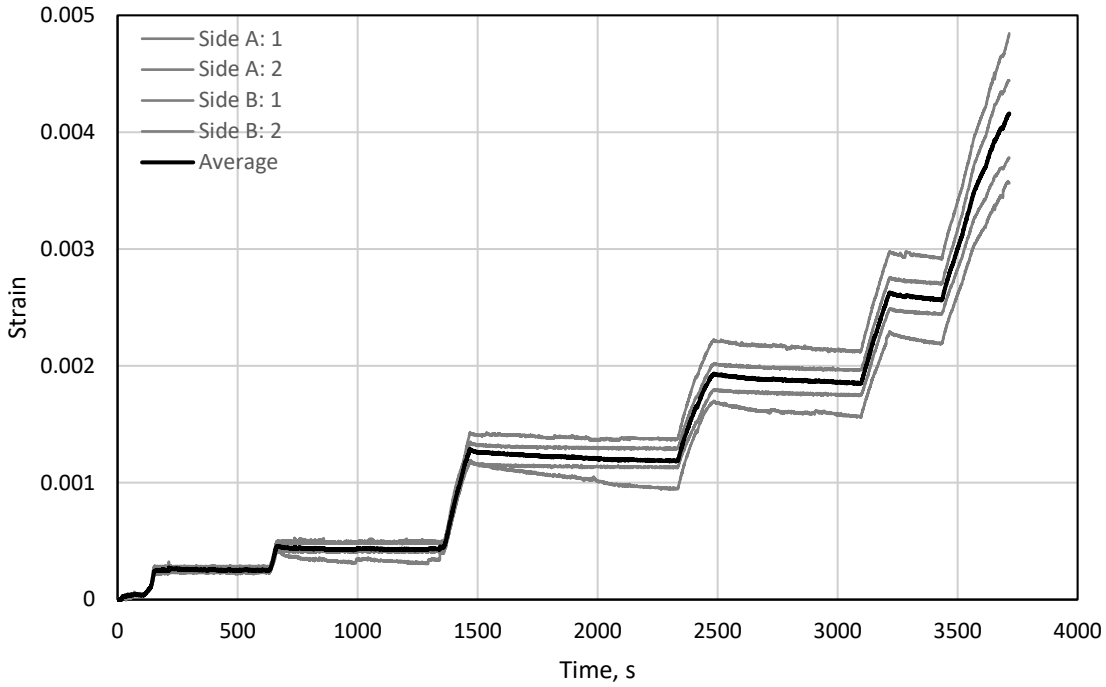

Figure F.7: Longitudinal bar strains for 14-g

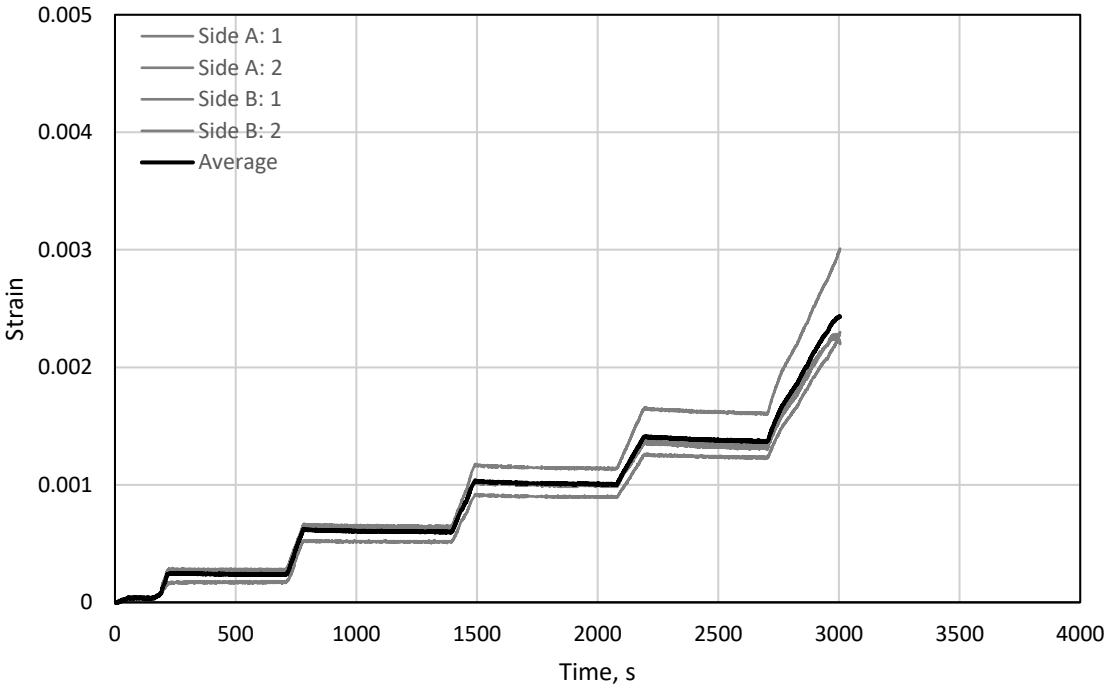

Figure F.8: Longitudinal bar strains for 18-a

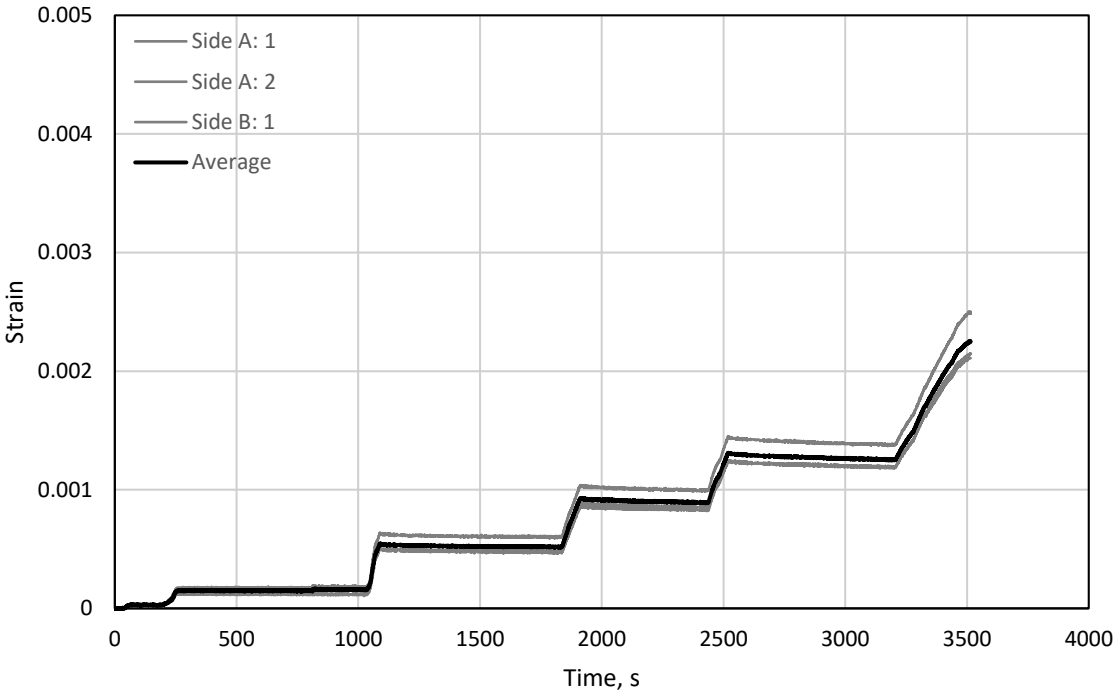

Figure F.9: Longitudinal bar strains for 18-b (Side B: 2, not recorded)

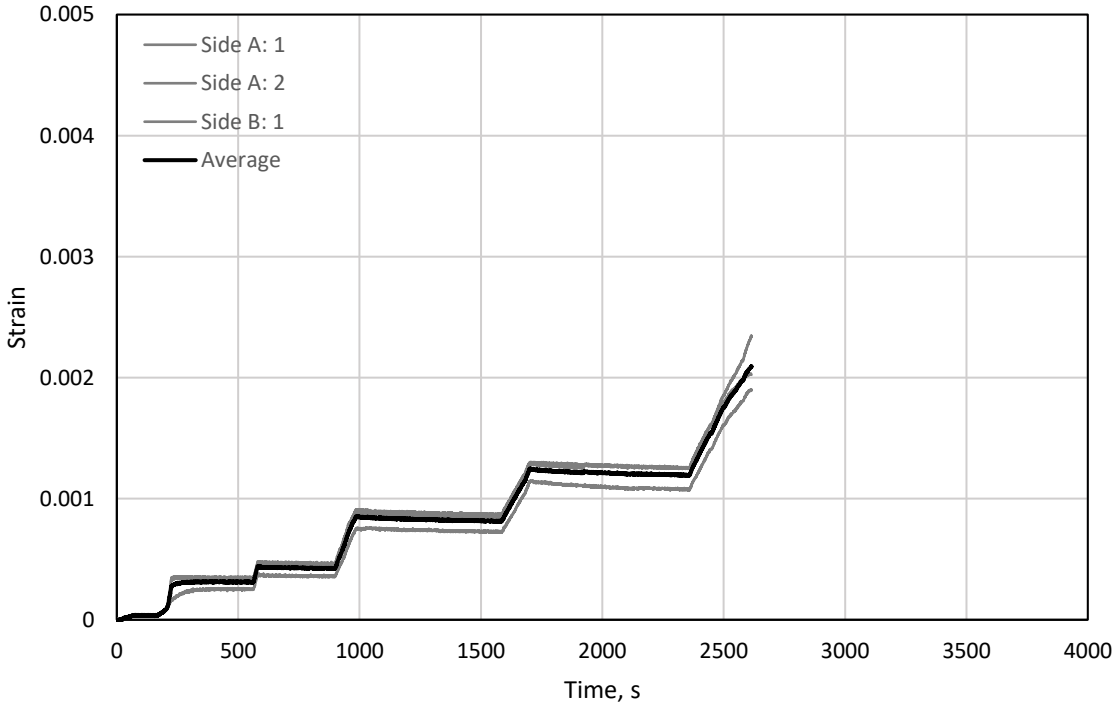

Figure F.10: Longitudinal bar strains for 18-c (Side B: 2, not recorded)

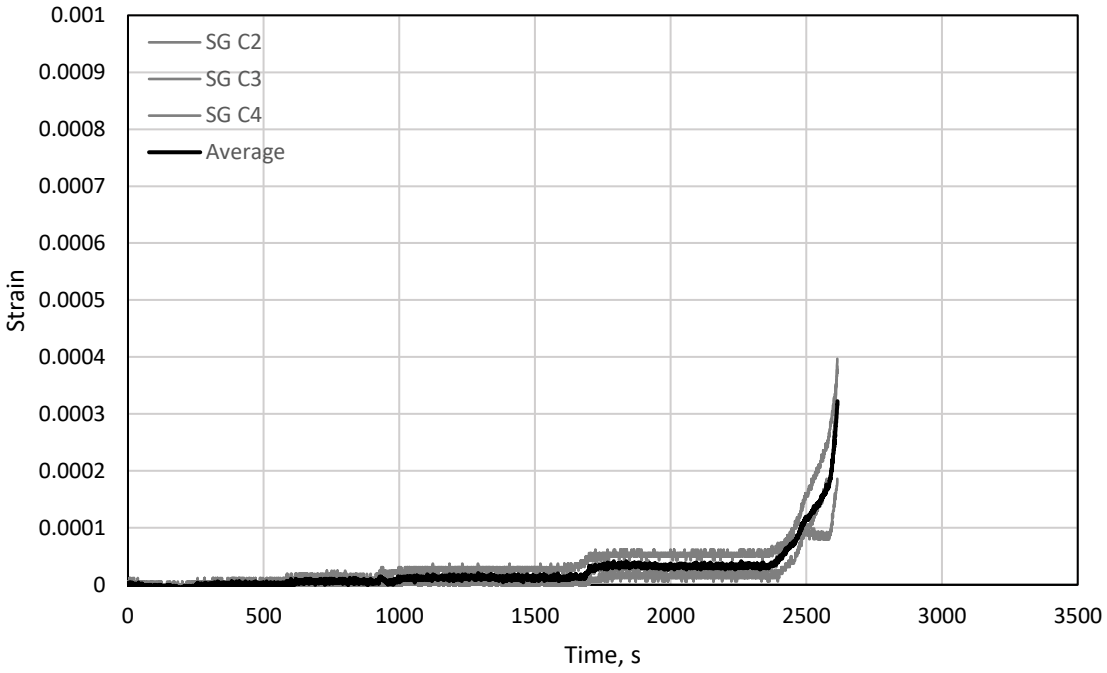

Figure F.11: Transverse reinforcement strains for 18-c (SG C1 not recorded)

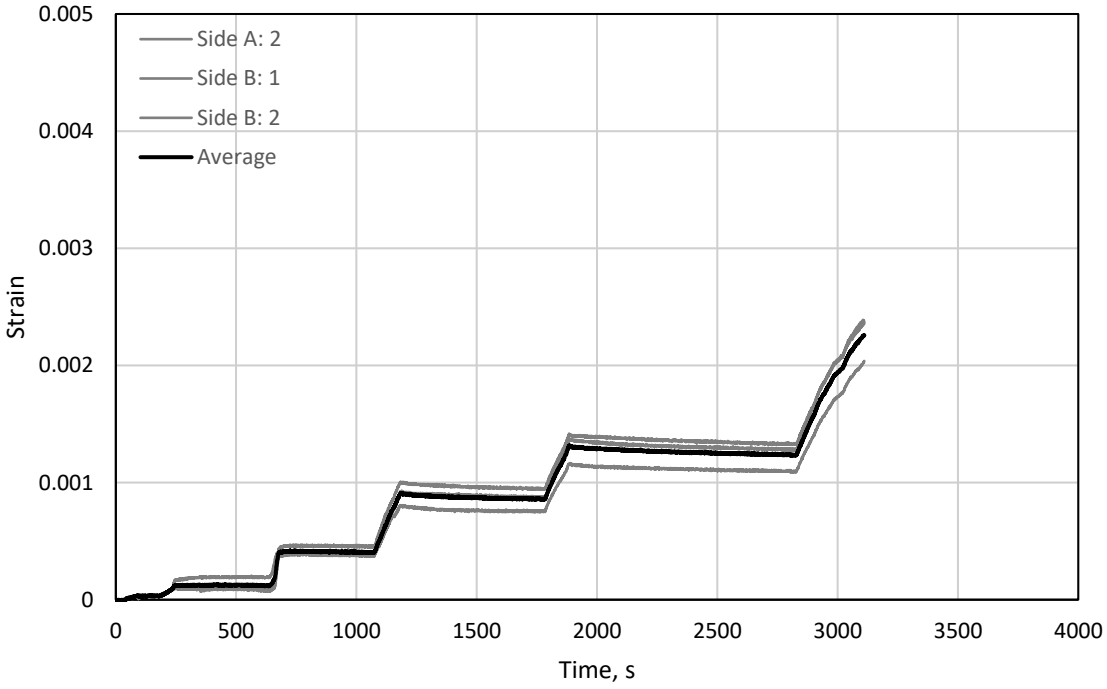

Figure F.12: Longitudinal bar strains for 18-d (Side A: 1, not recorded)

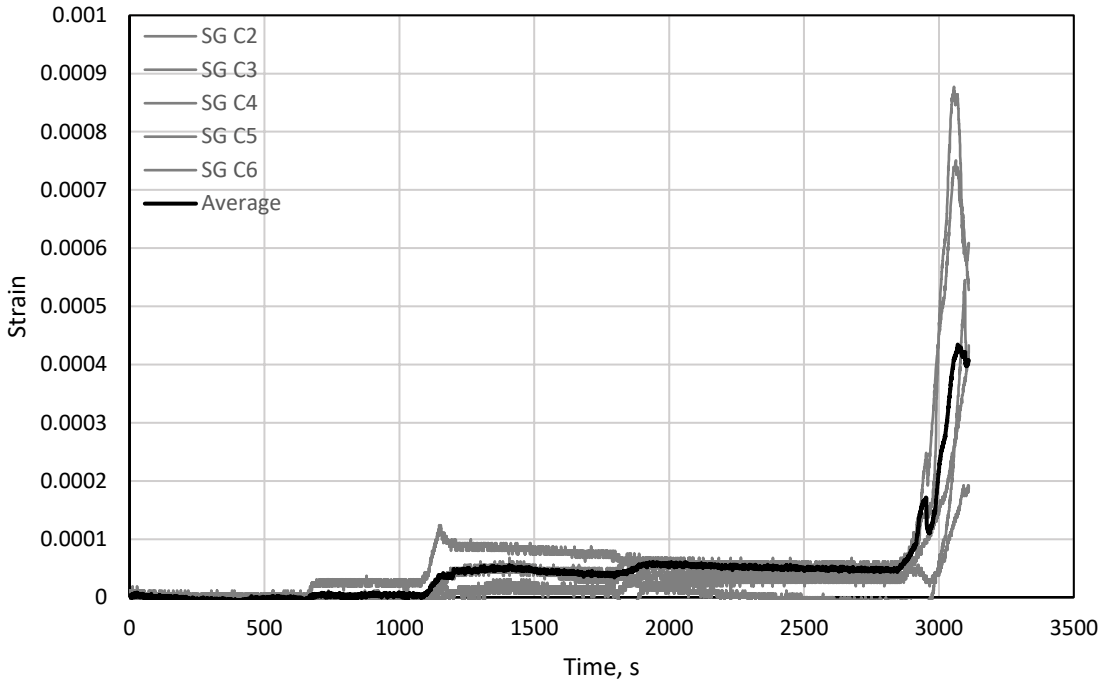

Figure F.13: Transverse reinforcement strains for 18-d (SG C1 not recorded)

Table F.1: Bar stress at failure based on measured strains [a]

ID	E_{nom} (ksi)	$\varepsilon_{f,avg}$ [b]	$\sigma_{f,nom}$ [c] (ksi)	% Error [d] ((+) means > reference)
14-a	29,000	0.00177	51.3	(-) 4.6%
14-b	29,000	0.00205	59.5	(+) 8.4%
14-c	29,000	0.00198	57.4	(-) 4.7%
14-d	29,000	0.00167	48.4	(-) 6.9%
14-e	29,000	0.00157	45.5	(-) 14.7%
14-f	29,000	0.00239	69.3	(-) 5.3%
14-g	29,000	0.00416	109 [e]	(-) 0.3%
18-a	29,000	0.00243	70.5	(+) 5.2%
18-b	29,000	0.00225	65.3	(-) 2.0%
18-c	29,000	0.00209	60.6	(-) 1.3%
18-d	29,000	0.00226	65.5	(+) 4.1%

[a] 1 ksi = 6.895 MPa
[b] Average of functioning strain gauges at time of failure (same moment in time as splice failure)
[c] Product of E_{nom} and $\varepsilon_{f,avg}$ unless noted otherwise.
[d] Bar stress calculated from beam moment method is used as reference (Table 4.2)
[e] Stress was determined from measured stress-strain results plotted in Appendix B (due to nonlinearity)

APPENDIX G: ROTATION ANALYSIS

Figures G.1 and G.2 show the layout of optical sensors on 18-c and 18-d. The location of each sensor in 3-dimensional space was recorded throughout the tests. The data were used to calculate the relative rotations between each successive pair of vertical columns of optical sensors. The rotations calculated at loads just before failure are listed in Tables G.1 and G.2 and plotted in Figures G.3(a) and G.4(a). The average curvatures within each portion of the beam span (e.g., A-B, B-C, etc.) were calculated as relative rotation divided by nominal horizontal distance and are given in Tables G.1 and G.2 and Figures G.3(b) and G.4(b).

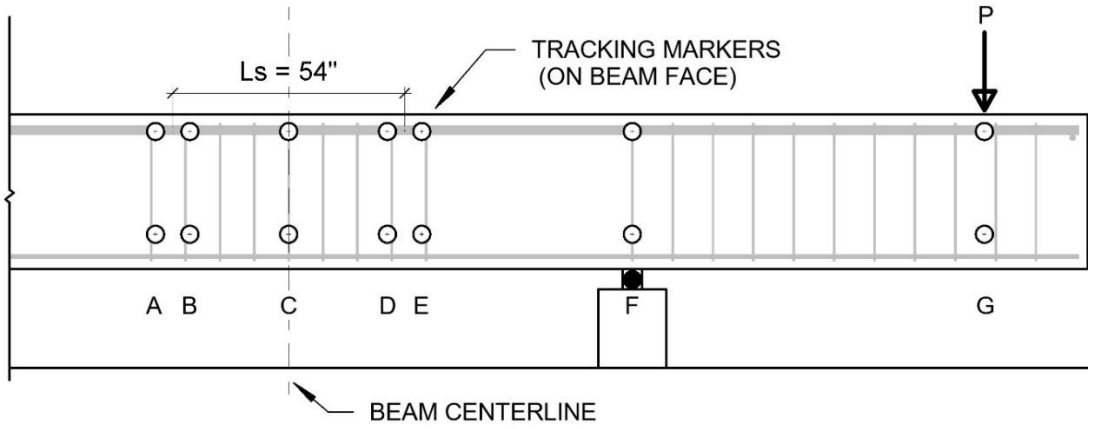

Figure G.1: Optical sensor layout for 18-c (1 in. = 25.4 mm)

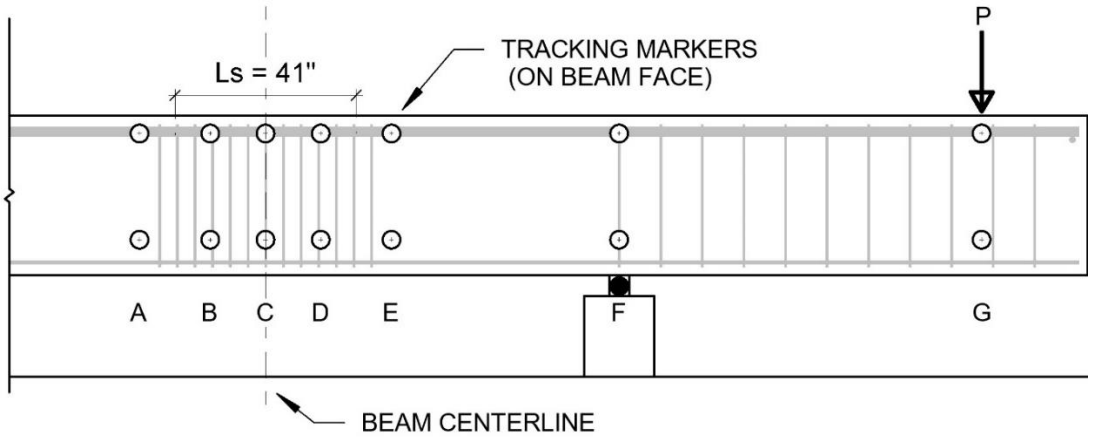

Figure G.2: Optical sensor layout for 18-d (1 in. = 25.4 mm)

Table G.1: Relative rotations for 18-c

Location	A - B	B - C	C - D	D - E	E - F	F - G	C- F
Description	Straddling splice end	Inside splice end to center line	Center line to inside splice end	Straddling splice end	Outside splice end to support	Support to load point	Center line to load point total
Relative Rotation rad	0.0050	0.0045	0.0025	0.0085	0.0021	0.0164	0.0295
Nominal Horizontal Distance in. (mm)	8 (200)	23 (580)	23 (580)	8 (200)	49 (1240)	82 (2080)	162 (4110)
Curvature x 10^{-4} 1/in. (1/mm)	6.25 (0.25)	1.96 (0.078)	1.09 (0.043)	10.6 (0.43)	0.43 (0.017)	2.0 (0.079)	1.8 (0.072)

Table G.2: Relative rotations for 18-d

Location	A - B	B - C	C - D	D - E	E - F	F - G	C- F
Description	Straddling splice end	Inside splice end to center line	Center line to inside splice end	Straddling splice end	Outside splice end to support	Support to load point	Center line to load point total
Relative Rotation rad	0.0184	0.0352	0.0110	0.0156	0.0050	0.0735	0.1051
Nominal Horizontal Distance in. (mm)	16 (410)	12.5 (320)	12.5 (320)	16 (410)	51.5 (1310)	82 (2080)	162 (4110)
Curvature x 10^{-4} 1/in. (1/mm)	11.5 (0.45)	28.2 (1.10)	8.8 (0.34)	9.8 (0.38)	0.97 (0.04)	9.0 (0.35)	6.5 (0.26)

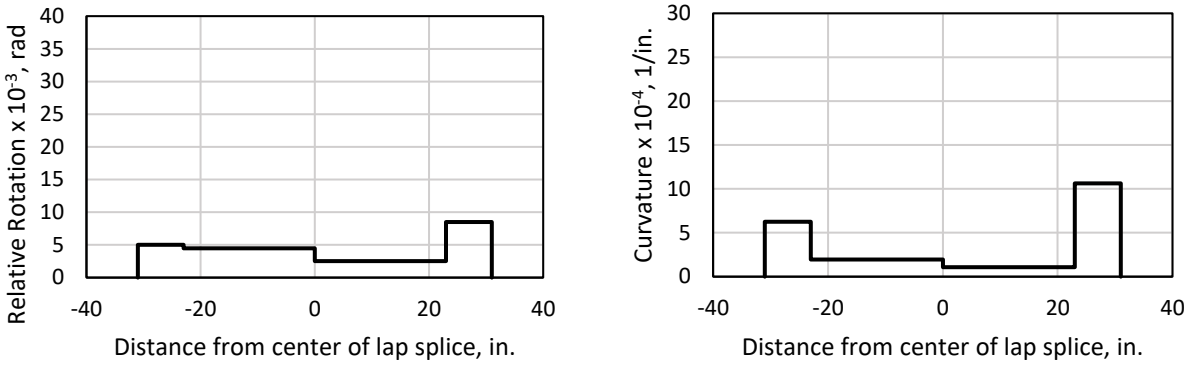

(a) (b)

Figure G.3: Specimen 18-c (a) relative rotation and (b) average curvatures within lap splice length (1 in. = 25.4 mm)

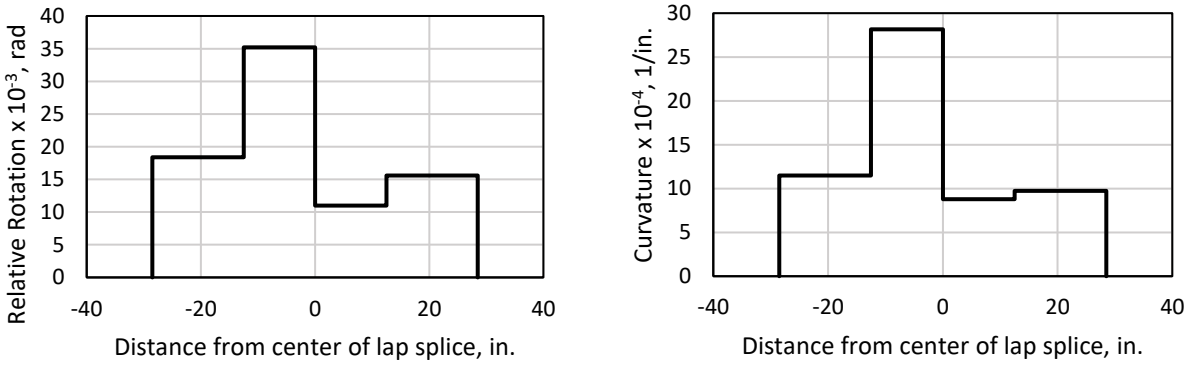

(a) (b)

Figure G.4: Specimen 18-d (a) relative rotation and (b) average curvature within lap splice length (1 in. = 25.4 mm)

Based on these results, the following analysis was done to examine whether bar bending/prying induced by beam curvature might have contributed to the observed bond-splitting failures at loads smaller than expected based on prior tests with smaller bars. In other words, does the greater flexural stiffness of large diameter bars cause them to tend to pry the cover off in a manner that reduces the bond strength?

For this analysis, it was assumed that plane sections remain plane and reinforcing bars remain perpendicular to the beam cross-section. Based on this assumption, reinforcing bars must bend to remain compatible with beam bending, so beam curvature and bar curvature are equal. Figures G.3(b) and G.4(b)

therefore represent beam curvature and bar curvature. For the following analyses, only results from 18-c are used because 18-d had a prominent inclined crack within the lap splice that clearly violated the plane sections remain plane assumption (Figure G.5).

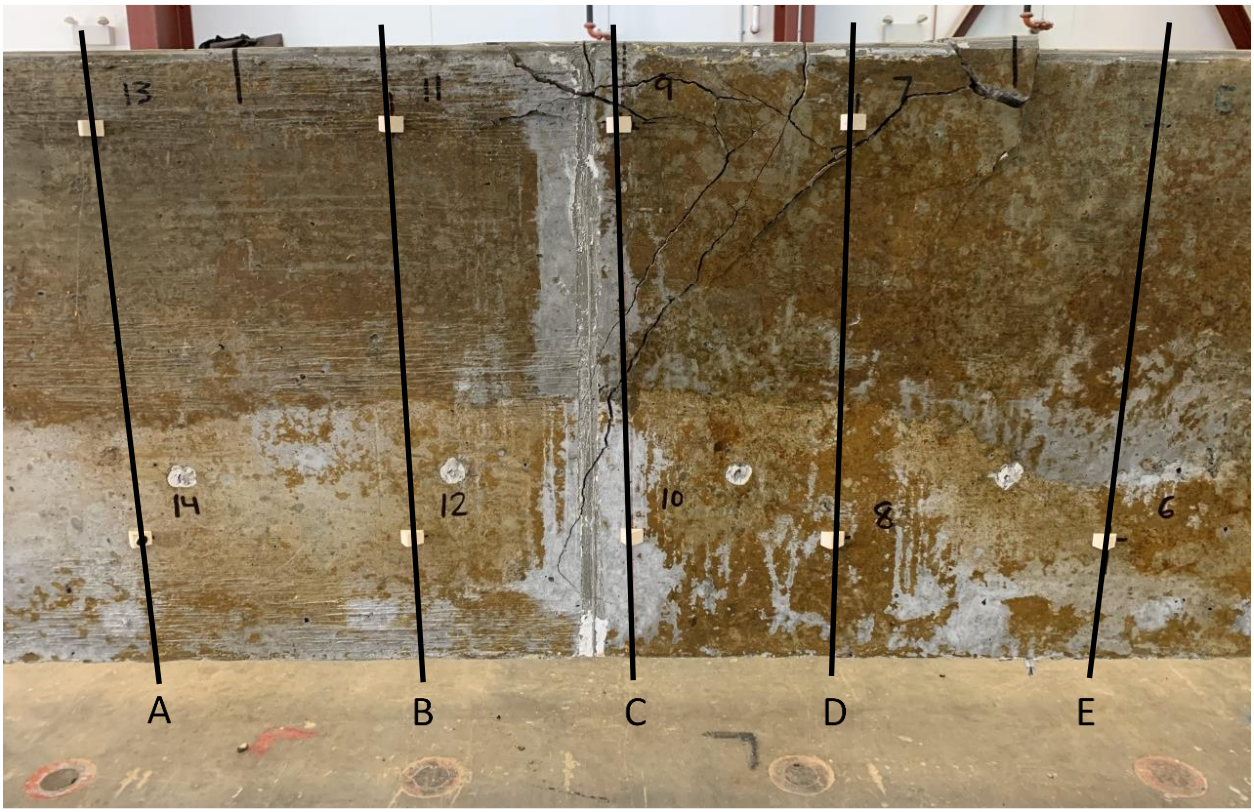

Figure G.5: Specimen 18-d with inclined crack spanning from the compression fibers in B-C to the D-E tension face after failure

Due to symmetry, to simplify the analysis, and reduce the localized effects of concentrated rotations at a single crack, curvatures were averaged as follows: curvatures in A-B and D-E, which straddled the splice ends, were averaged, as were curvatures in B-C and C-D, which represent the middle portion of the lap splice. The resulting average curvatures are given in Table G.3 and Figure G.6(a). Figure G.6(a) shows average curvatures versus position within the lap splice. The distribution in Figure G.6(a) cannot be the real distribution of curvature because a discontinuity in bar curvature implies a discontinuity in moment on the bar. This is not possible since no concentrated moments were applied to the bars.

Table G.3: Averaged curvatures

Location	A - B	B - C	C - D	D - E
Description	Straddling splice end	Inside splice end to center line	Center line to inside splice end	Straddling splice end
18-c Average Curvature x 10^{-4} 1/in. (1/mm)	8.44 (0.34)	1.52 (0.060)	1.52 (0.060)	8.44 (0.34)

To obtain a more realistic estimate of bar curvature distribution, the following assumptions were made:

1. Bar curvature is a maximum at the start of the splice and decreases linearly over a length *x*. The total rotation over *x* is equal to that measured in the test.
2. Bar curvature is zero at the end of a lap-spliced bar. This must be true because there is no moment applied to the bar end. But, this also requires some incompatibility in bending deformations near the end of the lap splice between the terminating end of one bar (zero curvature) and the continuous parallel bar (which experiences maximum curvature). The total rotation over *x* at the terminating bar end is therefore *not* equal to that measured in the test.
3. Bar curvature varies linearly over a length *x* from zero at the bar end towards mid-splice.
4. Bar curvature is constant over a length ($\ell_s - 2x$) centered on the mid-length of the lap splice. This constant curvature is equal to 1.52 x 10^4 1/in. (0.060 x 10^4 1/mm) for 18-c (Table G.3).

Based on these assumptions, and an assumed *x* of 6 in. (150 mm), the curvature distribution in one lap-spliced bar within the lap splice is plotted in Figure G.6(b). Since the bars remained linear elastic, the bar moments in Figure G.6(c) can be obtained by multiplying curvatures in Figure G.6(b) by *EI*, where *E* is 29,000 ksi (200 GPa) and *I* is 1.27 in.^{4} (530000 mm^4) assuming a No. 18 (57 mm) bar is represented as a circle with a diameter of 2.25 in. (57 mm). The shear in the bar (Figure G.6(d)) thus equals the slope of the moment distribution in Figure G.6(c). The above analysis ignores the presence of stirrups and their effect on the distribution of shear on the spliced bar.

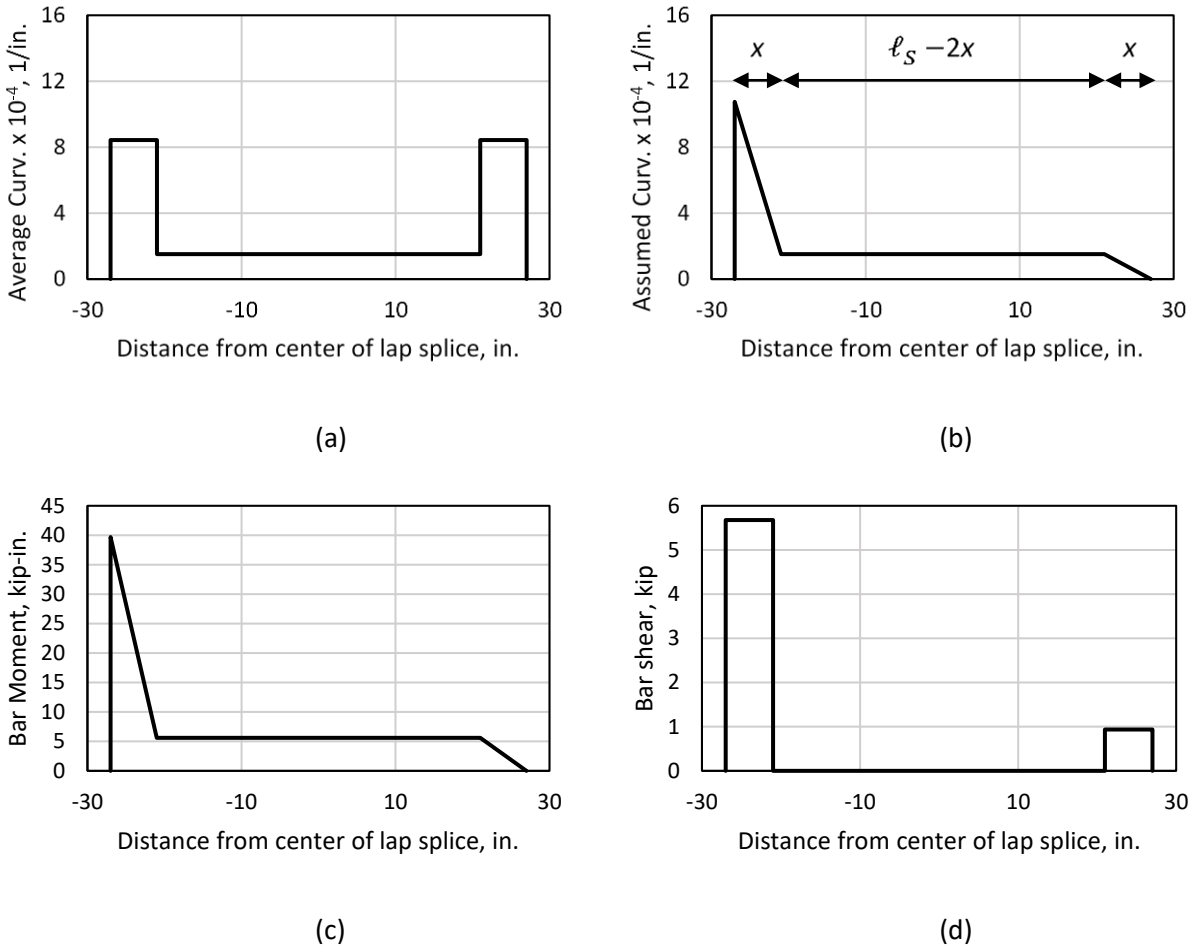

Figure G.6: Specimen 18-c (a) averaged bar curvature, (b) assumed bar curvature distribution for x = 6 in. (150 mm) based on stated assumptions with bar continuous to the left and terminating at the right end of the lap splice, (c) bar moment implied by curvature in G.6(b), and (d) bar shear implied by moment in G.6(c)

(1 in. = 25.4 mm, 1 kip = 4.448 kN)

The shear in the bar in Figure G.6(d), which is 5.7 and 0.9 kips (25 and 4 kN) at the continuous and terminating bar ends, respectively, can be a basis for estimating the force that must exist perpendicular to the bar axis within the lap splice to produce a bent-bar shape compatible with the shape of the flexing beam. The specimens had two lap splices, each consisting of two parallel bars. So, the cover at one end of the lap splice must provide a total clamping force equal to $2(5.7 \text{ kips} + 0.9 \text{ kips}) = 13.2 \text{ kips}$ (59 kN). If the area

of concrete in a plane parallel to the lap-spliced bars that is active in providing this clamping force is *x* times the quantity beam width, *b*, minus the width of the four lap-spliced bars, then bar prying/bending induced a tensile stress in the concrete perpendicular to the bar axis equal to $13.2 \text{ kips}/\big(x(b-4d_b)\big) = 150$ psi (1.0 MPa). The cracking stress of the cover is approximately $4\sqrt{f_c'} = 400$ psi (2.8 MPa), so resisting bar prying required approximately 1/3 of the available resistance to splitting provided by the cover concrete.

This analysis requires a series of assumptions that may not be valid, so it should not be interpreted as a means of accurately assessing the tension stress that bar prying/bending induces in the cover concrete. Nevertheless, this model is useful for comparisons and can be used to demonstrate how larger bar diameters can result in substantial increases in the concrete tensile stress required to resist bar prying/bending, and that the force required to resist bar prying/bending might be non-negligible for large bars.

Figure G.7 shows the estimated concrete stress required to resist bar prying/bending for different bar sizes and lengths *x*. The calculated concrete stress is heavily dependent on both *x* and bar diameter. Regardless of *x*, and assuming that everything else is equal, prying of a No. 14 (43 mm) bar induces concrete splitting stresses that are nearly six times larger than a No. 9 (29 mm) bar and two times larger than a No. 11 (36 mm) bar. Likewise, prying of a No. 18 (57 mm) bar induces concrete splitting stresses that are twenty times larger than a No. 9 (29 mm) bar and eight times larger than a No. 11 (36 mm) bar.

Figure G.7 shows that although small bar bending may be negligible, it may not be appropriate to neglect the concrete stresses induced by bending of large diameter bars. Assuming this model produces a reasonable estimate of concrete tensile stresses, prying/bending of large bars induces stresses in the concrete cover that compromise the ability of the cover to resist bond-induced splitting. Figure G.7 shows that for *x* = 3 or 6 in. (75 or 150 mm) the No. 18 (57 mm) bars produce concrete tensile stresses that are approximately 0.4 and 2.7 times the splitting stress for 10,000 psi (70 MPa) concrete ($4\sqrt{f_c'} = 400$ psi (2.8 MPa)).

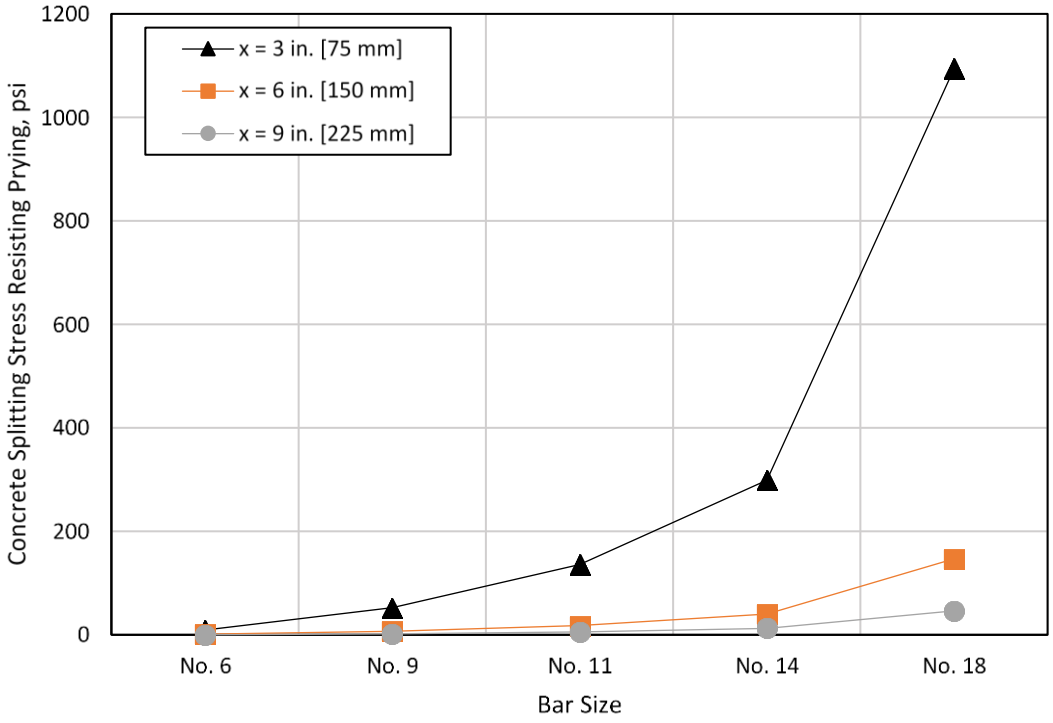

Figure G.7: Estimated stress in concrete cover perpendicular to bar axis required to resist bar prying/bending for varied bar size and length *x* (1 psi = 6.895 Pa, No. 6, 9, 11, 14, and 18 bars = 19, 29, 36, 43, and 57 mm)